Engineering probiotic bacteria to express vaccine derived antigens to enhance immune responses to vaccination

Isobel Ozra Khoshbooie

Supervisor: Professor David Lynn
Head Lynn Systems Immunology Group., South Australian Health and Medical Research Institute (SAHMRI) and Flinders University.

Co-supervisor: Dr. Todd Norton
Lynn Systems Immunology Group., South Australian Health and Medical Research Institute (SAHMRI).

Master of biotechnology
Department of medicine and public health, Flinders university

Student Name

Isobel Ozra Khoshbooie

Title

Engineering probiotic bacteria to express vaccine derived antigens to enhance immune responses to vaccination

Supervisor: Name and Department

Professor David Lynn, Head Systems Immunology Lab., South Australian Health and Medical Research Institute (SAHMRI) and Flinders University

Co-Supervisor: Name and Department

Dr. Todd Norton, Lynn Systems Immunology Group., South Australian Health and Medical Research Institute (SAHMRI)

Examiner 1: Name and Department

Dr. Damon Tumes, Head of the Allergy and Cancer Immunology laboratory in the Centre for Cancer Biology (CCB), University of South Australia and SA Pathology

Examiner 2: Name and Department

Dr. Bart Eijkelkamp, College of Science and Engineering, Flinders University

Due Date

31 October 2024

Table of Contents

List of Tables

List of Figures

Abbreviations/Glossary

i.m-Intramuscular

BCR- B cell receptor

Th1- T helper 1 cells

Th2- T helper 2 cells

Th17- T helper 17 cells

Treg- T regulatory cells

Tfh- T follicular helper cell

TGF-β- Transforming growth factor beta

IL-10- Interleukin 10

MN- Microneutralization

HIV- Huma immunodeficiency virus

SARS- COVID-19- Severe acute respiratory syndrome coronavirus 19

Phe- Phenylalanine

EcN- *Escherichia coli* Nissle

IFNs-Interferon

S. epi- *Staphylococcus epidermidis*

TT- Tetanus toxoid

NadA- Neisseria Adhesin A

OmpA- Outer membrane protein A

ColE1- Origin of replication carrying genes for colicin E1

pAIDA- Adhesin Involved in Diffuse Adherence (AIDA) plasmid construct

AIDA- Adhesin-involved-in-diffuse-adherence

PCV13- 13-valent pneumococcal polysaccharide vaccine

CRM 197- Cross-reactive material 197

PCR- Polymerase chain reaction

DNA- Deoxyribonucleic acid

E. coli DH5α- DH5- Alpha *Escherichia coli*

HEPA- High-efficiency particulate air

CFU- Colony forming units

IPTG- Isopropyl ß-D-1-thiogalactopyranoside

OD- Optical density

LB- Luria-Bertani broth

PBS- Phosphate-buffered saline

ELISA- Enzyme linked immunosorbent assay

ELISpot- Enzyme-linked immunospot assay

Ova- Ovalbumin

PBS-T- Phosphate-buffered saline -Tween

TMB- Ultra tetramethylbenzidine

cRPMI - Roswell Park memorial institute medium, complete cell culture media

GIBCO PBS- Grand Island Biological Company, Phosphate-buffered saline

HRP- Horseradish peroxidase

H2O- Water

SYTO™ BC- Green Fluorescent Nucleic Acid Stains

His tag- Polyhistidine protein tag fused to either the C- or N-terminus of a protein

Myc tag- polypeptide protein tag derived from the c-myc gene that can be fused to either the C- or N-terminus of a protein

RBS- Ribosome Binding Site

mRNA-Ova- mRNA based vaccine designed to deliver ovalbumin protein

ASC- Antibody secreting cells

GCB- Germinal center B cells

Bmem- Memory B cells

FSC- Forward scatter

SSC- Side scatter

LN- Lymph node

LacUV5- Promoter from the *Escherichia coli* to promote recombinant protein expression

EcN-WT-*Escherichia coli* Nissle carrying wild type

EcN-EV-*Escherichia coli* Nissle carrying an empty vector

EcN-CRM-*Escherichia coli* Nissle carrying cross-reactive material protein

BL21-EV-strain of *Escherichia coli* carrying a empty vector

BL21-CRM- Strain of *Escherichia coli* carrying cross-reactive material protein

BL21-WT- Strain of *Escherichia coli* carrying wild type

SEM- Standard error mean

V- Time of vaccination

V+0, 2, 4- Weeks of vaccination

TAE- Tris acetate ethylenediaminetetraacetic acid buffer

AEC-3-Amino-9-ethylcarbazole substrate

FACS- Fluorescence-activated cell sorting

Abstract

Immune responses to vaccination are highly variable between different individuals and within any given population. Further, those most vulnerable to infectious often show suboptimal immune responses to vaccination, leaving them more susceptible to infection following vaccination. Thus, developing strategies that can enhance vaccine-specific immune responses would be an enormous benefit. Most licensed vaccines are delivered intramuscularly and only induce a systemic immune response, however, they do not prime an immune response at mucosal tissues. This is a major limitation of current vaccine technologies as mucosal-induced immunity generates a resident B and T cell response and the production of mucosal Immunoglobulin (Ig) A which, combined, provide protection at the entry site for many vaccine-targeted pathogens. A challenge in developing strategies that promote mucosal immunity is finding a delivery method for the antigen of interest that is immunogenic enough without driving potentially harmful inflammation. Recent evidence suggests that the commensal bacteria that occupy our mucosal surfaces are a major source of foreign antigen that can prime effector and helper T cell responses, are capable of priming microbiota-pathogen cross-reactive T and B cell responses within mucosal tissue. Importantly, the priming of these cross-reactive responses seemingly occurs in the absence of inflammation, suggesting that commensal bacteria may be the perfect vehicle for the delivery of antigen to mucosal tissues to safely prime an antigen-specific immune response. Thus, I conclude that this potential mechanism can be exploited by engineering a commensal / probiotic bacterium to express antigen of interest.

I hypothesized that treating specific opportunistic pathogen free (SOPF) mice with an engineered probiotic bacterium expressing a vaccine-derived antigen will prime vaccine specific immunity in mucosal tissues and enhance vaccine specific immune responses upon subsequent vaccination. To investigate this, I constructed a pUC57 plasmid to express Ovalbumin- (Ova) derived peptides in the bacterial cytoplasm and transformed this plasmid into the probiotic *Escherichia coli* Nissle 1917 (EcN) strain (EcN-Ova ^{Cyto}). Two weeks prior to intramuscular vaccination with an mRNA-Ova vaccine I demonstrated that there was a significant increase in vaccine-specific IgG_{total} and IgM in the serum, and vaccine-specific IgA in the faces. Additionally, EcN-Ova treated mice had significant increase in splenic germinal Centre B cells, and antibody secreting cells. These finding confirmed that probiotic bacteria (EcN) engineered to express vaccine-derived peptides can enhance subsequent immune response to vaccination. To confirm these observations in a more relevant model of vaccination, I expressed a component of the polysaccharide conjugate vaccine-13 valent

(PCV13) cross-reactive material 197 (CRM) in the *Escherichia coli* strain BL21 and administer it to mice prior to vaccination with PCV13. Despite successful expression of CRM as a full-length protein on the surface of BL21 we saw no major differences in the outcome of PCV13 vaccination in mice. Together my data demonstrates that probiotics engineered to express vaccine-derived antigens can alter subsequent immune responses to vaccines containing the same antigen. However, careful consideration of the bacterial strain used, and the nature of the antigen expressed in the bacteria, may be required to exploit this mechanism to its full potential.

Declaration

I certify that this thesis does not incorporate without acknowledgement any material previously submitted for degree or diploma in any university; and the research within will not be submitted for any other future degree or diploma without the permission of flinders university; and to the best of knowledge and belief, does not contain materials previously published or written by another person where due reference is made in the text.

Isobel Ozra Khoshbooie

31 October 2024

Statement of Contribution

This thesis presents research conducted in fulfillment of the requirements for a Masters in Biotechnology. The majority of the experimental work, data analysis, and manuscript preparation were carried out by the author. However, specific contributions were made by colleagues, as detailed below:

- **Chapter 3:** The engineering of bacteria to express vaccine-derived antigens was completed by the author, with assistance by Dr. Yi Lu. Treatment of mice with engineered bacteria was performed by the author with assistance by Dr. Todd Norton, while vaccination of mice was performed by the author. Collection of mouse faecal samples was performed by the author while collection of blood was performed by Dr. Todd Norton. Cell staining for flow cytometry was completed by the author while acquisition of the data on a Flow Cytometer was performed by Dr. Todd Norton. Analysis of B cell populations by flow cytometry was performed by the author, with assistance from Dr. Todd Norton. All ELISAs were performed by the author, while ELISpots were performed by Dr. Todd Norton.

Overall, the data presented in this thesis reflects the author's primary responsibility for data analysis, with noted assistance in specific experimental techniques and data acquisition.

Acknowledgement

O boy, what an emotional roller-coaster this year was.

I would like to express my deepest gratitude to my supervisor Professor David Lynn, for giving me the opportunity to be part of the systems immunology lab. Your level of knowledge is truly aspiring and your guidance and expertise was essential in making this thesis possible. I am truly privilege for his encouragements to participate in lab meetings, journal clubs and lab presentations.

I am deeply thankful to my co-supervisor Dr. Todd Norton for taking me under his wing, giving me constant feedbacks and encouragements that made this thesis more enriching. His selfless support and passion for research specifically in regards to T cells is truly colorful to witness.

I would also like to give a special thanks to Dr. Miriam Lynn for investing her time in training me in all the laboratory skills and mice works during the first months. Thank you from the bottom of my heart.

I would also like to extend my special appreciation to the Dr. Natalie Stevens, Dr. Stephen Blake, Georgina Eden, PHD students; Yee Chern Tee, Joyce Mugabushaka, Charne Rossouw, Luka Ilic, and finally Dr. Yi Lu for your kindness and friendship. I am very thankful to you guys for being so welcoming.

And lastly, I would like to thank my family for being my constant emotional support and to my sister who picked up the phone every single time I called to listen to me talk non-stop, and for believing in me, which made this journey even more bearable. I am truly blessed to have you guys.

Chapter 1. Introduction

Vaccination remains one of the most effective public health interventions for preventing morbidity and mortality from infectious diseases. At the height of the SARS-CoV-2 pandemic alone vaccines were estimated to have saved over 20 million of lives (Watson et al., 2022). While vaccination programs have been enormously successful in reducing global morbidity and mortality, some individuals mount poor immune responses to vaccination that leave them susceptible to infection even after vaccination (Lynn et al., 2022). Even individuals with robust responses to certain vaccines see a waning of antibody responses in the months following vaccination that requires annual boosters to retain full protection (Levin et al., 2021). For example, elderly individuals are less likely to respond to influenza vaccination, with vaccine effectiveness estimated to be as low as 30-50%, requiring an increase in vaccine dose to provide the necessary protection (DiazGranados et al., 2014 , Ciabattini et al., 2018). These studies highlight the importance of developing interventions that can enhance the immunogenicity and durability of vaccine-specific immune responses which will have enormous public health and economic benefits.

Most vaccines licensed today are administered intramuscularly (i.m) and while they are effective in generating systemic IgG and IgM immune responses, they do not stimulate immune responses at mucosal surfaces (Winklmeier et al., 2024). However, priming vaccine specific immune responses at this location would generate localized tissue-resident memory B and T cells that are better poised to rapidly respond to infection than memory B and T cells generated from conventional intramuscular vaccinations (Lavelle, et al.,2022, Moradi-Kalbolandi et al., 2021). Despite the benefits of mucosal vaccination there are very few vaccines that promote these responses. Several challenges have limited their development, such as their stability and delivery in the harsh mucosal environment which can limit the ability of antigen to reach immune cells, and the requirement for them to be immunogenic enough to prime an immune response, without driving potentially harmful inflammation (Lavelle & Ward, 2022). Recent studies have revealed that the mucosal microbiota is a major factor that influences the behavior of immune cells both within mucosal tissues, and systemically (Lynn et al., 2022). Although the mechanisms through which the microbiota influence the immune system are many, and not fully understood, one potential way that the microbiota alters immune cell activity is through the ability to encode pathogen/vaccine-like epitopes that prime an immune response that cross-reacts with similar, if not exactly the same, epitopes present in vaccines or pathogens (Welsh & Fujinami, 2007 , Murray et al., 2023). These microbes encoding cross-reactive epitopes may

act as a “first dose” of antigen and prime memory T and B cells that are able to respond to subsequent cross-reactive vaccine or pathogen-derived antigens in a greater magnitude, thereby enhancing that immune response. Recently there has been significant interest in using commensal/probiotics as living biotherapeutics to express and deliver therapeutics which are used to prevent, treat, or cure diseases in humans, with many of these therapeutics making their way into phase I/II clinical trials (Cubillos-Ruiz et al., 2021). There is also a growing interest in using commensal/probiotic bacteria as immunogenic vehicles for the delivery of antigen to mucosal tissue to prime protective immune responses (Chen et al., 2023 , Bousbaine et al., 2024 , Wang et al., 2019 , Laver et al., 2021). However, whether this approach can be used to prime a mucosal immune response that both is enhanced by, and itself enhances, conventional intramuscular vaccination remains unexplored. Thus, the combination of mucosal vaccine priming by commensal/probiotics with conventional vaccination may boost the effectiveness of vaccination by enhancing systemic immunity and enhance the quality by promoting a mucosal immune response.

1.1. Mechanism by which immune system responds to vaccination

The primary correlate of protection for vaccination is the generation of high-affinity vaccine-specific antibodies by B cells (Shishido et al., 2012). Following vaccination, recognition of antigen by B cell receptors (BCR) on the surface of B cells allows differentiation of B cells into class-switched germinal center B cells (GCBs) (Roco et al., 2019). In the weeks following vaccination GCBs undergo rounds of proliferation and hypermutation to increase the affinity of their BCR for the vaccine antigen. The outcome of the germinal center reaction is long-lived plasma cells that continuously secrete vaccine-specific antibodies, and memory B cells that are poised for rapid differentiation into high-affinity antibody secreting cells, and secondary GCB cells, upon encounter of the target pathogen (Nutt et al., 2015). In the case of infection with the vaccine-targeted pathogen the antibodies produced are capable of neutralizing pathogens, by binding to key invasion receptors, or inhibiting the function of virulence factors, preventing them from establishing a foothold in the host. These antibodies also have secondary roles such as enhancing phagocytosis and complement activation (Lu et al., 2018). Conventional i.m. vaccination induces high titers of IgG antibodies in serum and while these antibodies are effective at neutralizing pathogens they often have poor penetration into mucosal tissues at homeostasis (Mao et al., 2022). As IgG antibody titers naturally wane in the months following

vaccination so does their ability to penetrate mucosal tissue and neutralize invading pathogens, which can lead to an increased susceptibility to breakthrough infections (Lipsitch et al., 2022). In contrast to systemically induced IgG, the antibody isotype IgA is specifically generated when B cells are primed in lymphoid tissue that drains mucosal tissues (Bemark & Angeletti, 2021 , Mao et al., 2022). The IgA isotype is primarily produced by antibody-secreting B cells that are resident within the mucosal tissue (i.e. the respiratory, gastrointestinal, and urogenital tracts) and is transported across the epithelium to accumulate in the mucosa. Unlike the IgG isotype, the IgA isotype is also more resistant to degradation. Combined, all these features of IgA make it a superior isotype in providing protection from invading pathogens within mucosal tissues (Woof & Russell, 2011). However, intramuscular vaccination only induces poor IgA responses, and even then IgA is largely restricted to the circulation, and poorly represented at mucosal surfaces (Lavelle & Ward, 2022).

Although less appreciated than B cell responses, vaccination also drives a T cell mediated immune response. These vaccine-induced T cells can directly kill pathogen-infected cells and provide critical assistance in the production of high-affinity, class-switched, antibodies described above (Shishido et al., 2012). Additionally, helper T cells ($CD4^+$ T cells) once activated will also differentiate into different subsets of T helper cells such as T helper 1(Th1), T helper 2 (Th2), T helper 17 (Th17), T regulatory cells (Treg), and T follicular helper (Tfh) cells (Pulendran & Ahmed, 2011). While these helper subsets are all crucial in vaccine-mediated protection in their own ways, the subset considered most vital to the outcome of humoral-mediated immunity are T follicular helper (Tfh) cells. These cells are responsible for initiating and maintaining the germinal center reaction in lymphoid tissues that would allow B cells to differentiate into different subsets, and ultimately produce high-affinity vaccine-specific antibodies (Pulendran & Ahmed, 2011 , Nutt et al., 2015).

1.2. Intestinal microbiota is an important factor in influencing immune responses to vaccination

The gut microbiota consists of a collection of microorganisms including bacteria, fungi, yeast, viruses, phage and archea. There is a balanced relationship between the host and its microbiota which has a large impact in the development and function of the immune system (Jandhyala et al., 2015). From early life, the microbiota has a major role in shaping the developing immune

system and, if disrupted, can have life-long impacts on the function of the host immune system (Al Nabhani et al., 2019 , Lynn et al., 2021). Changes in the microbiota later in life are also able to influence the composition and function of the immune system, for example, a study conducted in mice colonized with Clostridium strains promoted the production of Treg cells and TGF-β that promoted resistance to colitis (Atarashi et al., 2011). Additionally, in a study conducted in mice with experimental colitis induced by *Helicobacter hepaticus*, colonization with *Bacteroides fragilis* leads to production of polysaccharide A that protected these mice from inflammatory diseases due to the activity of interleukin 10 (IL-10) producing $CD4^+$ T cells (Mazmanian et al., 2008). Given that the gut microbiota plays a role in regulating immune development, it is likely that alterations in its composition can impact vaccine immunogenicity as well.

Although many factors such as host intrinsic, environmental, behaviour and nutritional could potentially contribute to differences to vaccine immunogenicity several lines of evidence suggest that composition of the intestinal microbiota may play a key role (Ponziani et al., 2023). For example, it was demonstrated that the composition of the intestinal microbiota was significantly different in infants in rural Ghana that responded to oral rotavirus vaccination relative to infants that did not respond to rotavirus vaccination (Harris et al., 2017). It was further shown that the composition of the intestinal microbiota in Ghanian rotavirus responders was more similar to that of Dutch infants than it was to Ghanian non-responders, with an increased abundance of *Streptococcus bovis* and a decreased abundance of Bacteroidetes (Harris et al., 2017). Similar observations were made in infants receiving rotavirus vaccination in Pakistan, relative to Dutch infants. It was found that Dutch and Pakistani infants responding to rotavirus vaccination had higher relative abundance of *Clostridium* cluster XI and Proteobacteria, relative to non-responders (Harris et al., 2018). These results demonstrate that the composition of microbiota correlates with an optimal immune response to vaccination.

While many observational studies suggest a link between the composition of the intestinal microbiota and immune responses to vaccination, they do not demonstrate a causal relationship. To formally demonstrate the relationship between the microbiota and immune response to vaccination our laboratory had investigated immune responses to early life vaccination in a model of antibiotics-induced dysbiosis. Neonatal mice were exposed to ampicillin and neomycin antibiotics to induce early life dysbiosis, characterized by the loss of

Bacteroidetes species, prior to vaccination. Antibiotics exposure significantly impaired antibody responses to a range vaccine that are routinely administered to infants in the first year of life, relative to antibiotics untreated controls (Lynn et al., 2018). This demonstrated a direct link between the composition of gut microbiota during early life and the outcome of vaccination (Rossouw et al., 2024).

Similar observations have been made in human studies where individuals have had their microbiomes disrupted prior to vaccination. Healthy individuals were subjected to a 5-day broad-spectrum antibiotic regimen consisting of an oral neomycin, vancomycin, and metronidazole, to deplete the microbiota prior to vaccination with a trivalent influenza vaccine. Microneutralization (MN) titers were measured after vaccination and showed that individuals exposed to antibiotics had impaired antibody responses following influenza vaccination. However, the reduction in MN titers was only observed in participants that had low levels of pre-existing influenza-specific antibodies prior to vaccination, suggesting that the microbiota may have a greater impact on *de novo* vaccine specific immune responses (Hagan et al., 2019). We have since made similar observations in human infants exposed to antibiotics during the neonatal period which significantly impaired their immune response to certain vaccines that are administered at six weeks of life, particularly polysaccharide-conjugate vaccines (unpublished observation). These observations highlight that intestinal microbiota plays an important role in modulating immune responses to vaccination and offers an attractive target to enhancing vaccine specific immune responses in individuals.

1.3. Microbiota-specific immune response may cross react with vaccine and disease-associated antigens.

There are several hypotheses that seek to explain how the gut microbiota may influence vaccine immunogenicity. One of those hypotheses suggests that microbial derived antigen may prime memory B and T cells that cross-react with the same vaccine-derived antigens, also referred to heterologous immunity (Agrawal, 2019), altering the outcome of vaccination (Welsh & Fujinami, 2007). It has been demonstrated that healthy human adults have a high abundance of activated T cells that are specific for bacterial phyla dominant in the gut (Hegazy et al., 2017). Moreover, these cells predominately possess an effector phenotype suggesting that, far from being strictly tolerated, intestinal microbes are an abundant source of antigen driving

potentially inflammatory effector responses. It has also been demonstrated that individuals seronegative for certain pathogens, such as human immunodeficiency virus (HIV), still have detectable levels of memory phenotype HIV-specific T cells in their blood, despite never having been infected (Su et al., 2013). These HIV-specific T cells are also functional as stimulation with their cognate antigen results in cell division and cytokine secretion. The authors went on to show that certain commensal and environmental bacteria encode pathogen-like antigens that could have provided the activation signal for these HIV-specific T cells (Su et al., 2013). During the SARS-CoV-2 pandemic multiple studies reported the presence of COVID-reactive T cells in unexposed, unvaccinated individuals (Bacher et al., 2020 , Saggau et al., 2022). While the exact origin of these cells is not entirely clear, it has been suggested that these T cells may have been primed during prior exposure to a similar antigen found in common cold coronaviruses, or antigens present in commensal microbiota, generating cross reactivity toward SARS-CoV-2 antigen (Bartolo et al., 2022). Although several studies have demonstrated the presence of pathogen or vaccine cross-reactive T cells, relatively few studies have investigated the impact they may have on the outcome of immune responses to infections or vaccines that contain the same antigen. While one study in COVID-19 vaccination suggested pre-existing, cross-reactive, T cells negatively impacted the outcome of vaccination, (Saggau et al., 2022), another study in yellow fever vaccination suggested they increase the overall quality, but not magnitude, of the T cell response (Pan et al., 2021). Cross-reactive T cells in other settings, however, have been shown to correlate with positive outcomes. It has been demonstrated that *Enterococcus hirae* encodes a bacteriophage-derived antigen, tape measure protein 1 (TMP1), that generates $CD8^+$ T cells that cross-react with similar epitopes present in MCA205 fibrosarcoma tumors (Fluckiger et al., 2020). Mice that were pre-treated with the *E. hirae* showed better control of MAC-205 tumors after immunotherapy with cyclophosphamide or anti-PD1 antibodies. Another study showed that the oral commensal bacteria *Streptococcus salivarius* can induce IgG antibodies against a membrane protein that cross-react with SARS-CoV-2 Spike protein (Bondareva et al., 2023). In a mouse model of SARS-CoV-2 infection, pre-treatment with *S. salivaris* led to the induction of COVID cross-reactive antibodies that enhanced the clearance of the virus from the lung, relative to untreated controls. These studies demonstrate how immune responses toward the gut microbiota can induce cross-reactive immune responses that may have the potential to alter later immune responses to vaccination or infection.

1.4. Engineering commensal bacteria to prime antigen-specific immune responses.

Several lines of evidence suggest that commensal microbes may serendipitously encode pathogen- or vaccine-like antigens that prime an immune response that may alter subsequent antigen-specific immune responses when encountered in the form of a vaccine. Rather than rely on these cross-reactive epitopes to arise naturally, it may be possible to engineer commensal microbes to encode a component of a vaccine and use these engineered microbes to prime an immune response, which can enhance the size and quality of later vaccination. In recent years there has been a growing interest in the use of probiotics as living biotherapeutics that alter immune cell activity and treat human diseases (Cubillos-Ruiz et al., 2021).The majority of these biotherapeutics that have progressed to clinical trials focus on the use of bacteria for the targeted delivery of disease-modifying molecules or enzymes. Examples include engineered *E. coli* Nissle (EcN) for the treatment of phenylketonuria, a genetic disease that is characterised by an inability to metabolise phenylalanine (Phe) (Isabella et al., 2018). Treating humans with an EcN strain engineered to express enzymes that convert Phe to harmless secondary metabolites, that are then excreted in the urine, was able to alleviate disease symptoms. Another example is an engineered *Lactococcus lactis* that secretes the mucosal protectant human trefoil factor 1 (TFF1) to treat oral mucositis, a painful inflammatory condition that can develop in the oral mucosa following certain chemotherapies (Limaye et al., 2013). Additionally, in another study EcN was again engineered to promote anti-tumour activity through the secretion of a STING agonist that activates antigen-presenting cells, enhances production of type I IFNs, and the cross-presentation of tumour neoantigens that all combines to promote anti-tumour activity (Leventhal et al., 2020).

The selection of bacterial strains for the development of biotherapeutic platforms is heavily dependent on the safety profile of the strain. The examples provided above utilise food-derived *Lactobacillus* or the commensal turned probiotic *E coli* Nissle. However, for a bacterium to be effectively used as a vehicle for the delivery of antigens to prime an immune response it must also be immunogenic. While a traditional view of the commensal microbiota is that the bacteria that cover our external surfaces are strictly tolerated, (Blum et al., 2024) and, thus, would not be effective at priming an effector response, However, we now know that individual microbes within a complex community stimulate a spectrum of effector and regulatory immune responses (Nagashima et al., 2023). Some commensal bacteria, such as the skin-derived commensal *Staphylococcus epidermidis* (S. epi), have been shown to prime a robust effector T cell response, seemingly in the absence of inflammation (Naik et al., 2015). In this case, these

bacteria are acting as the perfect adjuvant for the antigen that they carry, naturally stimulating a strong immune response, without any noticeable impact on the host. This observation has recently been exploited to re-direct these immune responses toward antigens of interest (Chen et al., 2023 , Bousbaine et al., 2024). *S. epi* engineered to express the model antigen Ovalbumin were able to prime an Ova-specific immune response that could be redirected to provide anti-tumour activity against Ova-expressing B16 melanomas (Chen et al., 2023). This bacterium was also engineered to express tetanus toxoid (TT) on its surface, generating a TT-specific humoral immune response that protected mice from a lethal challenge with TT (Bousbaine et al., 2024). The approach of using commensal bacteria as a mucosal vaccine has also made it into human studies. A commensal *Neisseria lactamica*, isolated from the airways of healthy humans, has been engineered to express the meningococcal antigen Neisseria Adhesin A (NadA). Administration of this bacterium to humans by intranasal inoculation generated NadA-specific IgG- and IgA-secreting cells and the formation of NadA-specific memory B cells after colonization (Laver et al., 2021).

The above examples utilize human and murine commensal bacteria as immunogenic vectors, but food-associated and probiotic bacteria have also been utilized to prime antigen-specific responses. Genetically engineered strains of food-derived *Lactococcus* have been engineered to deliver recombinant, Outer membrane protein A (OmpA), or influenza-derived hemagglutinin to mucosal sites which elicit both mucosal and systemic immunity in the form of antigen-specific IgG, IgG1, IgG2 in the serum and faecal IgA (Yagnik et al., 2019). Similarly, the probiotic *E coli* Nissle has been used as a vehicle for the expression and delivery of ancestral SARS-CoV-2 spike protein to the gastrointestinal tract mice (Sarnelli et al., 2023). Treatment of mice with this bacterium generates a spike-specific humoral immune response, including systemic anti-spike IgG and mucosal IgA responses, that provides protection from COVID-19 induced lung damage in a murine model of infection (Sarnelli et al., 2024).

These studies highlight the potential for genetic manipulation of commensal/probiotic bacteria to act as immunogenic vectors that prime immune responses to pathogen antigens. However, whether combining these immunogenic bacteria with conventional intramuscular vaccination to enhance the quality of vaccination has not been explored. Boosting the mucosal immune response has been shown to provide superior protection against breakthrough infection with COVID variants (McMahan et al., 2024). Such a approach has been explored before in the form of “prime and pull” vaccination where, after i.m. vaccination, pure vaccine antigens or peptides are delivered to mucosal tissues to encourage the formation of resident memory

cells and mucosal IgA (Riglar & Silver, 2018; , Mao et al., 2022, Shin & Iwasaki, 2012). While effective, this requires large amounts of purified vaccine antigen, which is expensive and laborious to manufacture. In contrast, bacteria have the ability to interact with their host to modulate an immune response at mucosal surfaces (Riglar & Silver, 2018). Many of these bacteria have a proven safety profile and are relatively easy to modify, and are affordable to produce on large scale. They are mostly stable at room temperature, in which it reduces their need for cold-chain logistics.

Hypothesis and Aims

I hypothesized that colonizing specific opportunistic pathogen free mice with an engineered probiotic bacterium expressing a vaccine-derived antigen will induce a pre-existing immunity and enhance vaccine specific immune responses to vaccination. To assess this hypothesis, I aimed to:

1. Clone and express vaccine-derived antigens in probiotic bacteria.

2. Assess whether there is an enhanced cellular and humoral response in mice treated with the engineered strain following intramuscular immunisation with the same vaccine antigen.

Chapter 2. Materials and methods

2.1. Construction of plasmids

To generate pUC57-Ova ^{cyto}, the backbone of the pUC57 plasmid (Thermo Scientific Massachusetts, USA), including the ampicillin resistance cassette and the ColE1 origin of replication, was amplified by PCR reaction to introduce EcoRI and XbaI restriction sites at the 5' and 3' ends of sequence, respectively, using primers FFmer-EcoR-F and rrnB-Xba-R (**Table 1**). The cytoplasmic Ovalbumin expression sequence, including the FFmeIR promoter, RBS, Ova-peptides, and T7 terminator, flanked by EcoRI and XbaI restriction sites, was synthesized by Twist Bioscience (San Francisco, USA) into a pTwist medium copy cloning vector (pTwist-Ova). The pTwist-Ova and pUC57 plasmids were digested using the EcoRI and XbaI restriction enzymes, and purified DNA fragments were ligated to form pUC57-Ova ^{cyto} (**Figure 1**).

To generate Adhesin Involved in Diffuse Adherence-Cross-reacting material 197 (pAIDA-CRM 197), the pAIDA plasmid was purchased from AddGene (Massachusetts, USA, Plasmid # 79180) and used for the expression of fusion proteins (CRM) on the outer membrane of *E. coli*. The codon optimised gene for PCV13-derived CRM 197 was synthesised as a gene block by Twist Bioscience. For cloning into the pAIDA plasmid the CRM gene block was amplified using primers CRM 197-Kpn-F and CRM 197-Sac-R (**Table 1**) to introduce KpnI and SacI restriction sites. The pAIDA plasmid and PCR amplified CRM gene were digested with KpnI and SacI restriction enzymes and the purified DNA fragments ligated to form pAIDA-CRM (**Figure 14**) (Sarnelli et al., 2023 , Lynch et al., 2023 , Zhang et al., 2022). The individual methods used to assemble these plasmids are detailed below.

Table 1. Table of primers used to amplify the Ova ^{Cyto} and CRM genes.

Primer (Ova ^{Cyto})	Sequence (5’ -> 3’)
FFmer-EcoR-F	CTTGTCTGTAAGGAATTCCCGGGGAT
rrnB-Xba-R	GCAACGCAATTAATGTCTAGAGAGAGCG

Primer (CRM 197)	Sequence (5’ -> 3’)
CRM 197-Kpn-F	GCGCGGGGTACCGATGACGTCGTAGACAG
CRM 197-Sac-R	CCGCGCGAGCTCGCTTTTTATCTCGAAAAAC

2.2. Engineering of plasmids

2.2.1. Restriction digestion

Restriction digestion is a procedure that uses sequence-restricted endonucleases to cut DNA fragments at specific locations. DNA samples were mixed with the appropriate restriction digestion enzymes: EcoRI/XbaI or KpnI-HF^{R}/SacI-HF^{R} in rCutSmart buffer (New England Biolabs Massachusetts, USA) and ultrapure water (Fisher Biotec, Subiaco WA, AUS) in a 0.2 ml PCR tubes (Corning Life Sciences, Wujiang, China) by pipetting gently. The reaction was then incubated at room temperature for one hour. Reaction volumes are shown in (**Table 2)**.

Table 2. Restriction digestion reaction

Components	Volume/sample	company	Catalogue number
Ova ^{Cyto} DNA concentration 10 ng/ml	4.29 µl	Twist Bioscience	N/A
CRM 197 DNA concentration 10 ng/ml		Twist Bioscience	
pUC57 DNA concentration 0.5 µg/µL		Thermo Scientific	SD0171
pAIDA DNA concentration 76.22 ng/µl		AddGene	79180
Restriction enzyme Ova-EcoRI 20000 U/ml	1 µl	New England Biolabs	R0101S
CRM 197-KpnI-HF ^{R} 20000 U/ml		New England Biolabs	R3142S
Restriction Enzyme Ova-XbaI 20000 U/ml	1 µl	New England Biolabs	R0145L
CRM 197-SacI-HF ^{R} 20000 U/ml		New England Biolabs	R3156S
rCutSmart buffer 10x	5 µl	New England Biolabs	B6004S

Ultra-pure water (PCR grade) 100 ml	39 µl	Fisher Biotec, Australia	UPW-100
Final volume	To make 50µl		

2.2.2. Gel Electrophoresis

Gel electrophoresis is a procedure that separates the DNA fragments based on their size. This was performed here to visualize and confirm the size of the DNA fragments produced after restriction digestion, PCR amplification, or DNA clean up and concentration. Digested DNA samples (Ova ^{Cyto}/CRM 197) were mixed with the 6x purple loading gel dye (New England Biolabs Massachusetts, USA) and 2 µl of DNA or 1.5 µl DNA ladder (New England Biolabs Massachusetts, USA) loaded into 1.5% weight for volume (w/v) agarose gel supplemented with gel red nucleic acid dye (1:10000, Merck Millipore, USA) for subsequent visualisation of bands (**Table 3**). The gel was run at 140V and imaged using a TM XR imaging system (Bio-RAD Laboratories).

Table 3. Agarose gel electrophoresis

Components	Volume/sample	Company	Catalogue number
1kb DNA ladder 500 µl	1.5 µl	New England Biolabs	N3232S
Loading gel dye purple 6x	1 µl	New England Biolabs	B7024S
Gel red ^{R} nuclei acid stain 10000x	4 µl	Merck Millipore	SCT123
Agarose powder 100 gm	0.5 gm	Scientifix, France	9010B
Tris acetate EDTA (TAE) buffer 1x	40 ml		N/A

2.2.3. DNA gel extraction

DNA gel extraction enables the isolation of DNA strands of a specific size for downstream applications such as ligation. The isolation provides a pure product free of DNA fragments of unwanted size and contaminants from previous steps, such as restriction enzymes, all of which may reduce the efficiency of downstream methods. DNA was extracted from agarose gel using Monarch® nucleic acid purification/DNA gel extraction kit (New England Biolabs Massachusetts, USA, cat # T1020S) as per manufacturer's instructions as shown in (**Table 4**). In brief the DNA bands were visualized under blue UV transilluminator. Using a standard blade, the DNA bands were excised from the agarose gel. The gel slices were pre-weighed in 1.5 ml microfuge tube and appropriate amount of Monarch® gel dissolving buffer (New England Biolabs) were added. The gel slices were incubated between 37-55 °C inverting periodically until the gel was completely dissolved. Spin column tubes were used for elution of DNA from digested gel fragments as per manufacturer's instructions.

Table 4. Monarch ^{R} nucleic acid purification/DNA gel extraction reaction

components	Volume/sample	Company	Catalogue number
Agarose gel with DNA bands Ova ^{Cyto} CRM 197 pUC57-empty vector pAIDA-empty vector	0.335 g	Twist Bioscience Thermo Scientific AddGene	
Monarch ^{R} dissolving buffer 47ml	1000 µl	New England Biolabs	T1021L
Monarch ^{R} washing buffer 5ml	400 µl	New England Biolabs	T1014L
Monarch ^{R} elution buffer	10 µl	New England Biolabs	T1016L

2.2.4. DNA Ligation

DNA ligation involves the covalent linking of two compatible strands of DNA by the enzyme DNA ligase. The reaction was setup in a 1.5 ml microfuge tube that contains insert DNA, plasmid DNA, T4 DNA ligase buffer, T4 DNA ligase and ultra-pure water as presented in (**Table 5**). The reaction was placed on ice and gently mixed with a pipette up and down then the ligation reaction was incubated overnight at 16 °C.

Table 5. DNA ligation reaction

Components	Volume/sample	Company	Catalogue number
Insert DNA 1 kb Ova ^{Cyto} CRM 197	6 µl	Twist Bioscience	N/A
plasmid DNA 4 kb pUC57-empty vector pAIDA-empty vector	2 µl	 Thermo Scientific AddGene	N/A
T4 DNA Ligase 400000 U/ml	1 µl	New England Biolabs	M0202S
T4 DNA Ligase Buffer 10x	2 µl	New England Biolabs	M0202S
Ultra-pure water (PCR grade) 100 ml	9.6 µl	Fisher Biotec, Australia	UPW-100
Final volume	20 ml		

2.2.5. Transformation

Transformation is the process by which bacteria take up foreign DNA from their surroundings, plasmid DNA in this setting. 50 µl chemically competent cells; *E. coli* DH5α (Thermo Fisher Scientific, Massachusetts, USA), *E. coli* Nissle (Evidence Based Probiotics, Adelaide, AUS), *E. coli* BL21 (New England Biolabs, Massachusetts, USA) were used for transformation. 50-100 ng of plasmid was mixed with the competent cells and incubated on ice for 30 mins. The cells were then heat shocked for 45 sec at 42 °C. The cells were incubated on ice for 2-3 mins and 950 µl of Luria-Bertani Broth (LB) (Sigma-Aldrich, Missouri, USA) broth was added. The tube was then placed in a shaking incubator for 60 mins at 180 rpm at 37 °C to enable expression of antibiotic resistance genes. 100 µl of the transformed cells were plated onto an LB agar plate containing the appropriate antibiotics for selection of successful transformants and cultured overnight at 37 °C.

2.2.6. Colony PCR

After the transformation step this procedure is done to amplify a specific region of the introduced plasmid DNA directly from individual bacterial colonies to screen for the presence of plasmid with the correct insert. Individual transformant colonies were selected and placed into 0.2 ml PCR tubes with the PCR reaction mixture for amplification of transformed plasmid (**Table 6**). Tubes were heated in incubator at 37 °C for 5 mins. A PCR machine (Veriti 96 well thermocycler, Applied Biosystems, Waltham, USA) was then setup at the cycling conditions for the primers a shown in (**Table 1**) and insert size as follows: Denaturation: 95 °C for 1 mins and 30 sec, Annealing: 95 °C for 30 sec, second stage of annealing: 63 °C for 30 sec, Extension: 72 °C for 1 mins and 50 sec, Final extension: 72 °C for 10 mins.

Table 6. Colony PCR reaction

Components	Volume/sample	Company	Catalogue number
DreamTaq master PCR mix 2x	12.5 µl	Thermo Scientific	K1071
Forward Primer FFmer-EcoR-F CRM 197-Kpn-F	0.5 µl	Sigma-Aldrich Invitrogen, Thermo Fisher Scientific	N/A
Reverse Primer rrnB-Xba-R CRM 197-Sac-R	0.5 µl	Sigma-Aldrich Invitrogen, Thermo Fisher Scientific	N/A
Ultra-pure water (PCR grade) 100 ml	10.5 µl	Fisher Biotec	UPW-100
Final volume	25 µl		

2.2.7. Plasmid extraction

Following colony PCR, bacterial colonies confirmed to carry the desired plasmid are cultured and the transformed plasmid can be isolated for further manipulation, transformation into a different strain, or further confirmation through restriction digest and gel electrophoresis. Plasmid extraction was performed using ZymoPURE Plasmid Miniprep Kit (California, USA cat # D4210) as per manufacturer's instructions as presented in (**Table 7**). In brief, 250 µl of ZymoPURE P1 (red) were added to the bacterial cell pellet. Followed by 250 µl of ZymoPURE P2 (blue). 250 µl of ZymoPURE P3 (yellow) was then added next. The neutralized lysate was then centrifuged for 5 mins at 16,000 x g. 260 µl of ZymoPURE binding buffer were added to the lysate. 800 µl ZymoPURE wash 1 and 800 µl ZymoPURE wash 2 were added next, then centrifuged for 1 mins at 10,000 x g before adding the ZymoPURE elution buffer and incubated for 1 mins.

Table 7. ZymoPURE Plasmid Miniprep Kit reaction

Components	Volume/sample	Company	Catalogue number
ZymoPURE P1 (red)	250 µl	Zymo Research	D4200-1-13
ZymoPURE P2 (blue)	250 µl	Zymo Research	D4200-2-13
ZymoPURE P3 (yellow)	250 µl	Zymo Research	D4200-3-13
ZymoPURE binding buffer	260 µl	Zymo Research	D4200-4-14
ZymoPURE wash 1	800 µl	Zymo Research	D4200-5-20
ZymoPURE wash 2	800 µl	Zymo Research	D4200-6-23
ZymoPURE elution buffer	30 µl	Zymo Research	D4200-7-12

2.3. Mice

Specific pathogen free (SPF) C57BL/6J mice were bred and maintained in individually ventilated cages (Techniplast, Buguggiate, Italy) at the South Australian Health and Medical Research Institute (SAHMRI). Colony founders were sourced from the Jackson Laboratory. Mice were housed in positively pressurised, high-efficiency particulate air (HEPA) filtered isolators, with access to autoclaved commercially pelleted food and sterilised water *ad libitum* with regulated daylight, humidity, and temperature. All procedures were executed in accordance with protocols approved by the SAHMRI Animal Ethics Committee.

2.3.1. Bacterial cultures and oral gavages

Overnight cultures of Ova-expressing *Escherichia coli Nissle* (EcN-Ova ^{Cyto}) or EcN carrying an empty pUC57 plasmid (EcN-EV) were cultured in LB containing 25 µg/mL ampicillin under anaerobic conditions to enable expression of the Ova ^{Cyto} construct under the control of the anaerobically active FFmeIR promoter. Cultures were grown to an OD of ~0.6-1, washed twice in phosphate buffered saline (PBS; Sigma-Aldrich, St. Louis, USA), and serial dilutions of bacteria were plated on LB agar plates supplemented with ampicillin to determine colony forming units (CFU) per mL of culture. Enumerated bacterial cultures were resuspended in PBS supplemented with 30% v/v glycerol, to prevent ice formation that can damage bacterial cell during freezing allowing the bacteria to be preserved for extended period without loss of viability to a concentration of 10^{10} CFU/mL and stored at -80 °C Overnight cultures of CRM-expressing BL21 (BL21-CRM) or BL21 carrying an empty pAIDA vector (BL21-EV) were grown in LB containing 25 µg/mL erythromycin. To induce high expression of the CRM construct from the LacUV5 promoter 200 mM Isopropyl ß-D-1-thiogalactopyranoside (IPTG, Sigma-Aldrich, Missouri, USA, I1284-5ML) was added when cultures reached an OD of ~0.2. Cultures were grown to an OD of ~0.6-1 and cryopreserved as described for EcN strains. Monocultures of EcN or BL21 strains were administered to mice by daily oral gavage of 100 µl of a 10^{10} CFU/mL solution for two weeks.

2.3.2. Confirmation of colonization of bacterial species by culture

Faecal samples were sterilely collected from mice two weeks post-vaccination and homogenized in 1x PBS. A 1:10 serial dilution was performed and 10 µl of faecal diluents were inoculated on LB agar plates supplemented with (ampicillin/erythromycin) and incubated overnight at 37 °C to allow for colonies to grow. The bacterial colonies from *Escherichia coli* Nissle and *E. coli* BL 21 were visually enumerated on the agar plate.

2.3.3. Immunization

Mice were anesthetized with isoflurane then vaccinated intramuscularly (i.m) with 0.15 µg mRNA-Ova (Synthesised at the University of Queensland and encapsulated in lipid nanoparticles at the University of Adelaide, AUS) or 1.5 µg 13-valent pneumococcal vaccine (PCV13- Link healthcare, AUS) / leg. Vaccine responses were boosted 2 weeks after initial vaccination using the same dosage and route of administration.

2.3.4. Serum sampling and faecal sampling

Mice were cheek bled into serum separator tubes. The collected blood was centrifuged at room temperature for 5 mins at 5000 x *g* to collect the serum. Serum was stored at -80 ^{o}C until processing. Faecal samples were collected, weighed and resuspended to 100 mg/mL with 1x PBS and stored at -80 ^{o}C until processing.

2.3.5. Assessment of vaccine-specific antibody responses by Enzyme-Linked Immunosorbent Assay (ELISA)

This procedure is used to detect the vaccine-specific antibody titres in serum based on the principle of antigen-antibody interaction. ELISA Nunc-Immuno™ MicroWell™ 96 well solid plates (Sigma-Aldrich, Cat # 442404) were coated with 1 µg/mL Ovalbumin (Ova) or PCV13 diluted in ELISA coating buffer and incubated overnight at 4 °C. After coating with target

antigen the plates were washed three times with PBS-Tween (PBS-T) (containing 1x PBS supplemented with 0.05% (v/v) Tween-20, Sigma-Aldrich, Missouri, USA, D1408-500ML) using an immune wash^{TM} microplate washer (BIO RAD, California, USA). The plates were then blocked with 1x ELISA/ELISpot buffer (Invitrogen, Thermo Fisher Scientific, Massachusetts, USA, Cat # DS98200) overnight at 4 °C. After blocking, the plates were washed three times in PBS-T and serum and faecal homogenate samples were diluted in 1x ELISA/ELISpot buffer to incubate overnight at 4 °C. The plates were washed three more times with PBS-T and Ova or PCV13 specific antibodies were detected using horse radish peroxidase (HRP) conjugated anti-mouse IgG_{total}, IgM or IgA antibodies (**Table 8)**. After another five washes the plates were developed with 1-Step™ Ultra tetramethylbenzidine (TMB) substrate (Thermo Fisher Scientific, Waltham, USA, Cat # 34028) at room temperature. The reaction was stopped with 1M (2N) sulfuric acid (Sigma-Aldrich, Missouri, USA). The developed plates were read with a Synergy HTX Multi-mode plate reader (Bio Tek, Vermont, USA) at 450 nm with correction by subtraction of 595 nm absorbance value.

Table 8. HRP-conjugated detection antibody concentrations

Antibody	Dilutions	Company	Catalogue number
Anti-IgG_{total} 1 mg/ml	1:1000	Invitrogen	A16066
Anti-IgM 1 mg/ml	1:1000	Abcam	ab5930
Anti-IgA 1 mg/ml	1:1000	Abcam	ab97235

2.3.6. Enzyme-Linked Immunosorbent Spot Assay (ELISpot)

To measure vaccine-specific antibody producing B cells, the ELISPOT tray was first coated with 10 µg/mL of Ova or PCV13 vaccine (1:50) diluted in PBS, and incubated at 4 °C overnight. Wells were then blocked with 50 µl of 1x ELISA/ELISpot blocking buffer per well for 60 mins. Wells were washed five times with sterile PBS before addition of $5x10^5$

splenocytes or bone marrow cells in Roswell Park Memorial Institute (RPMI) complete culture media (cRPMI) consisting of 1 x RPMI 1640 (RPMI- Sigma-Aldrich, Missouri, USA, Cat # R8758) supplemented with GIBCO minimal essential media amino acids (Gibco, Cat # 11140050), GlutaMAX L-glutamine (Thermo Fisher Scientific, USA), 10% foetal calf serum (FCS, Assay Matrix, AUS) and 55nM 2-Mercaptoethanol (Life Technologies, California, USA). Cells were incubated for 16-24 h at 37 °C, 5% $C0_2$. After incubation ELISpot trays were washed 5x with PBS 0.05% Tween (Tween-20 sigma-Aldrich, D1408-500ML) and 50 µl of 1:1000 horseradish peroxidase (HRP) conjugated anti-mouse IgG (AbCam, Cambridge, UK) or IgM (AbCam, Cambridge, UK) diluted in 1 x ELISA/ELISpot blocking buffer and incubated for 1 h at room temperature. Trays were then washed 5x times with PBS 0.05% Tween. To develop the plates, 50 µl of 3-Amino-9-ethylcarbazole (AEC) substrate (BD Biosciences, New Jersey, USA) was added until spots were clearly visible. Membranes were washed in H2O and dried and spots were counted via an ImmunoSpot ELISPOT Readers and Analyzer (ImmunoSpot, Cleavland, USA).

2.3.7. Single-cell suspension of spleen, iliac and inguinal lymph nodes and bone marrow

Spleen, iliac and inguinal lymph nodes were harvested and placed in a tissue culture plate containing RPMI wash media. The tissues were then dissociated through a 70 µm nylon mesh filter (Merck Millipore, USA) and transferred to 10 ml tubes. Cells were washed and splenocytes were treated with 1 ml of 1x Red Blood Cell (RBC) lysis buffer (Thermo Fisher Scientific, Massachusetts, USA). Cells were then washed two times, resuspended in PBS, and counted on a haemocytometer. For the generation of single cell suspensions from the bone marrow, femurs were removed from mice and flushed twice with 3 ml of PBS using a 3 ml syringe fitted with a 19-gauge needle. After washing, cells were lysed in 1 ml of 1x Red Blood Cell lysis buffer, washed in PBS and resuspended for counting. All counted cells were washed and resuspended again in cRPMI at a concentration of $2x10^7$ cells/mL for further processing for flow cytometry.

2.3.8. Flow Cytometry-Surface staining

Single-cell suspensions were plated into round-bottom 96-well plates at a concentration of 1.5-2x10^6 cells/well. Plates were washed with 1x PBS and resuspended in a solution containing Fixable Viability Stain 780 (1:2000, BD Biosciences, New Jersey, USA, Cat # 565388) and mouse FC block (1:500, BD Biosciences, New Jersey, USA, Cat # 553141) for 10-15 minutes at room temperature. Cells were washed in 1x FACS buffer (PBS, 1% BSA, 2mM EDTA) and stained with 50 µL of a fluorochrome-conjugated surface antibody master mix (**Table 9**) diluted in 1x FACS buffer for 20 mins at 4 °C. Cells were then washed and fixed with 4% formaldehyde (Thermo Fisher Scientific, Cat # J60401.AK) diluted in PBS and stored at 4 °C. Prior to acquisition of a BD FACS Symphony, 5 µL of BD™ Liquid Counting Beads (BD Biosciences, New Jersey, USA, Cat # 335925,) were added to enumerate the analysed cells. Data were analysed using FlowJo v10 (TreeStar).

Table 9. Surface staining antibody master mix panel for flow cytometry

Antibody	Fluorophore	Dilution	Clone	Company
CD19	PerCP-Cy5.5	1:300	1D3	BD Biosciences
CD138	PE	1:300	281-2	BD Biosciences
CD 267 (TACI)	BV421	1:300	8F10	BD Biosciences
IgM	BUV395	1:300	G20-127	BD Biosciences
CD 95 (Fas)	BV750	1:300	Jo2	BD Biosciences
GL7	AF647	1:600	GL7	BD Biosciences
B 220	FITC	1:300	RA3-6B2	BD Biosciences
CD 38	PE Cy7	1:600	HIT2	BD Biosciences

CD 45	BUV496	1:200	HI30	BD Biosciences
CD 3	PE-CF 594	1:600	17A2	Biolegend
CD 16/CD32 (FC Block)		1:200	2.4G2	BD Biosciences
IgD	BV510	1:300	11-26c.2a	Biolegend

2.3.9. Bacterial flow cytometry

Bacterial cultures, generated as described in **section 2.1**, were transferred into 1.5 ml microcentrifuge tubes. The tube was centrifuge at 500 x *g* for 5 mins at 4 °C and bacterial pellets were resuspended in PBS, supplemented with SYTO™ BC Green Fluorescent Nucleic Acid Stain (1:1000, Thermo Fisher Scientific, USA, Cat # S34855), mouse anti-histidine tag (1:900), anti Myc tag and anti CRM serum (1 uL/well) for 15 mins at 4 °C. After washing for 10 mins at 4 ℃, the pellet was resuspended in 100 µL of PBS containing AF647-conjugated anti-mouse IgG for 20 mins at 4 ℃. The suspension was then washed three times and resuspended in PBS for analysis using a BD Fortessa™ flow cytometer.

Statistical Analyses

The data gathered was analysed with GraphPad PRISM 10 (GraphPad Software Inc., La Jolla, USA). Statistical significance was assessed by student unpaired t-test to compare the level of statistical difference between two groups or One-way and two-way ANOVA followed by Šídák's multiple comparisons test to determine the significant differences between serum IgG_{total}, IgM and faecal IgA responses over time. Data are presented as the mean ± standard error of the mean (SEM). * $p \leq 0.05$, ** $p \leq 0.01$, *** $p \leq 0.001$, and **** $p \leq 0.0001$. ns = not significant.

Chapter 3. Results

3. Construction of plasmids pUC57 and engineering bacteria *Escherichia coli* Nissle 1917 (EcN)

3.1. Design of an Ovalbumin-peptide expressing pUC57 plasmid

To investigate the potential of engineered probiotic bacteria to enhance immune responses to vaccination I first addressed this hypothesis by expressing the model antigen ovalbumin (Ova) in our probiotic bacteria. Ova is a model antigen derived from egg whites that has well mapped T cell responses in C57B/6J mice (Bennek et al., 2019). Taking advantage of this prior knowledge I chose to express the Ova-derived immunodominant $CD4^+$ ($Ova_{323-339}$) and $CD8^+$ ($Ova_{257-264}$) peptides from our expression vector. Expressing only the immunodominant Ova-derived peptides reduces the translation burden on the bacteria and avoids potential problems with folding of full-length proteins, both of which can compromise bacteria viability. As the goal from the engineering of this expression vector was transformation into the probiotic *E. coli* Nissle (EcN) strain I used the pUC57 plasmid to construct the Ova-expression vector pUC57-Ova ^{cyto} (hereafter called Ova ^{Cyto}). This commonly used cloning vector contains the EcN compatible ColE1 origin of replication for replication of the plasmid in the EcN bacterium, as well as an ampicillin resistance gene for selection of EcN that have taken up the plasmid. For the expression vector we had a custom gene synthesised that included the FFmelR Promoter upstream of a Ribosome Binding Site (RBS) and the codon optimised sequences coding for a fusion of the $Ova_{323-339}$ and $Ova_{257-264}$ peptides, followed by a T7 terminator sequence that halts transcription (**Figure 1**). The FFmeIR promoter used in the construct is conditionally active in low-oxygen settings. The benefit in this setting is that the promoter should be active in the anoxic environment of the colon.

3.2. Construction of a pUC57 plasmid that expresses OVA peptides in the cytoplasm of *Escherichia coli* Nissle.

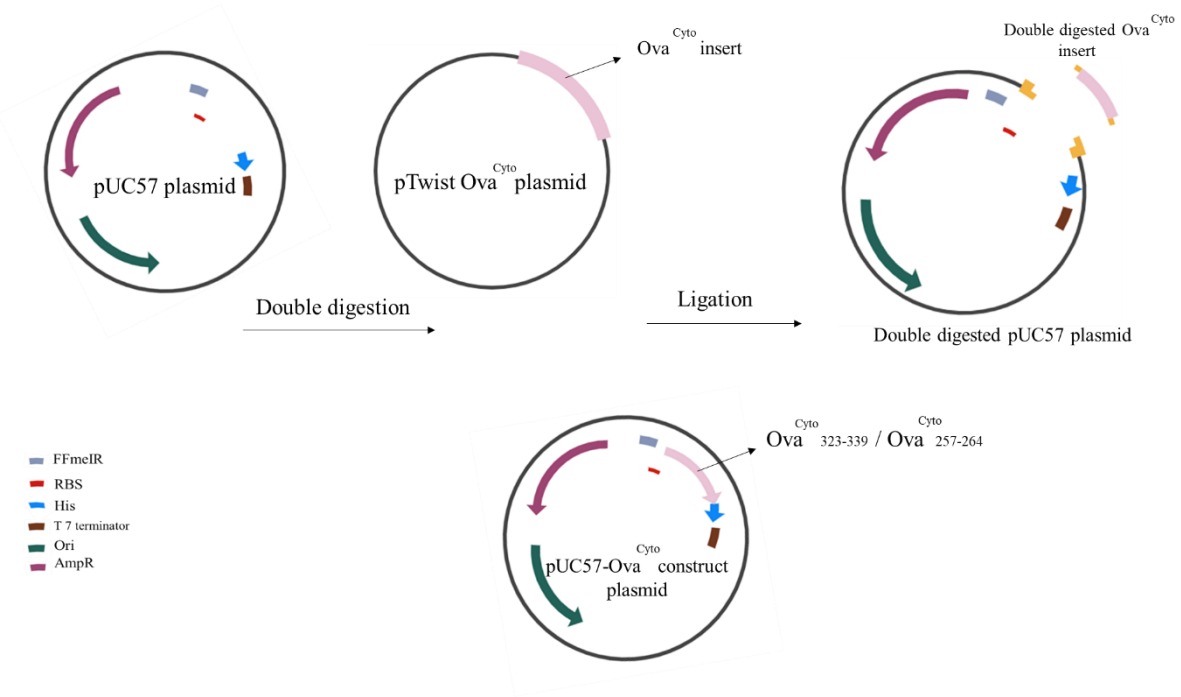

Figure 1. Overview of experimental design of pUC57-Ova ^{Cyto} construct for cytoplasmic expression of Ova epitope in EcN. (**A**) The 2677bp pUC57 plasmid used for the Cytoplasmic expression of protein flanked by His tag. (**B**) Ova ^{Cyto} sequence with a size of 478bp, PCR amplified to introduce the EcoRI and XbaI restriction enzyme sites. (**C**) EcoRI and XbaI digested pUC57 empty vector with a size of 2677bp and Ova ^{Cyto} insert with a size of 478bp. (D) Ligated pUC57-Ova ^{Cyto} construct with a size of 478bp.

To generate the pUC57-Ova ^{Cyto} plasmid with the size of 3155bp, the pUC57 backbone with the size of 2677bp was digested with the restriction enzymes EcoRI and XbaI to remove the LacZ operon from the plasmid. The Ova ^{cyto} expression cassette with a size of 478bp was similarly liberated from the pTwist cloning vector (**Figure 1**) (Hassan et al., 2016). Gel electrophoresis confirmed the expected DNA fragment sizes following double digestion of the pUC57-Ova ^{cyto} plasmid using the EcoRI and XbaI restriction enzymes (**Figure 2**). These DNA fragments were enriched from the agarose gel for subsequent ligation of the pUC57 backbone and the Ova ^{cyto} insert and ligation product was transformed into *E. coli* DH5α, a common strain used in cloning due to its high transformation efficiency and efficiency at plasmid amplification

for downstream manipulation (Hassan et al., 2016). Transformed DH5α were plated on LB agar plates containing ampicillin to select for bacteria containing the Ova ^{cyto} plasmid and colony polymerase chain reaction (PCR) performed to amplify the Ova ^{cyto} insert in select individual colonies to verify the correct insertion of the ligation product into the bacterial colonies. Gel electrophoresis of the colony PCR product confirmed the presence of the Ova ^{cyto} plasmid with DNA bands sizes corresponding to the Ova-insert PCR product of 478bp in *E. coli* DH5α (**Figure 3**). This observation was further confirmed by Ova ^{cyto} plasmid extraction followed by double digestion by the restriction enzymes EcoRI and XbaI and gel electrophoresis which confirmed the correct 2677bp band size of the pUC57 plasmid backbone and of the 478bp Ova ^{Cyto} insert, verifying that the two enzymes had successfully cut the plasmid and the Ova ^{Cyto} insert at the predicted sites and had been successfully ligated into the pUC57 plasmid backbone (**Figure 4**). After confirming the correct plasmid assembly in *E. coli* DH5α the recombinant plasmid was transformed into *E. coli* Nissle 1917 (EcN), an ideal probiotic strain that we have previously used as an immunogenic probiotic vector for the delivery of antigens to mucosal tissues (unpublished observations). After growth of EcN transformants on LB agar plates containing ampicillin, colony PCR was used to confirm bacterial colonies with bands corresponding to the correct size of the plasmid-inert PCR product of 478bp confirming successful transformation of Ova ^{Cyto} construct into *E. coli* Nissle (**Figure 5**).

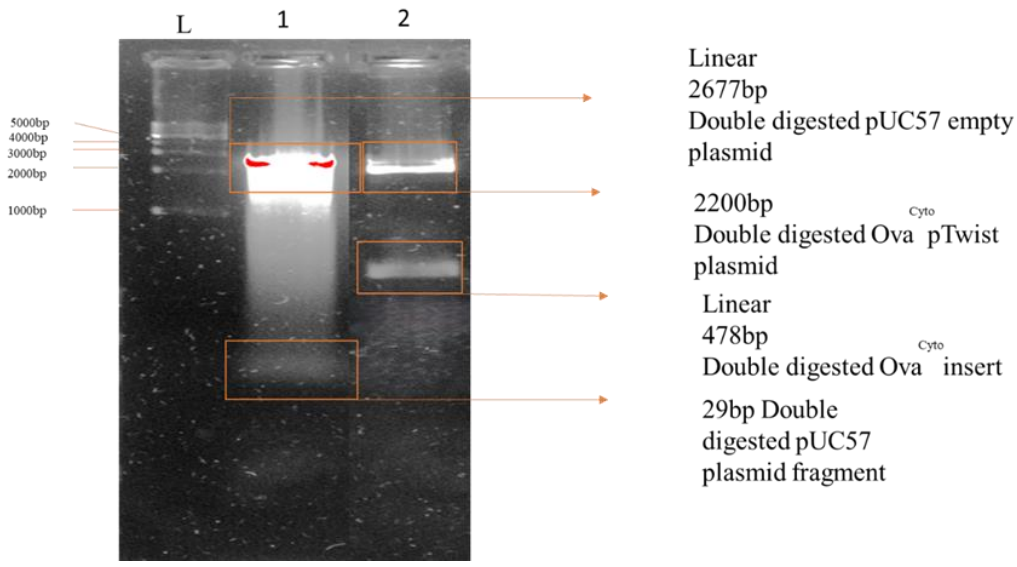

Figure 2. Gel electrophoresis of pUC57 plasmid DNA and ovalbumin ^{Cyto} insert following restriction enzyme double digestion. Agarose gel electrophoresis image showing the digestion of pUC57 plasmid and the expression construct for cytoplasmic ovalbumin (Ova ^{Cyto}) from the pTwist EF1 alpha plasmid using two restriction enzymes, EcoRI and XbaI. **L**: 1kb DNA ladder. **Lane 1**: Double digestion of plasmid DNA pUC57. **Lane 2**: Double digestion of pTwist OVA ^{Cyto} plasmid.

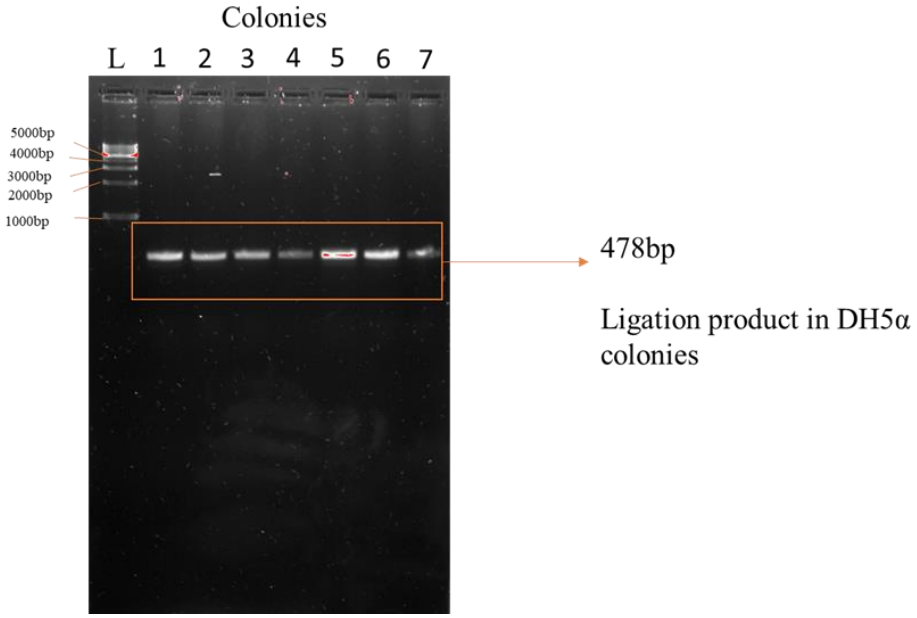

Figure 3. Confirmation of ligation product using colony PCR after transformation in *Escherichia coli (E. Coli)* DH5α. Agarose gel electrophoresis image of ligation product following colony PCR of DNA extracted from DH5α colonies transformed with pUC57-Ova ^{Cyto} . **L**: 1kb DNA ladder. **Lane 1-7**: pUC57-Ova ^{Cyto} transformants in *E. coli* DH5α.

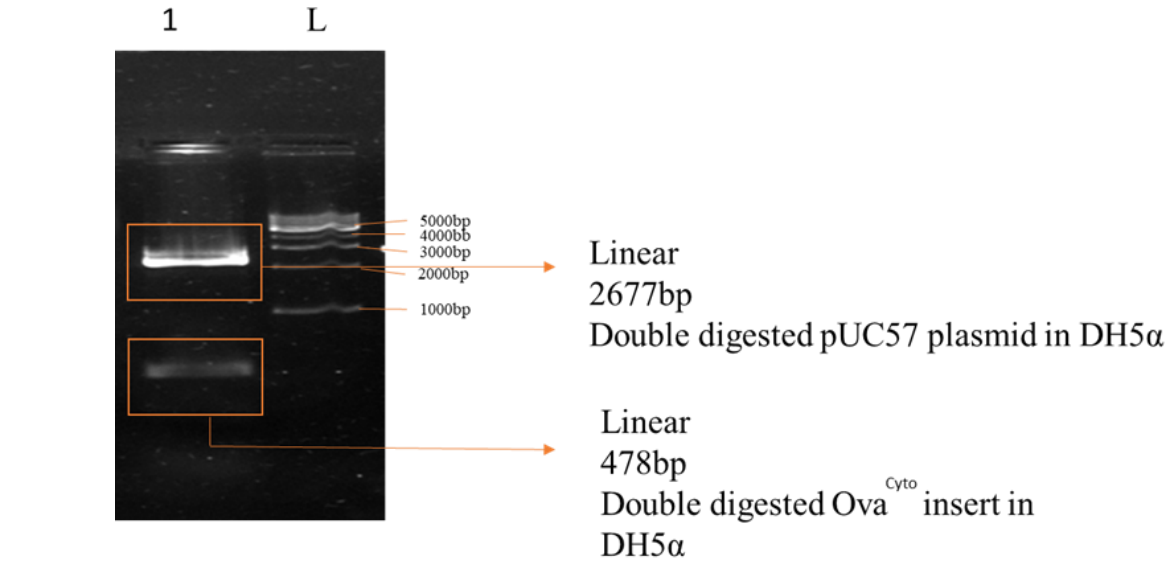

Figure 4. Gel electrophoresis of pUC57 plasmid DNA and ovalbumin ^{Cyto} insert following restriction enzyme double digestion. Agarose gel electrophoresis image of pUC57-Ova ^{Cyto} construct vector subjected to double digestion with EcoRI and XbaI. **L**: 1kb DNA ladder. **Lane 1**: Double digestion of DNA plasmid pUC57 and Ova ^{Cyto} insert.

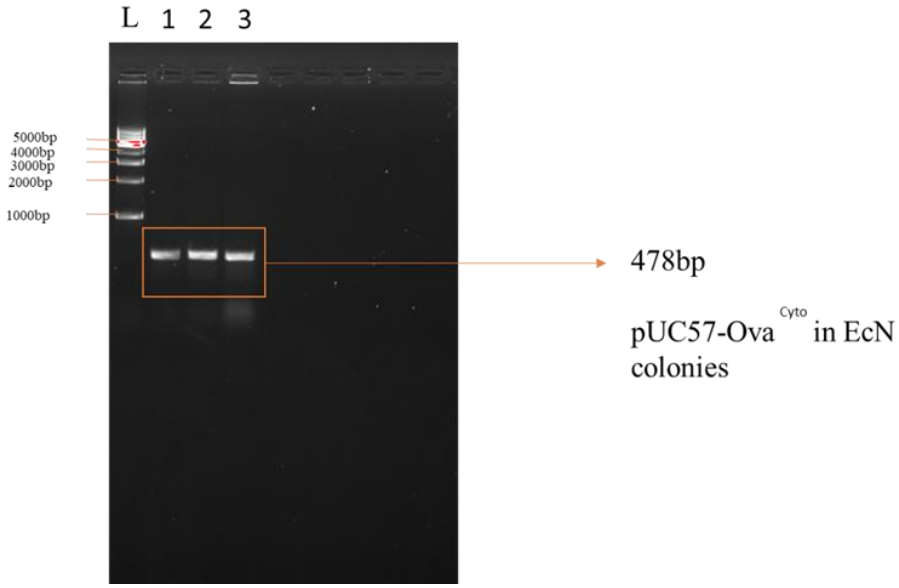

Figure 5. Confirmation of pUC57-Ova ^{Cyto} using colony PCR after transformation in *Escherichia coli* Nissle (EcN). Agarose gel electrophoresis image of EcN colonies following colony PCR of DNA extracted from ECN colonies transformed with pUC57-Ova ^{Cyto} . **L**: 1kb DNA ladder. **Lane 1-3**: pUC57-Ova ^{Cyto} transformants in EcN.

3.3. Assessing vaccine-specific antibody responses in mice treated with engineered *Escherichia coli* Nissle (EcN) expressing Ova peptides two weeks post vaccination.

To assess the ability of EcN expressing Ova ^{Cyto} peptides to alter responses to vaccination, mice were orally administered with 1 x 10^{10} CFU of EcN expressing Ova peptides (EcN-Ova ^{cyto}) or EcN carrying an empty pUC57 vector (EcN-EV). Administering bacteria at this concentration has previously been demonstrated to engage a robust immune response in mice, while lower doses (<10^{8} CFU) are not immunogenic (Hapfelmeier et al., 2010). Engineered bacteria were given daily for two weeks to allow for sufficient stimulation of the immune system. After a two-week treatment of mice with the engineered bacteria mice were injected with 0.3 µg of mRNA-Ova vaccine (Synthesised at the University of Queensland and encapsulated in lipid nanoparticles at the University of Adelaide, AUS) intramuscularly to generate an Ova-specific immune response. Peripheral blood and faecal sample were collected weekly to assess the systemic and mucosal humoral antibody response. Two weeks after the initial vaccination mice were given a booster dose of mRNA-Ova by the same route of immunisation to allow a more robust response particularly in generating antibodies and memory B cells (**Figure 6 A**). Prior to boosting, Ova-specific IgG_{total} and IgA in the blood and faeces, respectively, were measured by ELISA. While there was a trending increase in serum IgG in EcN-Ova ^{cyto} treated mice two weeks after primary vaccination, this increase was not significantly different relative to EcN-EV treated mice (**Figure 7 A**). In contrast to the increase in serum Ova-specific IgG from pre-vaccination to post, Ova-specific IgA in faecal homogenates of mice were too low to be interpretable (**Figure 7 B**). Together, these data demonstrate that pre-treatment of mice with EcN-Ova prior to mRNA-Ova vaccination has minimal impact on the outcome of single-dose vaccination when compared to EcN-EV.

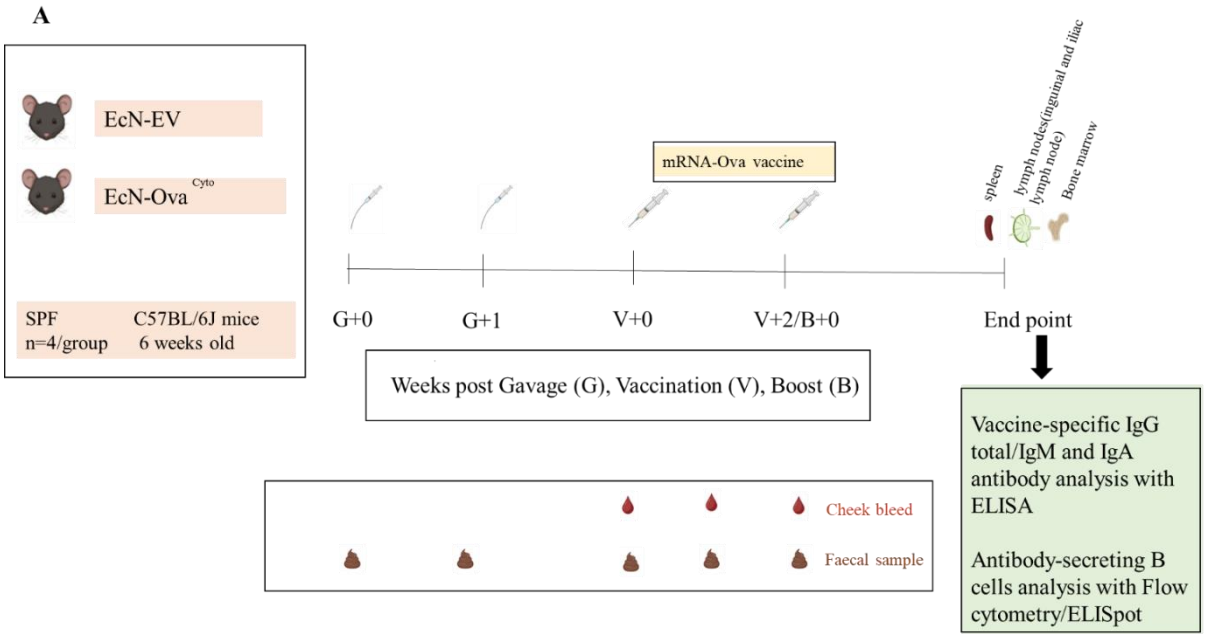

Figure 6. The experimental design used to establish whether bacteria engineered to express Ova ^{Cyto} protein alter subsequent immune responses to vaccination with mRNA-Ova. 6-week old SPF mice were treated orally with 10^{10} CFU EcN-Ova ^{Cyto} or EcN-EV (n=4 mice/group) daily for two successive weeks. Mice were then vaccinated with 0.15 µg of by intramuscular injection (i.m) at V+0 and V+2 weeks. Cheek bleeds and faecal samples were taken weekly to assess vaccine- specific antibody responses. Two weeks post-boost, mice were euthanized and immunologically relevant organs (inguinal and iliac lymph nodes, bone marrow and spleen) were harvested and processed for endpoint analyses to assess B cell immune responses.

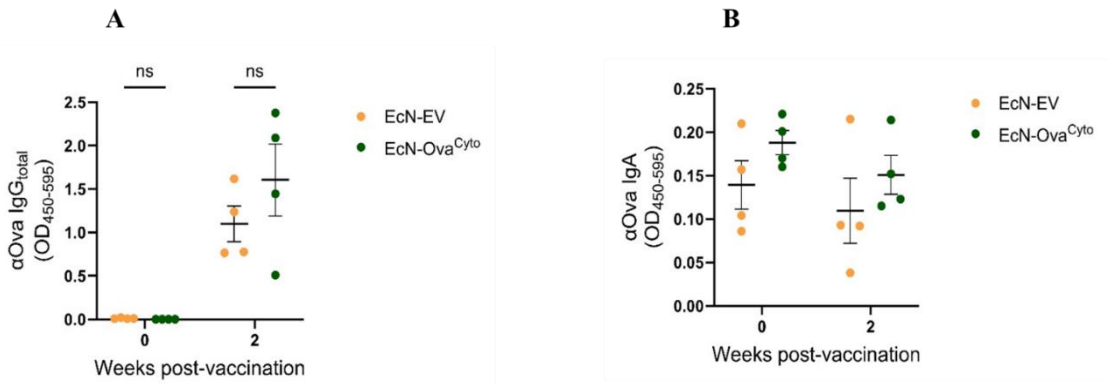

Figure 7. No statistically significant increase in Serum IgG total or faecal IgA response in SPF mice treated with EcN-Ova ^{Cyto} after mRNA-Ova vaccination at week two. Peripheral blood and faecal samples were collected at baseline and 2 weeks post mRNA-Ova vaccination to screen for vaccine-specific antibodies. (**A**) Ova-specific serum IgG total (1:1000 dilution) and (**B**) Ova-specific faecal IgA (1:1000 dilution) were assessed by ELISAs. Raw optical density (OD) readings from the ELISA are shown and represented as the mean ± SEM. A unpaired t-test was used to assess statistical significance. ns = not significant. n = 4 mice/group

3.4. Assessing vaccine-specific antibody responses post vaccination in mice treated with engineered *Escherichia coli* Nissle.

Two weeks after the 2nd dose of mRNA-Ova vaccination, Ova-specific IgG_{total} and, IgM and IgA were assessed by ELISA in the serum and faeces, respectively, of mice treated with EcN-EV and EcN-Ova ^{cyto}. Ova-specific IgG_{total} titres in serum were not significantly different in mice treated with EcN-Ova ^{Cyto} in the first 3 week following initial vaccination. Importantly, however, there was a statistically significant increase in serum IgG_{total} at day 28 in mice treated with EcN-Ova ^{cyto} , relative to EcN-EV treated mice (**Figure 8 A**). There was no statistically significant difference in Ova-specific IgM titres at any timepoint in mice treated with EcN-Ova ^{cyto} compared to control mice (**Figure 8 B**). Finally, Ova-specific IgA titres were assessed in faecal homogenates in the weeks following vaccination. There was an increase in Ova-specific IgA in the faeces in both groups of mice, particularly after the second dose of mRNA-Ova vaccination, which is unexpected given the intramuscular route of vaccination. Despite this, there was statistically significant increase in faecal IgA in EcN-Ova ^{cyto} treated mice, relative to EcN-EV control mice, at day 21 after primary vaccination (**Figure 8 C**). Together, these data demonstrate that pre-treatment of mice with a probiotic engineered to express Ova-derived

peptides can significantly enhance the subsequent class-switched antibody response to mRNA-Ova vaccination, both systemically, and within mucosal tissue.

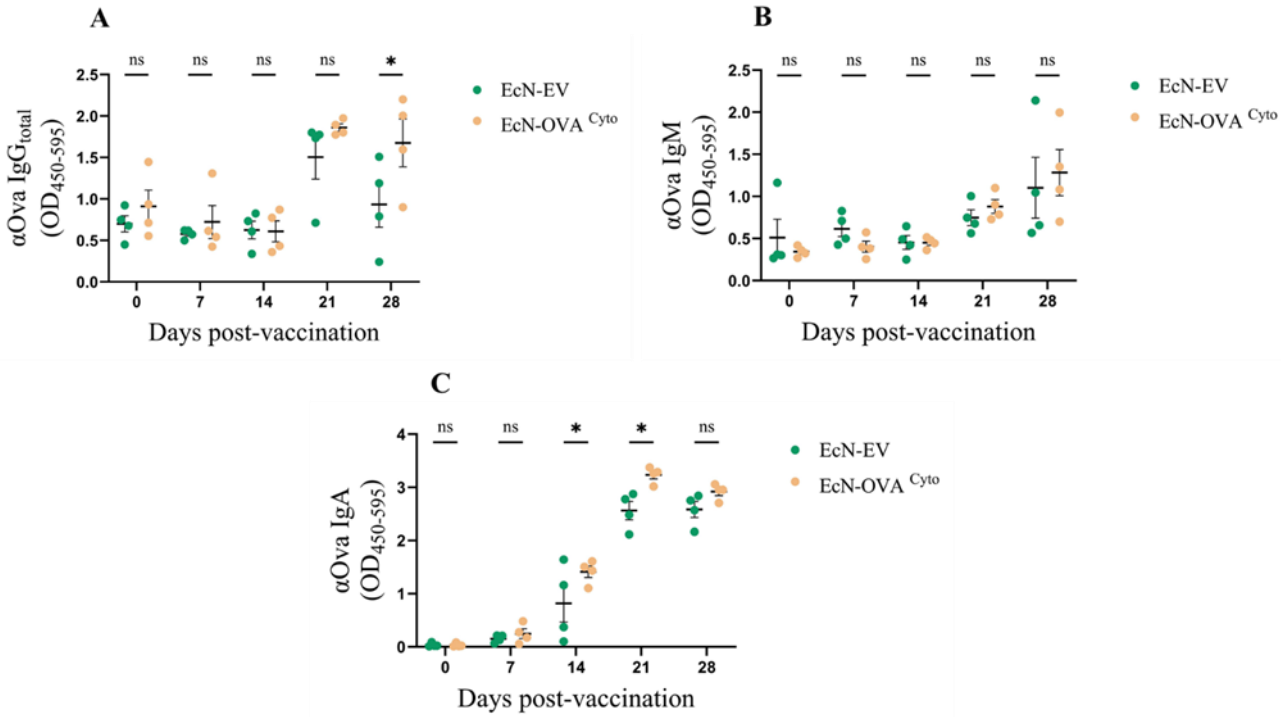

Figure 8. IgG and IgA antibody responses to an mRNA-Ova vaccine are increased in mice treated with EcN-Ova ^{Cyto}. Peripheral blood and faecal samples were collected weekly following mRNA-Ova vaccination to assess Ova-specific antibody responses in mice that were administered the engineered probiotic strains, EcN-EV (control) or EcN-Ova ^{Cyto}, for 2 weeks prior to vaccination. (**A**) Ova-specific serum IgG$_{total}$ (1:5000 dilution), (**B**) Ova-specific serum IgM (1:100 dilution), and (**C**) Ova-specific faecal IgA (1:2 dilution) were assessed by ELISA. Raw optical density (OD) readings from the ELISA are shown and are represented as the mean ± SEM. A unpaired t-test was used to assess statistical significance. * $p < 0.05$. ns = not significant. n = 4 mice/group.

3.5. Increased formation of splenic Ova-specific IgG antibody-secreting cells in EcN-Ova ^{cyto} treated mice.

Results from the ELISAs demonstrated that pre-treatment with EcN-Ova ^{cyto} enhanced the accumulation of Ova-specific IgG in the serum of mice that were immunised with two doses of the mRNA-Ova vaccine, relative to EcN-EV treated mice that were similarly immunised. The production of vaccine-specific IgG can be attributed to antibody-secreting B cells (ASCs) that develop in response to vaccination, suggesting that EcN-Ova ^{cyto} treated mice may have increased numbers of Ova-specific ASCs. To determine if this was true, I performed ELISpot analysis to quantify the number of Ova-specific IgG ASCs in the spleens and bone marrow of EcN-EV and EcN-Ova ^{cyto} treated mice. I observed no significant differences in the number of Ova-specific IgM ASCs in either the spleen or bone marrow (**Figure 9 A-B**), consistent with there being no difference in Ova-specific serum IgM titres between the two groups of mice (**Figure 8 B**). However, I did observe a statistically significant increase in the number of Ova-specific IgG-secreting cells in the spleen of EcN-Ova ^{cyto} treated mice relative to EcN-EV treated mice (**Figure 9 A**). This was not observed in the bone marrow (**Figure 9 B**).

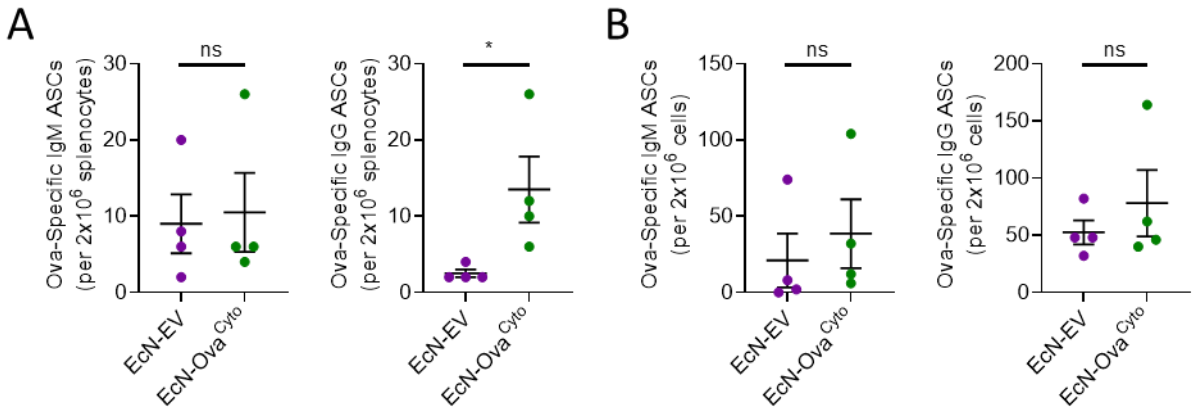

Figure 9. Ova-specific IgG secreting cells are significantly increased in the spleen, but not bone marrow, of EcN-Ova ^{cyto} treated mice. Four weeks post-initial mRNA-Ova vaccination Ova-specific IgM and IgG antibody-secreting cells in the spleen and bone marrow were assessed by ELISpot assay. (**A**) The total number of Ova-specific IgM and IgG antibody secreting cells in the spleen and (**B**) bone marrow. Data are presented as mean ± SEM. * $p < 0.05$. ns = not significant. n = 4 mice/group.

3.6. Assessing B cell populations in mice colonized with engineered *Escherichia coli* Nissle.

B cells responding to a stimulation such as vaccination can develop into distinct subsets, such as germinal centre B cells (GCB cells), antibody-secreting cells (ASCs), or memory B cells (Bmem) that can each contribute to the hosts pool of antigen-specific antibody titres. Thus, I used flow cytometry to determine if any of these B cell subsets were altered in magnitude in EcN-Ova ^{cyto} treated mice, relative to EcN-EV treated mice, using the flow cytometry gating strategy shown (**Figure 10**). Two-weeks post boost, mice were humanely culled and the vaccine-draining secondary organs, including the inguinal and iliac lymph nodes and the spleen as well as the bone marrow were harvested were for analysis.

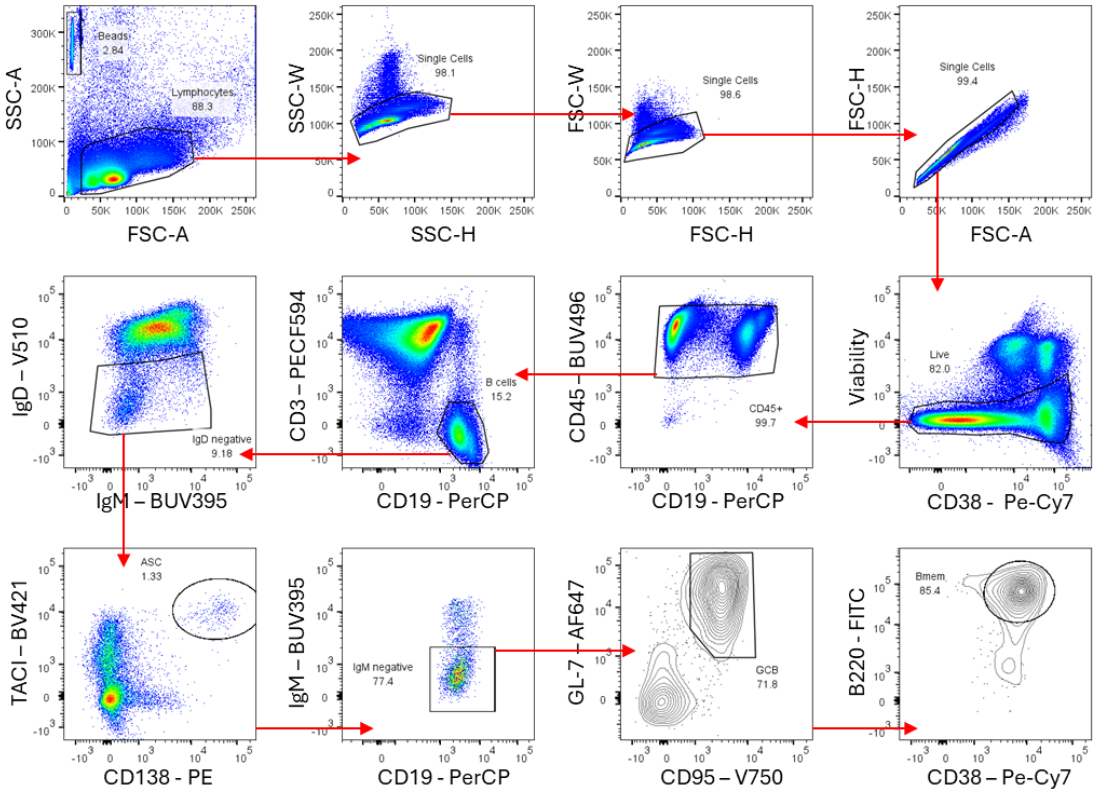

Figure 10. B cell gating strategy. Single cells were gated based on forward scatter (FSC) and side scatter (SSC) profiles for lymphocytes, followed by gating live cells using a viability dye, and all cells of hematopoietic origin using the marker CD45. B cells were then identified on the basis of CD19 expression, followed by exclusion of naïve B cells based on expression of IgD. B cells were then further gated into different subsets to include antibody-secreting cells (Live, $CD45^+$ $CD3^-$ $CD19^+$ IgD^- $CD138^+$ $TACI^+$), germinal centre B cells (Live, $CD45^+$ $CD3^-$ $CD19^+$ IgD^- IgM^- $CD138^-$ $TACI^-$ $GL\text{-}7^+$ $CD95^+$) and memory B cells (Live, $CD45^+$ $CD3^-$ $CD19^+$ IgD^- IgM^- $CD138^-$ $TACI^-$ $GL\text{-}7^-$ $CD95^-$ $CD38^+$).

3.6.1. The proportion of GC B cells is significantly higher in the spleen of EcN-Ova ^{cyto} treated mice.

Germinal centres are specialist lymphoid structures that form in response to vaccination or infection to support the proliferation, differentiation, and processes for the generation high-affinity, vaccine-specific, antibodies during an immune response (De Silva & Klein, 2015). Flow cytometry analysis was used to enumerate GCB cells in spleen, inguinal and iliac lymph nodes (**Figure 11 A**). There was a statistically significant increase in frequency of GCB cells in the spleen of EcN-Ova ^{cyto} treated mice, relative to EcN-EV treated mice, both as a percentage of all $CD19^+$ B cells (hereafter referred to as percentage), and as a frequency of live, $CD45^+$ cells (hereafter referred to as frequency) (**Figure 11 B**). However, although the total number of GCBs was higher in most of the EcN-Ova ^{cyto} treated mice, this did not translate to a statistically significant difference in the total number of GCBs in the spleens (**Figure 11 B**). In the vaccine-draining inguinal and iliac lymph nodes there was no statistically significant difference in the percentage, frequency, or total number, of GCB cells between EcN-EV and EcN-Ova ^{cyto} treated mice (**Figure 11 C-D**). Together, these data demonstrate that pre-treatment with EcN-Ova ^{cyto} can enhance the formation of a B cell subset in the spleen critical for the formation and production of high-affinity, vaccine-specific antibodies.

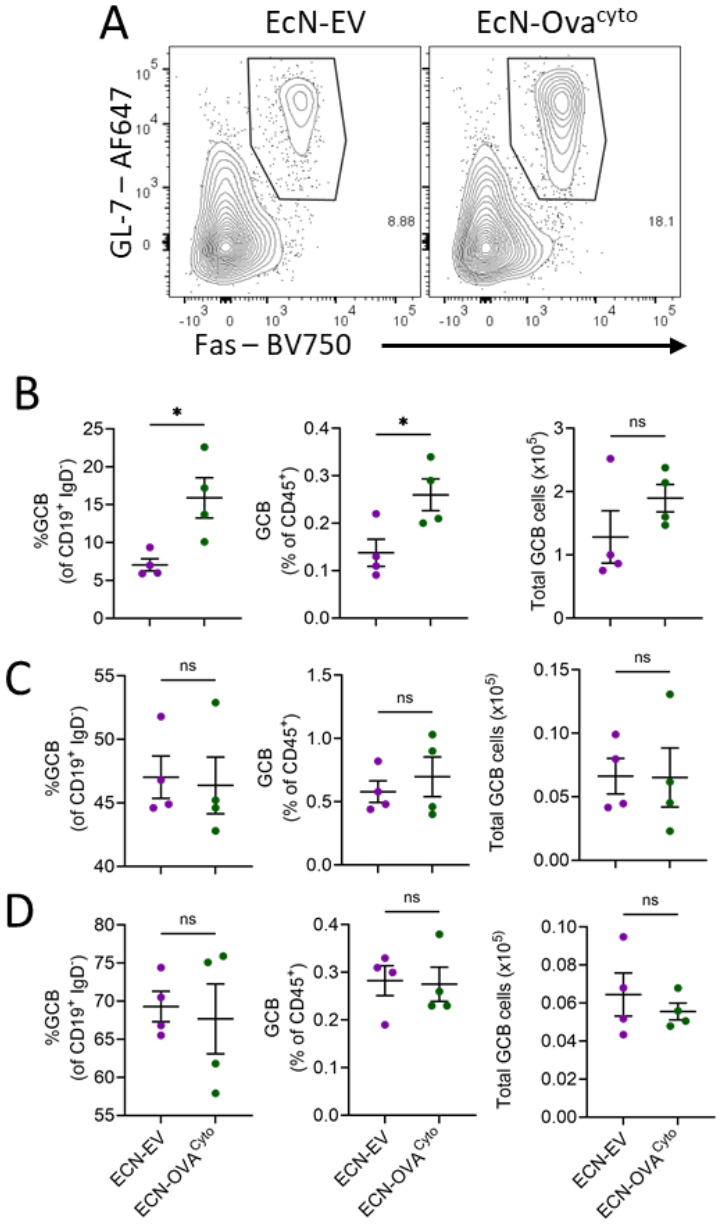

Figure 11. The proportion of germinal centre B cells was significantly higher in the spleen of EcN-Ova ^{cyto} treated mice after mRNA-Ova vaccination. Four weeks post-boost mRNA-Ova vaccination EcN-EV and EcN-Ova ^{cyto} treated mice were assessed for changes in germinal centre B cell responses by flow cytometry. **(A)** Representative flow cytometry of GCB cells ($CD19^+$ IgM^- IgD^- $GL7^+$ FAS^+) in the spleen of EcN-EV and EcN-Ova ^{cyto} treated mice 4 weeks post-boost vaccination. **(B)** Percentage, frequency and total number of germinal centre B cells in spleen, **(C)** inguinal lymph node (LN) and **(D)** iliac LN. Data are represented as the mean ± SEM. An unpaired t-test was used to assess statistical significance. * $p < 0.05$. ns = not significant. n = 4 mice/group.

3.6.2. The proportion of memory B cells in the iliac lymph node was significantly higher in EcN-Ova ^{cyto} treated mice.

A statistically significant increase in serum and faecal antibody tires in EcN-Ova ^{cyto} treated mice was only observed after boosting with mRNA-Ova. This potentially indicates that the primary mRNA-Ova vaccination generated higher numbers of Ova-specific Bmems in EcN-Ova ^{cyto} treated mice, which resulted in greater production of Ova-specific antibodies after boosting. Thus, we next analysed the formation of memory B cells in secondary lymphoid organs in response to vaccination (**Figure 12 A**). There was a small (~0.04%) but significant increase in the frequency of Bmems among all live, $CD45^+$, immune cells in the iliac lymph nodes of EcN-Ova ^{cyto} treated mice, relative to EcN-EV. However, this was not reflected as a statistically significant increase in the total number of Bmems in this organ, or as the percentage of Bmems among all B cells (**Figure 12 D**). We also observed no statistically significant differences in the percentage, frequency and total number memory B cells in the spleen and inguinal lymph nodes of mice treated with EcN-EV and EcN-Ova ^{cyto} four weeks after primary vaccination with mRNA-Ova (**Figure 12 B-C**). These data suggest that EcN-Ova ^{cyto} treatment only had a minimal impact on the formation of memory B cells. Although largely statistically not significant, more sensitive detection methods to identify vaccine-specific Bmems may be required to adequately address this question.

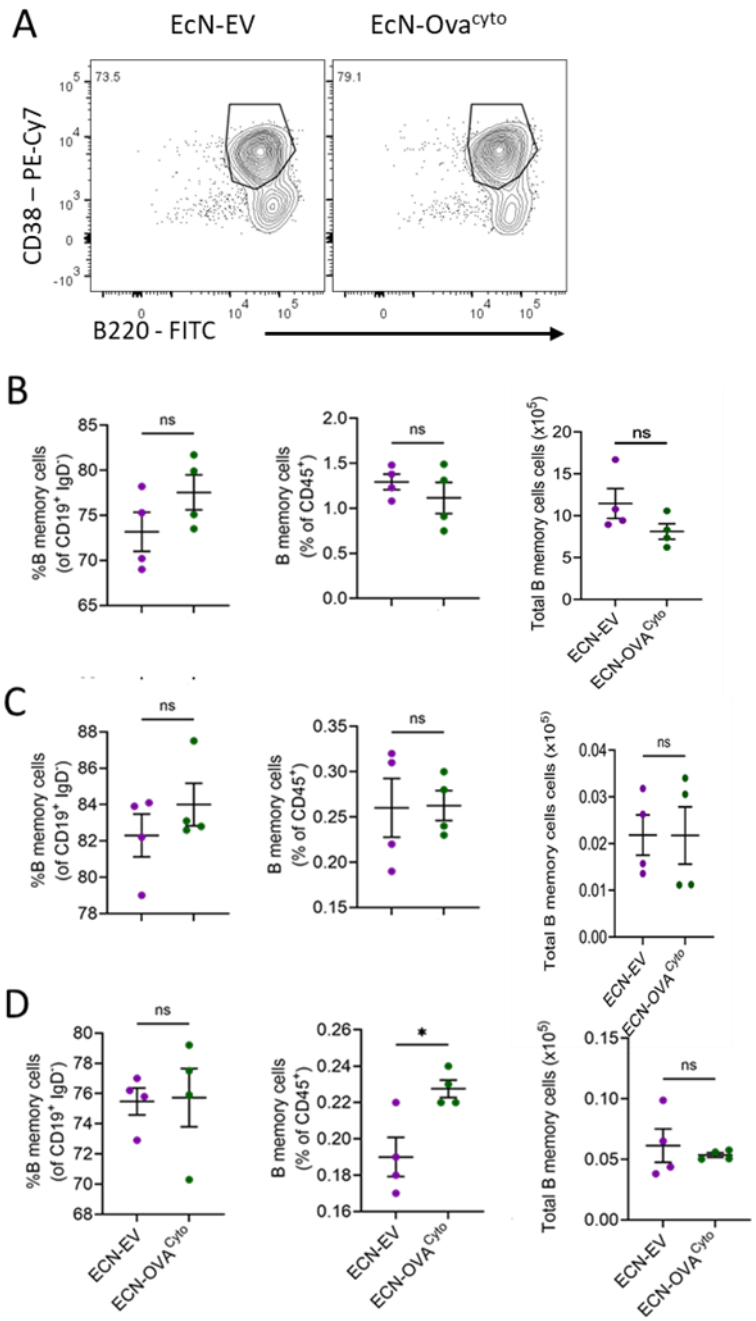

Figure 12. The proportion of memory B cells in the iliac lymph node was significantly higher in EcN-Ova ^{cyto} treated mice. Four weeks post-boost mRNA-Ova vaccination EcN-Ev and EcN-Ova ^{cyto} treated mice were assessed for changes in memory B cells by flow cytometry. **(A)** Representative flow cytometry analysis of memory B cells ($CD19^+$ IgM^- IgD^- $GL7^-$ FAS^- $CD38^+$) in the spleen of EcN-EV and EcN-Ova ^{cyto} treated mice 4 weeks post-boost vaccination. **(B)** Percentage, frequency and total number of memory B cells in spleen, **(C)** inguinal LN, and **(D)** iliac LN. Data are represented as the mean ± SEM. An unpaired t-test was used to assess statistical significance. * $p < 0.05$. ns = not significant. n = 4 mice/group.

3.6.3. Assessing antibody secreting cells (ASC) population in bone marrow and spleen.

Finally, ASCs were assessed using flow cytometry analysis in the bone marrow and spleen four weeks after vaccination (**Figure 13 A**). In contrast to the increased ASCs observed in the ELISpot assays (**Figure 8 A**), there was no statistically significant difference in the percentage, frequency or total number of ASCs in the spleens of mice treated with EcN-EV and EcN-Ova ^{cyto}, although all of these analyses were trending higher in the EcN-Ova ^{cyto} treated mice (**Figure 13 C**). Consistent with the ELISpot data, we observed no statistically significant differences in the percentage, frequency or total number of ASCs in the bone marrow of EcN-EV and EcN-Ova ^{cyto} treated mice (**Figure 13 B**). These data suggest that EcN-Ova ^{cyto} treatment had an impact in the formation of ASCs in the bone marrow and spleen, although statistically not significant and more replicates would be required to confirm this observation.

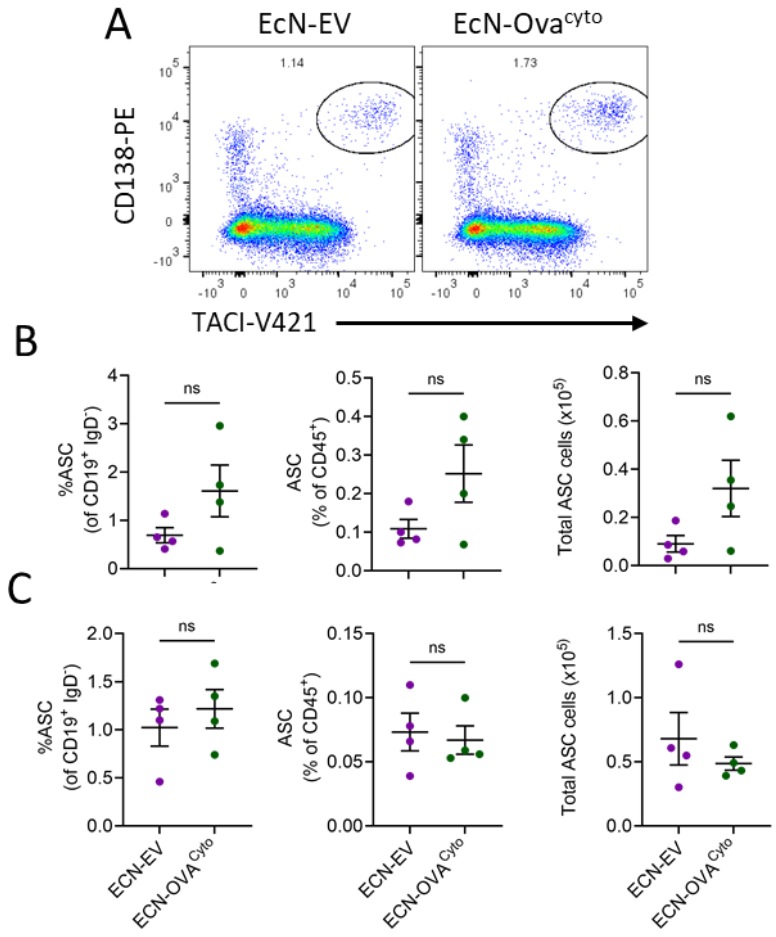

Figure 13. No statistically significant difference in Antibody secreting cells (ASC) in bone marrow and spleen of SPF mice colonized with EcN-Ova ^{cyto} and EcN-EV after vaccinated with mRNA-Ova. Four weeks post-boost mRNA-Ova vaccination EcN-EV and EcN-Ova ^{cyto} treated mice were assessed for changes in Antibody secreting cells (ASCs) cells by flow cytometry**. (A)** Representative flow cytometry of Antibody secreting cells (ASCs) ($CD19^+$ IgM^- IgD^- $GL7^-$ FAS^- $CD138^+$) in the bone marrow of EcN-EV and EcN-Ova ^{cyto} treated mice 4 weeks post-boost vaccination. **(B)** Percentage, frequency and total number of ASCs in the bone marrow and **(C)** spleen. Data are represented as the mean ± SEM. An unpaired t-test was used to assess statistical significance. ns = not significant. n = 4 mice/group.

Conclusion

I successfully constructed the pUC57 plasmid expressing OVA^{Cyto} peptide and transformed it into *Escherichia coli* Nissle 1917 (EcN). Following treatment with EcN-Ova ^{Cyto} or EcN-EV and post vaccination with mRNA-Ova there was a significant increase in antibody-specific immune response as seen in the enhancement of Ova-specific IgG, and IgA titres. Ova ^{Cyto} had an impact on formation of germinal B cells that are essential for differentiating into antibody secreting cells (ASC). Likewise, there was clearly an impact in the formation of ASC and memory B cells in Ova ^{Cyto} treated mice particularly demonstrated to be higher in iliac lymph node given the intramuscular administration. Given my original hypothesis colonizing the mice with expressed Ova ^{Cyto} peptide clearly can lead to an enhanced humoral immune response particularly mucosal immune response following mRNA-Ova vaccination.

3.7. Construction of pAIDA plasmids and engineering *Escherichia coli* to express full-length CRM 197

3.7.1. Design of plasmid construct to express full-length CRM 197

In the previous experiments we expressed select Ova-derived immunodominant peptides within bacteria to enhance immune responses to Ova vaccination. Administration of this bacteria to mice, prior to Ova vaccination, resulted in a significant increase in Ova-specific IgG and IgA antibodies, as well as an increase in Ova-specific IgG in the spleen, demonstrating that these bacteria can be used to enhance vaccine-specific immune responses. However, expressing only select epitopes from an antigen within bacteria, as we did with EcN-Ova, may restrict the full potential of immune activation. Thus, expressing the full-length protein, rather than an epitope, may stimulate a stronger immune response (Chen et al., 2023 , Pedersen et al., 2022), and prime both the cellular and humoral arms of the adaptive immune system. In addition, expressing the desired vaccine antigen on the bacterial surface, rather than in the cytoplasm might provide the immune system better access to the antigen particularly in eliciting B and T cell mediated immune response that are key for antibody production (Chen et al., 2023). These improvements, could significantly enhance the immunomodulatory effects observed in my earlier experiments leading to a better vaccine efficiency and immune memory formation (Chen et al., 2023, Pedersen et al., 2022).

To localise full-length, vaccine-derived, proteins to the cell surface we used the previously engineered Adhesin Involved in Diffuse Adherence (AIDA) plasmid construct (pAIDA) (Jarmander et al., 2012). This construct employs the AIDA protein for the surface display of a fusion protein, with the expressed protein being flanked by His and Myc tags that enable easy identification of AIDA-fusion constructs by standard laboratory methods such as flow cytometry. Expression of the AIDA construct is driven by the LacUV5 promoter, which has moderate constitutive expression that can be enhanced through addition of Isopropyl ß-D-1-thiogalactopyranoside (IPTG), an inducer commonly used to regulate lac-operon controlled genes. Additionally, an erythromycin resistance gene is incorporated into the plasmid to enable selection of bacteria after transformation of the plasmid (Jarmander et al., 2012). We chose cross reactive material 197 (CRM) as the vaccine antigen to express in these experiments. CRM is a genetically detoxified form of diphtheria toxin that is widely used as a carrier protein in polysaccharide conjugate vaccines, such as the 13-valent pneumococcal vaccine (PCV13) (Moginger et al., 2016). Our laboratory has extensive experience using this vaccine in

preclinical models having previously demonstrated that the humoral response to PCV13 vaccination is highly dependent on the composition of the microbiota (Lynn et al., 2018).

3.7.2. Construction of a pAIDA plasmid that expresses CRM 197 full protein on membrane surface of *Escherichia coli* Nissle.

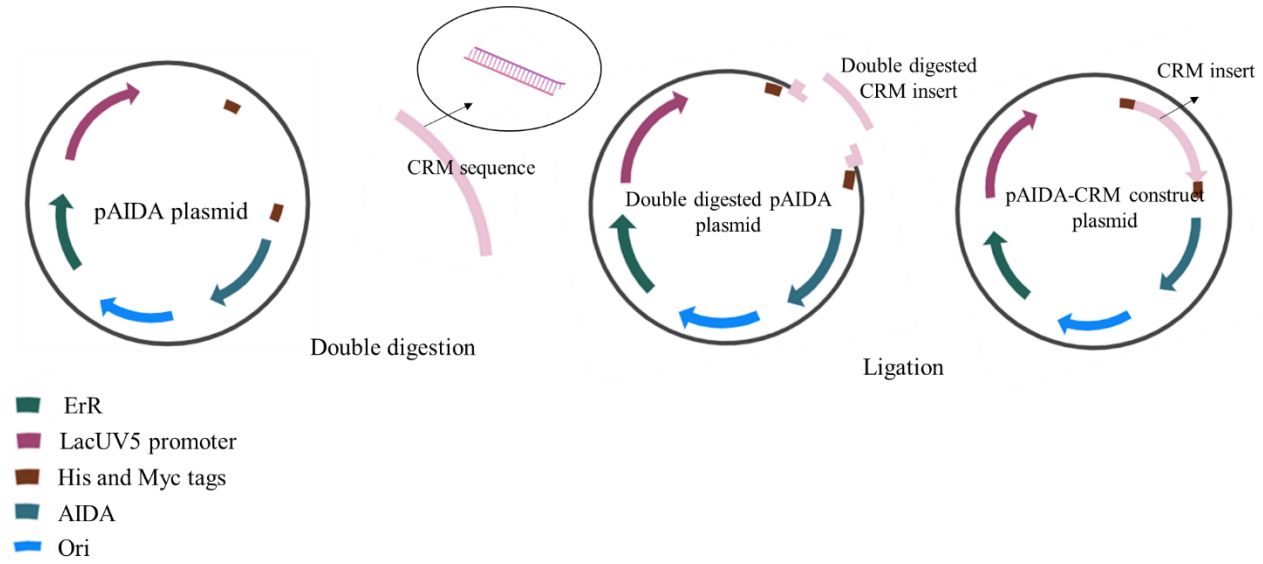

Figure 14. Overview of experimental design of pAIDA-CRM construct for outer membrane expression of full-length CRM expression in EcN. (**A**) The 5536bp pAIDA plasmid used for the surface display of a fusion protein flanked by His and Myc tags. (**B**) codon optimised full-length CRM sequence with a size of 1609bp, PCR amplified to introduce the KnpI and SacI restriction enzyme sites. (**C**) KpnI and SacI digested pAIDA empty vector with a size of 5536bp and CRM insert with a size of 1609bp. (**D**) Ligated pAIDA-CRM construct with a size of 7145bp.

To generate the pAIDA-CRM construct with the size of 5561bp, a linear CRM sequence was cloned into the pAIDA plasmid through restriction digestion and ligation (**Figure 14**). The codon optimised CRM sequence was first PCR amplified to introduce KnpI and SacI restriction sites at the 5' and 3' ends of the DNA sequence, respectively. The pAIDA plasmid and the PCR amplified CRM sequence were then digested with KpnI and SacI restriction enzymes,

which enables cloning of the CRM sequence in frame with the AIDA protein, with the addition of 6X His-tag N-terminal of the CRM protein, and a Myc-tag C-terminal of the CRM protein (**Figure 14**). Successful double digestion of plasmid, and PCR amplified CRM insert, was confirmed by gel electrophoresis with the expected linear pAIDA empty plasmid band observed around the expected 5536bp and the DNA sequence encoding the CRM protein at 1609bp (**Figure 15**). The desired pAIDA and CRM DNA sequences were extracted from the agarose gel and ligated to form the pAIDA-CRM plasmid before transformation into *E. coli* DH5α, a common strain used for its high transformation efficiency (Kostylev et al., 2015). Transformed DH5α were plated on LB agar plates containing erythromycin to select for bacteria containing the pAIDA-CRM plasmid and colony polymerase chain reaction (PCR) performed to amplify the CRM insert in select individual colonies to verify the correct insertion of the ligation product into the bacterial colonies. Gel electrophoresis confirmed the expected band sizes of the CRM plasmid-insert PCR product of 1609bp in transformed DH5α (**Figure 16**). The presence of the correct pAIDA-CRM was further confirmed by plasmid extraction from overnight cultures of transformed DH5α and double digestion using KpnI and SacI restriction enzymes. Gel electrophoresis of the digested plasmid revealed the expected band sizes for both the pAIDA plasmid at 5536bp and CRM insert at 1609bp, indicating successful digestion and ligation of the CRM insert into the pAIDA plasmid (**Figure 17**). The pAIDA CRM plasmid was then transformed into *E. coli* Nissle (EcN) to generate EcN-CRM and transformed bacteria plated on LB agar plates containing erythromycin to select for bacteria containing the pAIDA-CRM plasmid. Colony PCR once again confirmed correct band sizes for the CRM insert of 1609bp in EcN colonies, validating the successful transformation of the EcN-CRM strain (**Figure 18**). These results indicated the successful cloning of the CRM sequence into the pAIDA vector, and the transformation of this plasmid into the probiotic strain EcN.

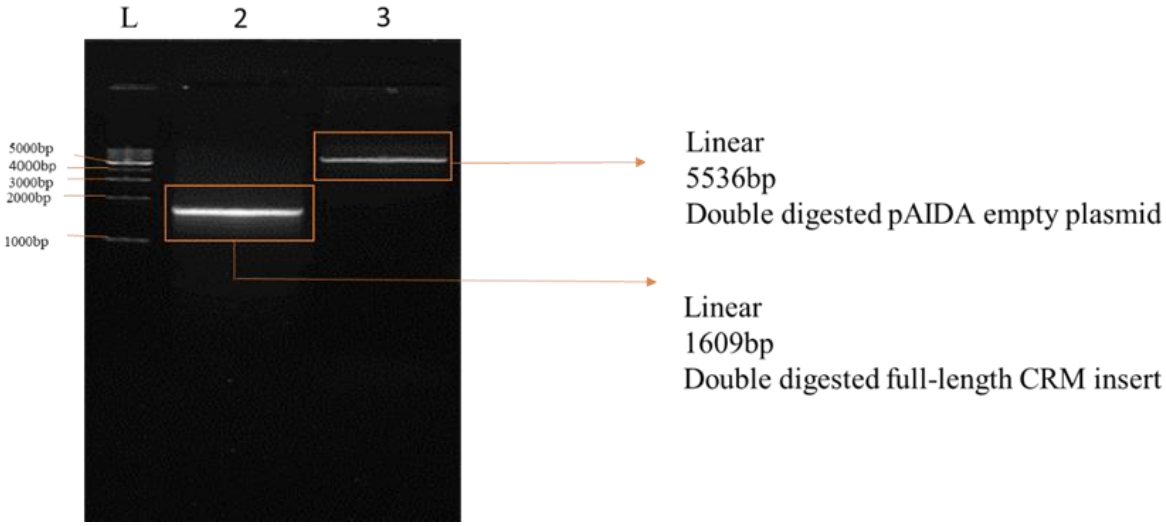

Figure 15. Gel electrophoresis of pAIDA plasmid DNA and CRM insert following restriction enzyme double digestion. Agarose gel electrophoresis image showing of the expected size of the pAIDA plasmid and the sequence encoding CRM following digestion using two restriction enzymes, KnpI and SacI. **L**: 1kb DNA ladder. **Lane 2**: DNA sequence encoding the CRM protein**. Lane 3**: pAIDA plasmid DNA

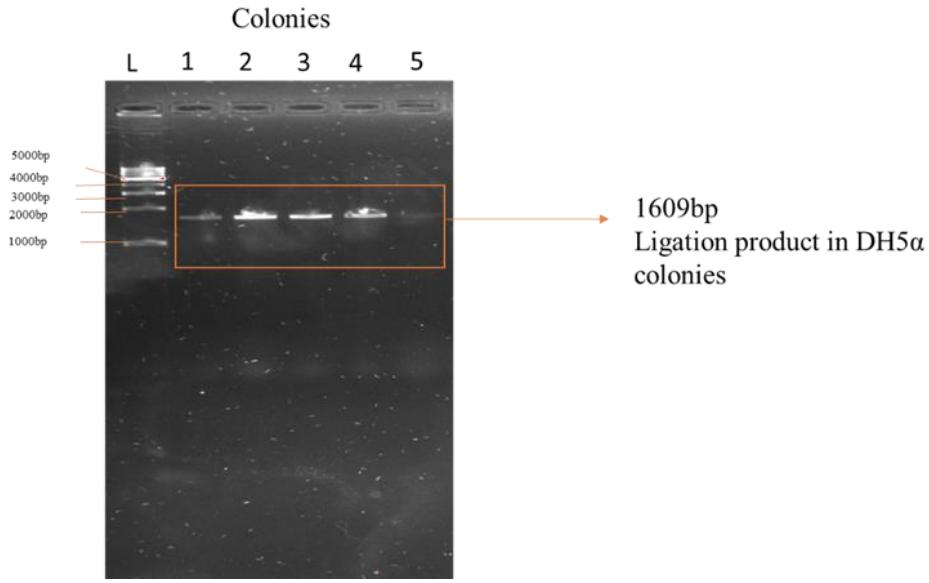

Figure 16. Confirmation of ligation product using colony PCR after transformation in E. Coli DH5α. Gel electrophoresis image showing the ligation product following colony PCR of DNA extracted from DH5α colonies transformed with pAIDA-CRM. **L**: 1kb DNA ladder. **Lanes 1-5**: pAIDA-CRM PCR product from individual DH5α colonies.

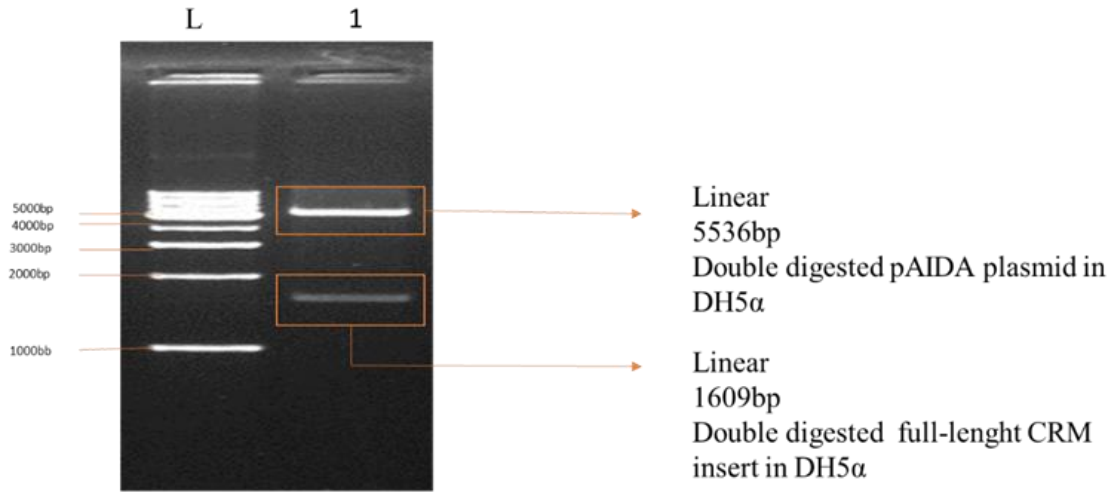

Figure 17. Gel electrophoresis image of double digestion of pAIDA-CRM product following restriction enzyme double digestion. Gel electrophoresis image showing digestion of pAIDA-CRM construct using two restriction enzymes, KnpI and SacI. **L**: 1kb DNA ladder. **Lane 1**: CRM construct DNA fragment sizes following double restriction enzyme digestion.

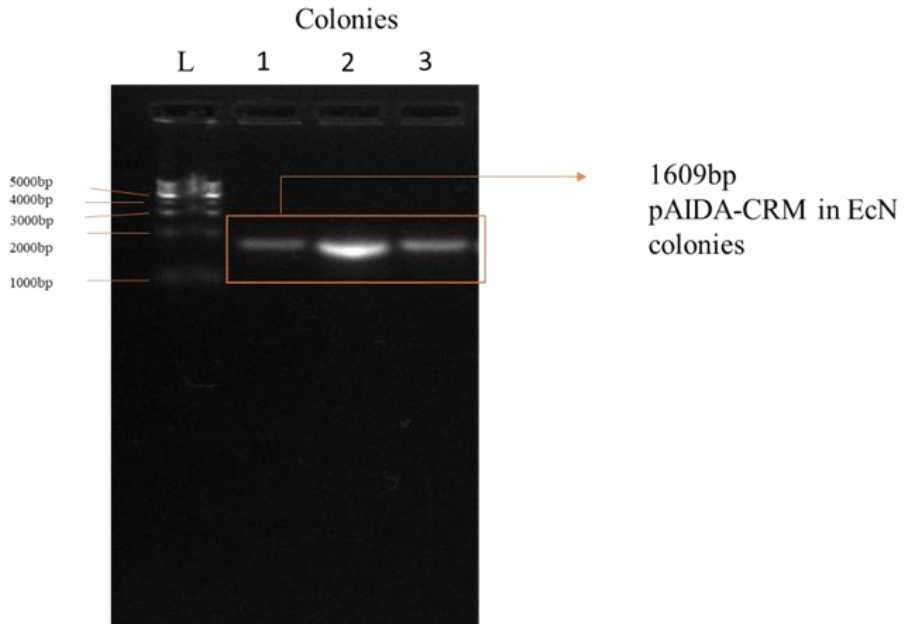

Figure 18. Confirmation of pAIDA-CRM using colony PCR after transformation in *Escherichia coli* Nissle (EcN). Gel electrophoresis image shows EcN colonies transformed with pAIDA-CRM. **L**: 1kb DNA ladder**. Lanes 1-3**: PCR amplification of pAIDA-CRM DNA from individual EcN transformants.

3.8. Evaluating outer membrane expression of full-length CRM protein in *E. coli* Nissle (EcN).

3.8.1. Absence of outer membrane localization of full-length CRM protein in EcN.

As previously mentioned in the first experiment, EcN was the probiotic of choice used to successfully express Ova in the cytoplasm and enhance Ova-specific immune responses when used *in vivo*. Hence, EcN was used again here for the expression of full-length CRM in the outer membrane. As mentioned previously, the pAIDA expression construct contains His- and Myc-tags N- and C-terminal of the inserted CRM sequence, respectively (**Figure 19 A**). Thus, as a readout of surface expression of the AIDA-CRM fusion protein, the His- and Myc tags was stained on bacteria using fluorescently conjugated monoclonal antibodies. Additionally, to detect the CRM protein, unconjugated, polyclonal, mouse anti-CRM serum from mice that had been previously vaccinated with PCV13 was used in combination with fluorescently conjugated anti-mouse IgG detection antibodies. The expression level of AIDA-CRM was measured in ECN-CRM in addition to EcN carrying an unmodified pAIDA plasmid (EcN-EV) and a wild-type (WT) EcN, carrying no plasmid. Bacteria were first identified based on scatter profile, and the binding of a nucleic acid dye (**Figure 19 B)**. As expected, there was no shift in fluorescence intensity for His, Myc, or CRM in the WT EcN strain, demonstrating minimal non-specific signal for any of these markers (**Figure 19 C**). In contrast, there was a significant increase in binding of the anti-His and Myc tag antibodies in the EcN-EV strain, indicating that the unmodified AIDA membrane anchor with its surface exposed Myc and His tags is present on the surface of EcN-EV. As expected, there was no increase in binding of the anti-CRM antibody, as the CRM sequence is not present in the EV strain (**Figure 19 D**). Surprisingly, there was no increase in binding of the anti-CRM antibody in the EcN-CRM strain, relative to EcN-WT or EcN-EV, suggesting that CRM is not present on the surface of this strain (**Figure 19 E**). Consistent with this observation, there was also a loss of His-tag binding, which should be present N-Terminal of the CRM protein. There was, however, still binding of the anti-Myc tag antibody, which is present in N-terminal, of the AIDA membrane anchor (**Figure 19 E**). Together, these data suggest that, in the EcN-CRM strain, the membrane anchor is present and localised to the outer surface of the EcN, as indicated by the presence of the Myc-tag, but there is a loss of the CRM fusion protein, and the His-tag at the N-terminus.

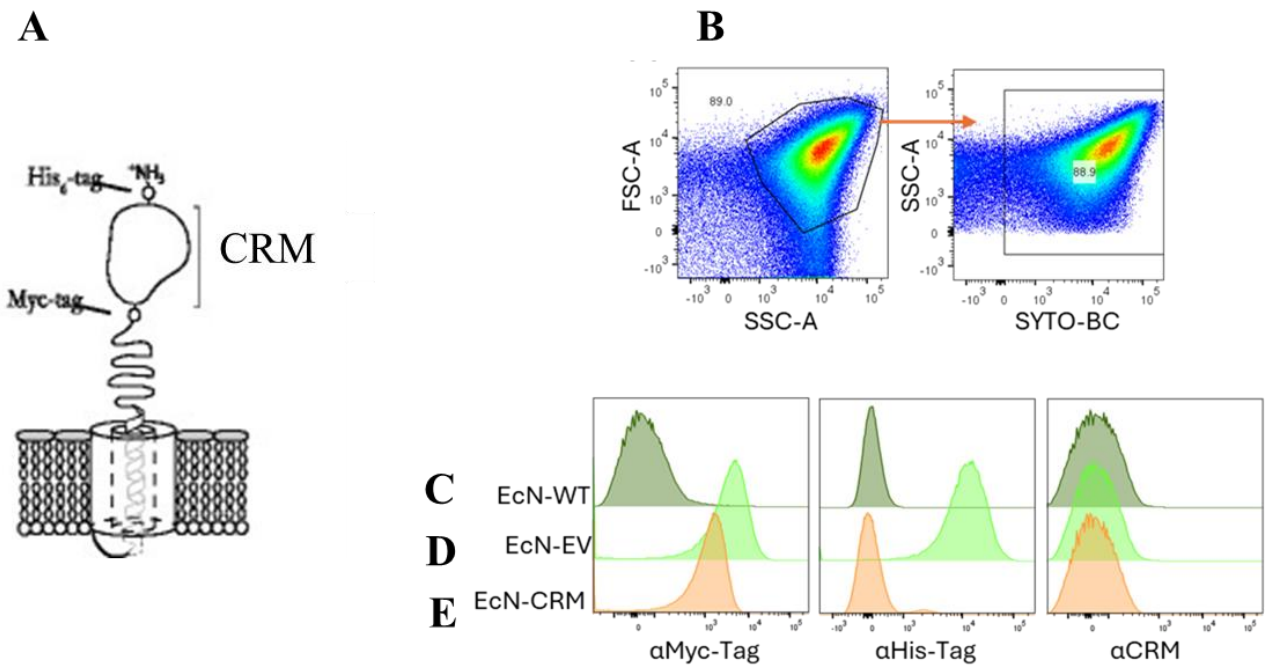

Figure 19. Flow cytometry analysis of full-length CRM surface expression in EcN. Wild type EcN, EcN transformed with a pAIDA empty vector (EcN-EV) or a pAIDA plasmid encoding an AIDA-CRM fusion protein (EcN-CRM) were stained to identify epitope tags within the AIDA protein, and the CRM protein. (**A**) Schematic presentation of AIDA-CRM fusion protein with His- and Myc-tags N- and C-terminal of the CRM protein. **(B**) Representative flow cytometry analysis identifying EcN cells based on forward and side scatter and nucleic acid binding dye SYTO™ BC Green Fluorescent. Histograms showing the presence of a cMyc (**C**) or His (**D**) epitope tags, or full-length CRM protein (**E**) in the indicated EcN strains.

3.8.2. Optimizing full-length CRM protein expression for enhanced recombinant protein production in *E. coli* BL21.

The initial attempt to express CRM in EcN did not yield the desired results. The lack of expression in EcN could be related to a strain-specific limitation, or an issue with the pAIDA-CRM plasmid itself. To investigate this further I opted to transform *E. coli* BL21, a strain of *E. coli* commonly used for recombinant protein expression. This strain is deficient in several proteases such as Lon and OmpT which are often responsible for protein degradation, reducing the likelihood of protein degradation and making it more likely to achieve successful protein expression (Du et al., 2021). If the CRM expression works in *E. coli* BL21 it may suggest the failure is strain-specific and related to EcN protease activity rather than plasmid design or expression. BL21-CRM and control strain were generated and stained for by bacterial flow cytometry as described above. As expected, there was no shift in fluorescence intensity for His, Myc, or CRM in the BL21-WT strain, demonstrating minimal non-specific signal for any of these markers in this *E. coli* strain (**Figure 20 A**). In contrast, there was a significant increase in binding of the anti-His and Myc tag antibodies in the BL21-EV strain, indicating that the unmodified AIDA membrane anchor with its surface exposed to Myc and His tags is present in BL21-EV. As expected, there was no increase in binding of the anti-CRM antibody, as the CRM sequence is not present in the EV strain (**Figure 20 B**). There was, however, an increase in binding of the anti-CRM antibody in the BL21-CRM strain, relative to BL21-WT and BL21-EV, suggesting that CRM is present on the surface of this strain (**Figure 20 C**). Consistent with this observation there was also His-tag binding, present at the N-Terminal end, as well as binding of anti-Myc tag antibody, present at the C-terminal, of the AIDA membrane anchor (**Figure 20 C**). Together, these data suggest that, in the BL21-CRM strain, the AIDA membrane anchor with the full-length CRM fusion is present and localised to the outer surface of the *E. coli* BL21, as indicated by the presence of the His-tag at N-terminus and Myc-tag, at C-terminus, and the positive binding of the anti-CRM antibody.

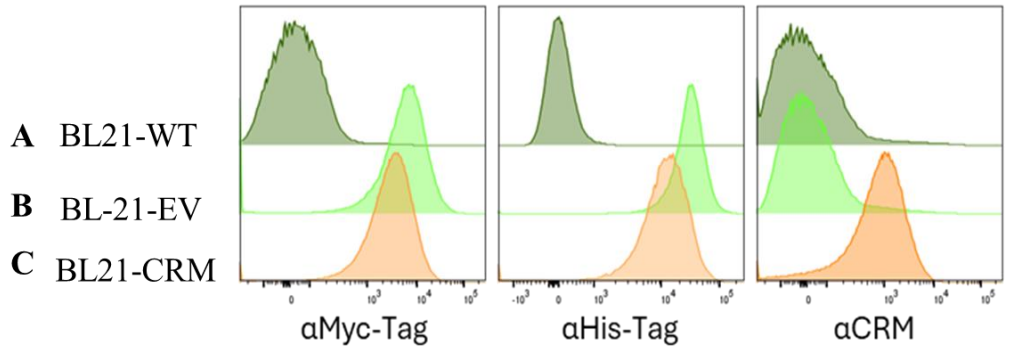

Figure 20. Flow cytometry analysis of full-length CRM protein expression in *E. coli* BL21. Wild type BL21, BL21 transformed with a pAIDA empty vector (BL21-EV) or a pAIDA plasmid encoding an AIDA-CRM fusion protein (BL21-CRM) were stained to identify epitope tags within the AIDA and the CRM proteins. Histograms showing the presence of cMyc (**A**) or His (**B**) epitope tags, or full-length CRM protein (**C**) in the indicated BL21 strains.

3.9. Effect of BL21-CRM pre-treatment on vaccine specific-antibody responses following PCV13 vaccination in mice treated with engineered *E. coli* BL21 expressing full-length CRM protein.

3.9.1. Overview of experimental plan.

My initial aim was to express the CRM in the probiotic bacterium EcN for later delivery to mice. However, we were unable to achieve expression of AIDA-CRM in EcN but were able to successfully express this fusion protein in the BL21 strain. Although BL21 is not a probiotic bacterium, like originally planned, we were able to successfully express CRM allowing progression to *in vivo* studies with this strain. To assess the ability of BL21-CRM to alter subsequent immune responses to vaccines containing the CRM antigen, mice were orally administered 1 x 10^{10} CFU of BL21-EV or BL21-CRM (n=10 mice/group). Engineered bacteria were given daily for 2 weeks to enable time for the immune system to mount a response against the administered bacteria. After two weeks, half of the BL21-EV and BL21-CRM treated mice (n=5 mice/group) were vaccinated intramuscularly with 1.5 µg of PCV13. The remaining mice were mock vaccinated with PBS (n=5 mice/group) (**Figure 21 A**). This

experimental approach enables us to determine if treatment of mice with BL21-CRM stimulates an anti-CRM response in the absence of vaccination (BL21-EV and -CRM mock treated groups) and, if present, if this response enhances subsequent vaccination (BL21-EV and -CRM PCV13 vaccinated groups). In the subsequent experiments we saw minimal differences between BL21-CRM and -EV treated, mock vaccinated, mice during our endpoint analyses, suggesting no homeostatic immune response against CRM expressed on the membrane of BL21. Therefore, this result section will largely focus on the differences between BL21-CRM and BL21-EV treated, PCV13 vaccinated mice.

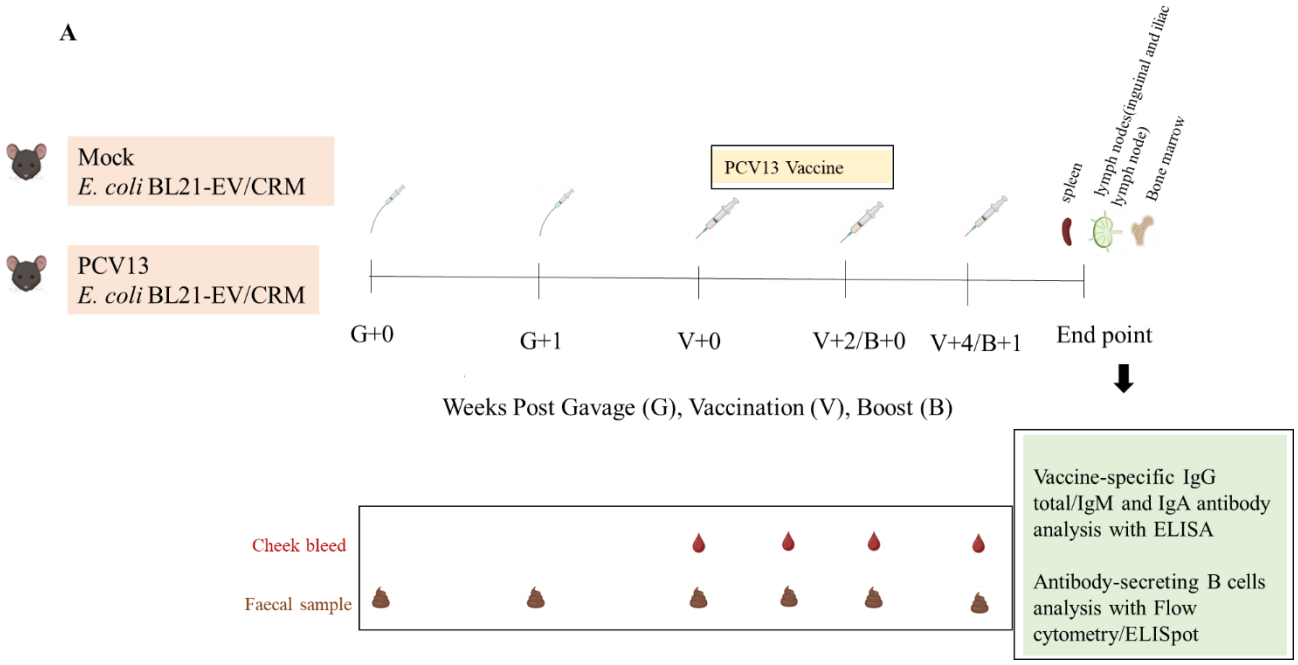

Figure 21. The experimental design used to establish whether bacteria engineered to express full-length CRM protein alter subsequent immune responses to vaccination with PCV13. 6-week old SPF mice were treated orally with 10^{10} CFU BL21-CRM or BL21-EV (n=10 mice/group) daily for two successive weeks. Mice were then vaccinated with 1.5 µg of PCV13 (n=5 per BL21 strain) or mock vaccinated with sterile saline (n=5 per BL21 strain) by intramuscular injection (i.m) at V+0-4 weeks. Cheek bleeds and faecal samples were taken weekly to assess vaccine-specific antibody responses. Two weeks post-boost, mice were euthanized and immunologically relevant organs (inguinal and iliac lymph nodes, bone marrow and spleen) were harvested and processed for endpoint analyses to assess B cell immune responses.

3.9.2. Mice treated with BL21-CRM had significantly higher IgG_{total} responses following PCV13 vaccination.

To assess systemic and mucosal PCV13-specific antibody responses in BL21 treated mice vaccinated with PCV13, peripheral blood and faecal samples were collected weekly. IgG_{total}, IgM, and faecal IgA were measured by ELISA at weeks 0-4 post-vaccination. Mice colonised with BL21-CRM exhibited a statistically significant increase in serum IgG_{total} at week 3 post-primary vaccination, relative to PCV13 vaccinated BL21-EV treated mice. However, this significant difference was lost at 4 weeks post-primary vaccination (**Figure 22 A**). These data suggest that pre-treatment with BL21-CRM transiently enhances the systemic humoral immune response to PCV13. Unexpectedly, PCV13 specific IgM antibodies in the serum were significantly higher in BL21-EV treated mice compared to the BL21-CRM treated mice at four weeks post-primary vaccination (**Figure 22 B**). These data suggest that treatment of mice with BL21-CRM may reduce IgM responses to the PCV13 vaccine. Interestingly, there was a notable increase in PCV13-specific IgM responses in mock and PCV13-immunised BL21-CRM, but not BL21-EV treated mice at V+2 weeks that disappeared from V+3. This suggest that colonisation with BL21-CRM may transiently induce CRM-specific IgM responses in the absence of PCV13 vaccine. In both PCV13-CRM and EV treated mice there was no significant difference in PCV13-specific IgA antibodies at week 3 and 4 relative to the mock group which suggests that after vaccination with PCV13, BL21-CRM treated mice do not generate a vaccine-specific mucosal IgA response, but rather a systemic immune response (**Figure 22 C**).

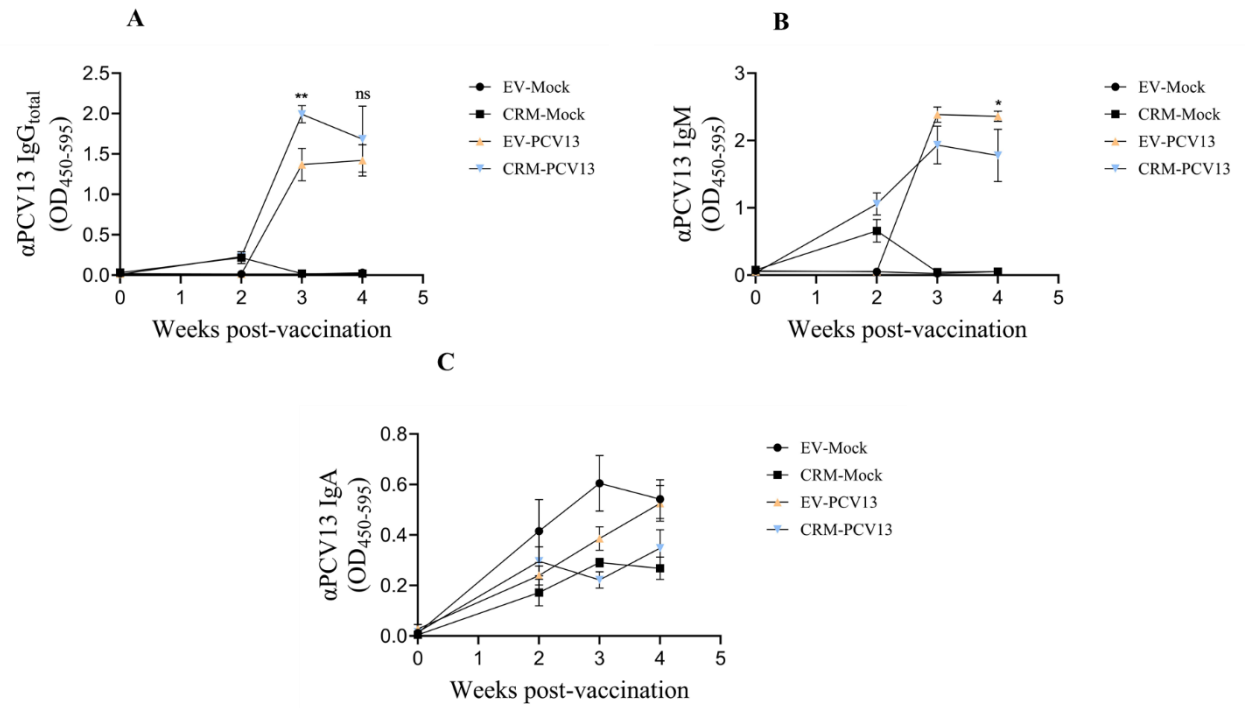

Figure 22. Significant increase in serum IgG$_{total}$ antibody responses after PCV13 vaccination in mice treated with BL21-CRM. Peripheral blood and faecal samples were collected weekly up to four weeks post-PCV13 vaccination and, PCV13-specific antibody responses in mice that were administered with engineered BL21 strains were measured by ELISA. (**A**) serum PCV13-specific IgG$_{total}$ (1:1000 dilution) titers, (**B)** PCV13-specific IgM tires (1:1000 dilution) and (**C**) faecal IgA (1:1000) titers were assessed by ELISA. Raw optical density (OD) readings from the ELISA are shown and presented as the mean ± SEM. A two-way ANOVA was used to assess statistical significance. * $p < 0.05$, ** $p < 0.01$. ns = not significant. n = 5 mice/group.

3.10. The percentage, frequency and total number of ASC B cells were significantly higher in the inguinal lymph node of BL 21-CRM treated mice.

Analysis of serum PCV13-specific antibody responses revealed small, although statistically significant, differences in the IgG and IgM response to vaccination in BL21-CRM treated mice, relative to BL21-EV. To determine if these differences were reflected in changes to B cell subsets required for humoral immune responses flow cytometry was used to quantify ASCs in different immune tissues namely the vaccine-draining inguinal and iliac lymph nodes, bone marrow, and spleen at four weeks post-initial vaccination (**Figure 23 A**). ASCs, expressed as a percentage of all $CD19^+$ B cells (hereafter referred to as percentage), or as a frequency of all live, or $CD45^+$ immune cells (hereafter referred to as frequency), were significantly higher in the inguinal lymph node of BL21-CRM treated, PCV13-vaccinated, mice (**Figure 23 B**), indicating that treating mice with the BL21-CRM strain does lead to significantly higher ASC responses in mice. In the iliac LN there was a statistically significant increase in total number of ASCs in PCV13 vaccinated mice, relative to mock vaccinated, regardless of the BL21 strain they were treated with. However, when comparing BL21-EV and BL21-CRM treated and vaccinated mice there was no statistically significant difference in percentage, frequency, or total number of ASCs controls (**Figure 23 C**). In the bone marrow, there was a near-significant increase in the percentage of ASCs ($p=0.0867$) in vaccinated mice colonized with BL21-CRM, relative to BL21-EV, suggesting that there may be greater trafficking of long-lived ASCs to the bone marrow in mice treated with BL21-CRM prior to vaccination (**Figure 23 D**). Finally, in the spleen there were no statistically significant differences in the percentage, frequency or total number of ASCs between any of the groups of mice, regardless of vaccination status (**Figure 23 E**). Together, these data suggest that recombinant bacteria expressing PCV13-derived CRM can selectively enhance the ASC response following PCV13 vaccination in the vaccine-draining inguinal lymph node.

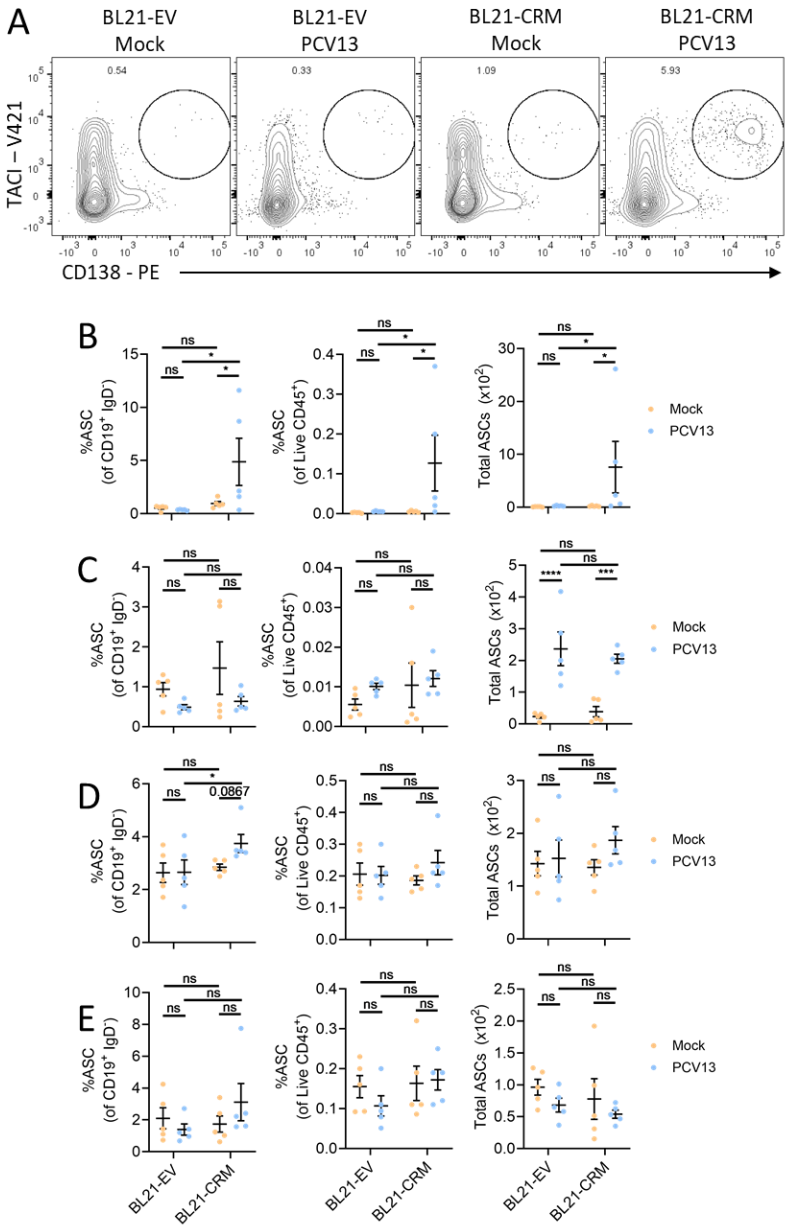

Figure 23. The percentage, frequency and total number of antibody-secreting cells (ASCs) in inguinal lymph node was significantly higher in BL21-CRM treated mice following PCV13 vaccination. Mice were treated with BL21 carrying an empty vector (BL21-EV), or expressing CRM (BL21-CRM), prior to mock vaccination or vaccination with PCV13. Four weeks after initial vaccination, the formation of (ASC) was assessed in primary and secondary lymphoid organs. (**A**) Representative flow cytometry of ASCs ($CD19^+$ IgD^- $TACI^+$ $CD138^+$ cells) in the vaccine-draining inguinal lymph nodes. (**B-E**) The frequency of ASCs among all class switched B cells ($CD19^+$ IgD^-), among all live cells, $CD45^+$ cells, and the total number of ASCs in the (**B**) inguinal lymph nodes, (**C**) iliac lymph nodes, (**D**) bone marrow, and (**E**) spleen. Data are presented as mean ± SEM. A one-way ANOVA was used to assess statistical significance. * $p < 0.05$. ns = not significant. n = 5 mice/group.

3.11. BL21-CRM treatment does not enhance the formation of germinal centre B cells following vaccination with PCV13.

Analysis of ASCs in BL21-CRM treated mice showed a significant increase in ASC populations in select organs of these mice after PCV13 vaccination. As ASCs are a B cell subset that are produced in the germinal centre reaction, we next analysed the formation of germinal B cells (GCBs) in secondary lymphoid organs in response to vaccination (**Figure 24 A**). In both the inguinal and iliac LN there was a dramatic increase in the percentage, frequency and total number of GCBs in PCV13 vaccinated mice, relative to mock (**Figure 24 B-C**). However, when comparing the GCB response between BL21-EV and BL21-CRM treated and vaccinated mice, there was no statistically significant difference in the percentage, frequency, or total number of GCB cells (**Figure 24 B-C**). In contrast to the vaccine-draining lymph nodes, the spleens of PCV13 vaccinated mice exhibited only a minor increase in percentage, frequency and total number of GCB cells, relative to mock vaccinated mice (**Figure 24 D**). Furthermore, the percentage, frequency and total number of GCB cells in the spleen was not significantly different in PCV13-vaccinated mice that were treated with the BL21-CRM strain compared to those treated with BL21-EV control strain. Together the distribution of GCBs across secondary lymphoid organs of vaccinated mice suggests that, when administered intramuscularly, PCV13 vaccination drives robust germinal centre responses in the draining lymph nodes, but little to no PCV13 drains to the spleen to fuel a germinal centre reaction there. These data suggest that treatment of mice with BL21-EV and BL21-CRM had no impact on the formation of GCBs, a critical part of adaptive immune response specifically in antibody producing cells.

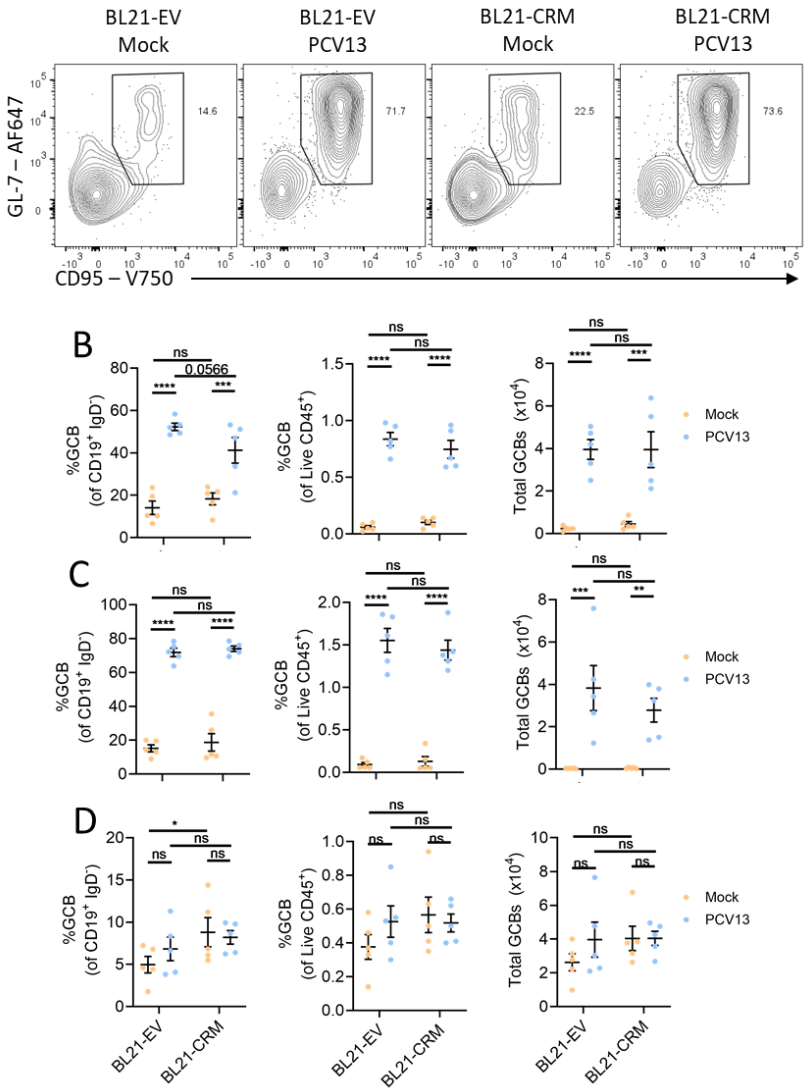

Figure 24. No statistically significant difference in the proportion of germinal B cells in mice treated with BL21-EV and BL21-CRM, following PCV13 vaccination. Mice were treated with BL21 carrying an empty vector (BL21-EV), or expressing CRM (BL21-CRM), prior to mock vaccination or vaccination with PCV13. Four weeks after initial vaccination the formation of germinal centre B cells (GCBs) was assessed in vaccine-draining secondary lymphoid organs. (**A**) Representative flow cytometry of GCBs ($CD19^+$ IgD^- $TACI^-$ $CD138^-$ $GL\text{-}7^+$ $CD95^+$) in the vaccine-draining iliac lymph nodes. (**B-D**) The frequency of GCBs among all class switched B cells ($CD19^+$ IgD^-), among all live cells, $CD45^+$ cells, and the total number of GCB cells in the (**B**) inguinal lymph nodes, (**C**) iliac lymph nodes, and (**D**) spleen. Data are presented as mean ± SEM. A one-way ANOVA was used to assess statistical significance. * $p < 0.05$, *** $p < 0.001$, **** $p < 0.0001$. ns = not significant. n = 5 mice/group.

3.12. No statistically significant difference in the CRM-specific germinal centre B cells in BL21-CRM treated mice following PCV13 vaccination.

Although BL21-CRM treatment had no significant impact on the formation of GCB cells following PCV13 vaccination (**Figure 21**), this assessment was performed on antigen-agnostic GCBs. However, pre-treatment with BL21-CRM is most likely to promote the development of CRM-specific B cells that may be more likely to enter the germinal centre reaction. Therefore, profiling CRM-specific GCBs, as opposed to all GCBs as performed previously, may reveal antigen-specific differences in BL21-CRM treated and vaccinated mice, relative to BL21-EV. To do this, we used a fluorescently labelled CRM protein that binds to the B cell receptor of CRM-specific B cells, enabling their identification by flow cytometry (**Figure 25 A**). Although we saw a statistically significant increase in the frequency of CRM-specific GCBs among all GCBs in PCV13 vaccinated mice, relative to mock, there was no significant difference between BL21-EV and BL21-CRM treated and vaccinated mice in the percentage and total number in the draining lymph nodes, or spleen (**Figure 25 B-D**). These data suggest that BL21-CRM treatment does not enhance CRM-specific GCB formation when compared to BL21-EV treatment even after vaccination with PCV13. This outcome indicates that CRM antigen expressed by *E. coli* BL21 does not contribute to the formation of GCB in the vaccine draining lymphoid organs.

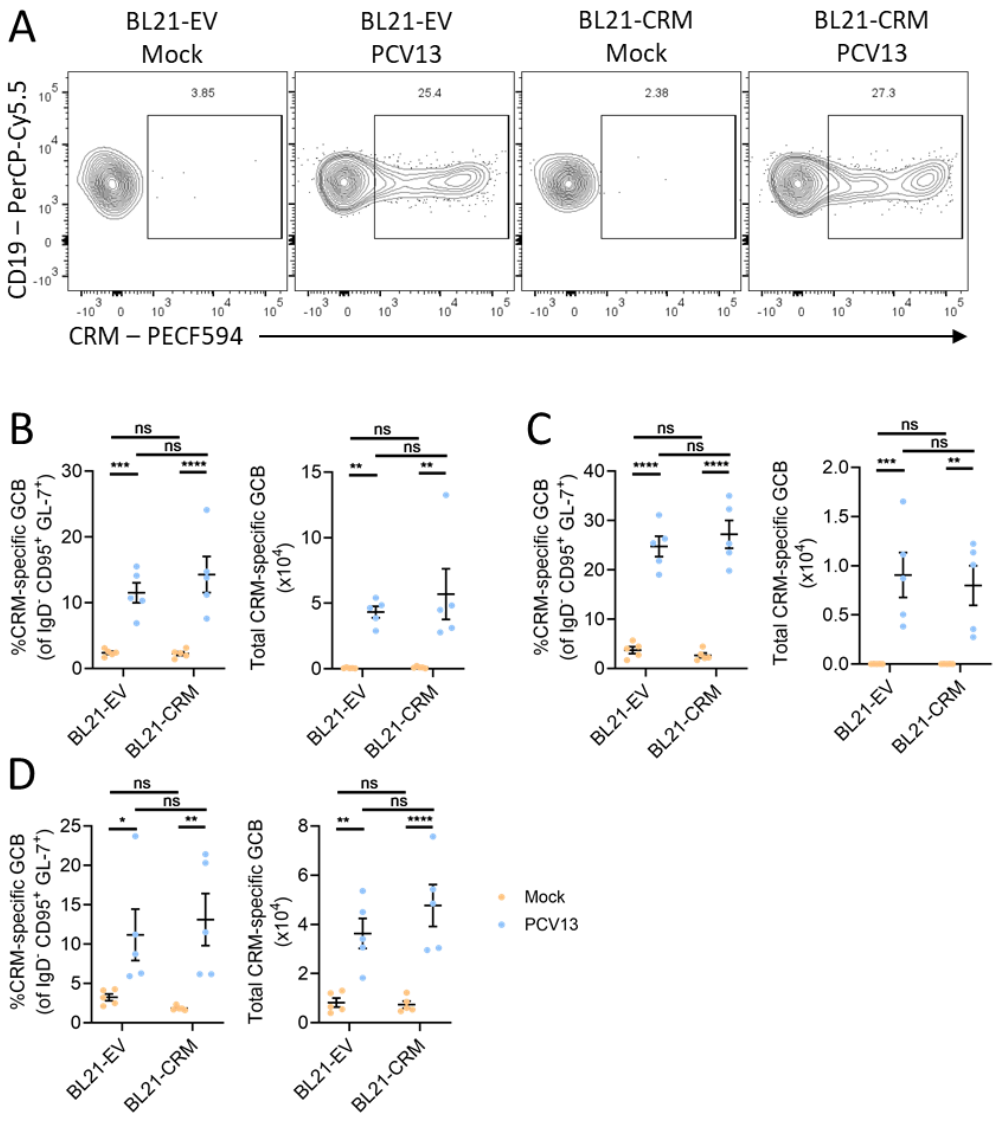

Figure 25. No significant differences in the proportion of CRM-specific germinal centre B cells in BL21-EV or BL21-CRM treated mice, following PCV13 vaccination. Mice were treated with BL21 carrying an empty vector (BL21-EV), or expressing CRM (BL21-CRM), prior to mock vaccination or vaccination with PCV13. Four weeks after initial vaccination the formation of CRM-specific germinal centre B cells (GCBs) in vaccine-draining secondary lymphoid organs was assessed using fluorescent CRM probes. (**A**) Representative flow cytometry analysis of CRM-specific GCBs ($CD19^+$ IgD^- $TACI^-$ $CD138^-$ $GL\text{-}7^+$ $CD95^+$ CRM^+) in the vaccine-draining iliac lymph nodes. (**B-D**) The frequency of CRM-specific GCBs among all class switched B cells ($CD19^+$ IgD^-), among all live cells, $CD45^+$ cells, and the total number of CRM-specific GCBs in the (**B**) inguinal lymph nodes, (**C**) iliac lymph nodes, and (**D**) spleen. Data are presented as mean ± SEM. A one-way ANOVA was used to assess statistical significance. * $p < 0.05$, ** $p < 0.01$, *** $p < 0.001$, **** $p < 0.0001$. ns = not significant. n = 5 mice/group.

3.13. Significant reduction in percentage, frequency and total number of memory B cells in spleen of BL 21-CRM treated mice, following vaccination with PCV13.

Finally, the formation of memory B cells (Bmems) following BL21 treatment and PCV13 vaccination was assessed in inguinal and iliac lymph nodes, and spleen (**Figure 26 A**). In the draining lymph nodes of vaccinated mice Bmems, as a percentage of all $CD19^+$ B cells, demonstrated a significant decrease, relative to mock vaccinated mice (**Figure 26 B-C**). This likely reflects the dramatic increase in GCB cells, as a percentage of all B cells, seen in the draining lymph nodes (**Figure 24 B-C**), which is in turn reducing the Bmems population as a percentage of all B cells. Although there was a small increase in the frequency and total number of Bmem cells in the inguinal LNs of BL21 treated, PCV13 vaccinated mice, relative to mock vaccinated, there was no statistical significance difference between BL21-EV and BL21-CRM vaccinated mice (**Figure 26 B**). Similarly, in the iliac lymph nodes, there were no statistically significant differences in the percentage, frequency or total number of Bmems between BL21-EV and BL21-CRM treated and vaccinated mice (**Figure 26 C**). In the spleens of BL21-CRM treated, PCV13 vaccinated, mice there was a statistically significant reduction in the percentage, frequency and total number of Bmem cells, relative to BL21-EV treated mice (**Figure 26 D**). These data suggest that treatment with BL21-CRM might significantly impair Bmems formation in response to PCV13 vaccination and thus potentially lead to a suppressed immune response. Therefore, CRM antigen expressed by BL21 does seem to have an impact on the Bmems cell compartment four weeks post-initial vaccination, particularly in the spleen, although this effect is not desirable in the context of enhancing immune memory.

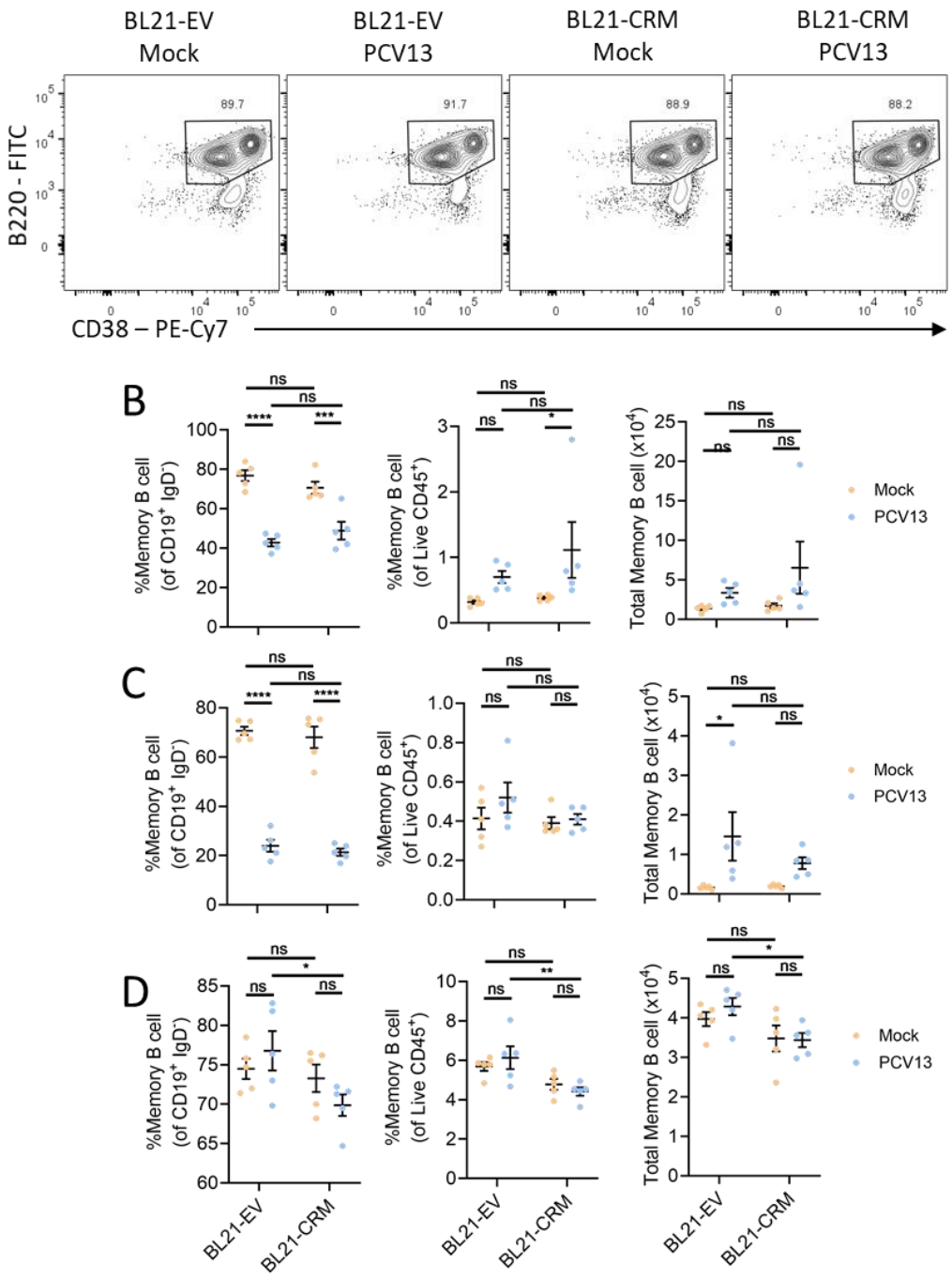

Figure 26. **Significant reduction in percentage, frequency and total number of memory B cells in spleen of BL 21 -CRM treated mice, following vaccination with PCV13.** Mice were treated with BL21 carrying an empty vector (BL21-EV), or expressing CRM (BL21-CRM), prior to mock vaccination or vaccination with PCV13. Four weeks after initial vaccination the formation of Memory B cells (Bmems) was assessed in vaccine-draining secondary lymphoid organs. (**A**) Representative flow cytometry of Bmems ($CD19^+$ IgD^- $TACI^-$ $CD138^-$ $GL\text{-}7^-$ $CD95^-$ $CD38^+$) in the spleen. (**B-D**) The frequency of Bmems among all class switched B cells ($CD19^+$ IgD^-), among all live cells, $CD45^+$ cells, and the total number of Bmems in the (**B**) inguinal lymph nodes, (**C**) iliac lymph nodes, and (**D**) spleen. Data are presented as mean ± SEM. A one-way ANOVA was used to assess statistical significance. * $p < 0.05$, ** $p < 0.01$, *** $p < 0.001$, **** $p < 0.0001$. ns = not significant. n = 5 mice/group.

Conclusion

After engineering *E. coli* BL21 strains to express CRM protein on the outer membrane I aimed to determine if the expressed antigen has an impact on the immune responses following PCV13 vaccination. Daily oral gavage of the engineered bacteria was performed for two weeks followed by PCV13 vaccination. Results showed a significant, albeit transient, enhancement in IgG response in mice treated with BL21-CRM along with an increase in formation of antibody secreting cells (ASC) in the vaccine-draining inguinal lymph node. Additionally, treatment had no impact in germinal centre B cells response. Likewise, there was also a reduction in memory B cells particularly in the spleen. These findings suggest that recombinant bacteria that expressed BL-21-CRM in *E. coli* can potentially modulate vaccine induce immunity more specifically a systemic humoral immune response, although the effect is marginal.

Chapter 4. Discussion

For reasons that are still poorly understood, immune responses to vaccination frequently vary between individuals, with some people mounting suboptimal immune responses, that leave them susceptible to infections. Therefore, developing interventions or therapeutics to enhance these responses would be an enormous public health benefit. In this study, I aimed to address this by cloning and expressing vaccine-derived antigens in the cytoplasm of a probiotic bacteria to assess whether these engineered microbes could be used to prime the immune system, prior to vaccination, and subsequently enhance vaccine-specific cellular and humoral responses in mice following intramuscular vaccination.

My study demonstrated that oral administration of a probiotic strain of *Escherichia coli*, *E. coli* Nissle, engineered to express immunodominant peptides derived from the model antigen ovalbumin (EcN-Ova ^{Cyto}), significantly enhanced Ova-specific Immunoglobulin (Ig) G titres in the serum following vaccination with an mRNA-Ova vaccine. Vaccine-specific titres were significantly higher at 3-4 weeks post-vaccination, compared to mice orally administered an empty vector control strain. Consistent with this observation, there was a significant increase in IgG Ova-specific antibody secreting cells in the spleen of EcN-Ova ^{Cyto} treated mice, relative to control mice, as measured by Enzyme-linked immunosorbent spot (ELISpot) analysis. Additionally, Ova-specific IgA antibody titres in faecal samples were significantly higher in EcN-Ova ^{Cyto} treated mice from 2-weeks post-vaccination. The presence of IgA antibodies in the faecal homogenates of mRNA-Ova vaccinated mice, regardless of the *Escherichia coli* Nissle (EcN) strain they were pre-treated with, is surprising, given that this vaccine is administered intramuscularly (i.m.) and the generation of antigen-specific IgA is usually associated with orally ingested antigen (Cerutti, 2008). Given this, future experiments should investigate the presence of vaccine-specific IgA at other mucosal sites, such as the respiratory and urogenital tracts, to determine if this phenomenon is restricted to the gastrointestinal tract or spread throughout the body. Regardless, prior exposure to antigen within mucosal tissue can generate antigen-specific IgA responses that are enhanced by subsequent i.m. vaccination, (Sano et al., 2022), and is likely what is observed in EcN-Ova ^{cyto} treated mice.

Increased Ova-specific antibodies in the serum and faeces results from increased antibody secreting cells activity which, in turn, is likely a result of increased germinal centre B activity. Flow cytometry analysis of germinal centre B cells in the spleen of EcN-Ova ^{Cyto} treated mice supported the idea that pre-treatment with the engineered bacteria facilitated their

enhanced differentiation into germinal centre B cells within the spleen. Moreover, a slight but significant increase in memory B cells was observed in the iliac lymph nodes, suggesting that B cell activation and germinal centre B cell differentiation may have led to enhanced memory B cell formation in this organ. These results indicate enhanced B cell activation following EcN-Ova ^{cyto} treatment and mRNA-Ova vaccination. However, the *E. coli* Nissle bacteria was only engineered to express peptides that would activate T cells, $Ova_{257-246}$ and $Ova_{323-339}$, and are not epitopes known to drive B cell activation. It is therefore likely that treatment with EcN-Ova ^{cyto} does not directly activate B cells, but rather may drive the activation of T follicular helper (Tfh) cells which, after mRNA-Ova vaccination, may provide enhanced help to naïve B cells responding to Ova to promote their differentiation into germinal centre B cells. This enhancement of the GC reaction would result in further differentiation into Ova-specific antibody secreting B cells leading to higher levels of IgG and IgA in the serum and faeces. These observations provide direct support to the hypothesis of "cross-reactive epitopes" present within the intestinal microbiota that can prime an immune response that cross-reacts with, and alters the outcome of, antigen-specific vaccination. This hypothesis suggested that certain pathogen-specific T cell clones bearing an antigen-experienced phenotype in the circulation of healthy humans had been activated by pathogen-like epitopes present in intestinal microbes, rather than during direct pathogen infection (Su et al., 2013, Lynn et al., 2022). Whether these microbiota-induced, cross-reactive, T cells could influence subsequent immune responses to infection or vaccination is unclear, despite attempts to address this question in several human studies (Lynn et al., 2022 , Pan et al., 2021, Saggau et al., 2022). The data present here suggest that these cross-reactive cells are primed in mice treated with bacteria expressing vaccine-derived antigens, and that these cells have a positive impact on vaccination in the form of enhanced humoral responses post-vaccination.

However, in the present study, the generation of $Ova_{323-339}$ cross-reactive $CD4^+$ T cell following EcN-Ova ^{cyto} treatment was not experimentally confirmed. To formally assess this, future experiments could use $Ova_{323-339}$ loaded major histocompatibility complex (MHC)-II tetramers to measure Ova-specific $CD4^+$ T cells following treatment and vaccination to determine if pre-treatment of mice with EcN-Ova ^{cyto} enhances the generation of Ova-specific T follicular helper cells. Together, these findings align with my initial hypothesis that EcN-Ova ^{Cyto}-treated mice would exhibit significant changes in vaccine outcomes, particularly in terms of eliciting a humoral response and enhancing the immunogenicity of the Ova-mRNA vaccine.

However, although successful, one limitation of this approach is that only two peptides, rather than the full-length protein, were expressed. This limits activation of immune cells to specific T cell clones, and is unlikely to directly drive activation of B cells. Furthermore, expression of the peptides was confined to the cytoplasm of the probiotic bacteria, which may have made it more difficult for the immune system to recognize the antigen (Chen et al., 2023 , Pedersen et al., 2022). To address these limitations, and potentially generate an engineered bacterium that drives better immune cell activation and even greater enhancement of vaccine-specific immune responses, I extended the approach of engineering a probiotic bacterium to express full length immunogenic proteins on the surface of EcN for enhancing vaccine efficiency. Building on this foundation, I hypothesized that cloning and engineering EcN to express the full-length cross-reactive material (CRM) protein, a carrier protein used in conjugate vaccines, could induce both B cell mediated humoral and cell mediated immune responses and enhance the effectiveness of the CRM-containing pneumococcal conjugate vaccine 13-valent (PCV13).

After successful assembly of the Adhesin Involved in Diffuse Adherence (AIDA) plasmid construct pAIDA-CRM, I evaluated the surface expression of full-length CRM protein in EcN transformed with the pAIDA-CRM vector. However, initial results revealed an unexpected absence of cross-reactive material protein localised to the outer membrane, despite the presence of the AIDA protein in the membrane to which CRM should have been fused. EcN expresses some proteases that are known to degrade recombinant expressed proteins and may have been responsible for the loss of surface-expressed CRM (Redenti et al., 2024). To confirm this hypothesis, I decided to use another strain of *E. coli*, namely *E. coli* BL21, which is genetically modified to remove key proteases, lon and OmpT, (Du et al., 2021), that may have been cleaving the cross-reactive material protein from the surface of EcN. Results indicated that this strain provided a more favourable environment for recombinant protein expression, minimizing the risk of degradation. Expression in BL21 showed a significant increase in fluorescence intensity for antibodies targeting both His and Myc tags, and the CRM protein itself, indicating that the Adhesin Involved in Diffuse Adherence membrane anchor and CRM protein were correctly expressed.

Next, I investigated the impact of BL21-CRM treatment on humoral immune responses to the PCV13 vaccine, which uses CRM197 as a carrier protein. The data demonstrated that pre-treatment with BL21-CRM led to a significant increase in total IgG levels three weeks post-vaccination, suggesting that BL21-CRM does, in fact, act as an immunogenic vector that

enhances systemic humoral responses to PCV13. However, in contrast to the earlier experiments with EcN-Ova ^{Cyto} treated mice, this significant increase was transient, as IgG levels dropped by the fourth week, indicating a short-lived enhancement of the humoral response. I also observed a decrease in IgM titres at weeks 3 and 4 in the BL21-CRM treated mice, that may suggest a delay in the class-switching mechanism necessary for generating high-affinity IgG antibodies post-PCV13 vaccination. While analysis of IgA in the faeces revealed no increase in PCV13-specific IgA in vaccinated mice, relative to mock, suggesting that, unlike mRNA-Ova vaccination, i.m. PCV13 vaccination does not induce a mucosal antibody response. Further analysis of B cell subsets with flow cytometry revealed only minimal differences in B cell activation in BL21-CRM treated and vaccinated mice, relative to BL21-EV. The only differences in BL21-CRM treated mice that were consistent were an increase in antibody secreting B cells in the inguinal lymph nodes, and a decrease in memory B cells in the spleen. Why the antibody secreting cell response was selectively enhanced in the inguinal lymph nodes is not clear, but this might be because the inguinal lymph nodes drain the lower part of extremities, and given the route of vaccination (i.m.), immune cell activation will be higher in inguinal compared to iliac lymph nodes. This increased ASC activity in this organ may also explain the elevated IgG levels seen in the serum of the mice. However, treatment seems to have had no impact in formation of CRM-specific germinal centre B cells, the precursor cells from which antibody secreting B cells and memory B cells eventually differentiate (Hamel et al., 2012). Therefore, given my hypothesis, BL21-CRM did provide a transiently enhanced systemic immune response, although with no mucosal immune response. However, this effect was minimal relative to the effect provided by EcN-Ova ^{cyto} and further refinement of the approach would be required for a full effect.

Differences between Ova ^{Cyto} and CRM model

Escherichia coli 1917 (EcN) a probiotic strain known for its ability to colonize the gut and interact with the mucosal immune system. In contrast, Escherichia coli BL21 is primarily used for the efficient production of recombinant protein production and is not typically used to colonise mice and is not known for its immunomodulatory capacity *in vivo*. This is likely why the EcN had a much stronger impact on the immune system following vaccination, as the mucosal priming by EcN, prior to vaccination, was greater using this strain. Although this immune priming would need to be formally assessed, as described earlier. However, the

enhancing of the IgA response in mRNA-Ova vaccinated, EcN-Ova ^{cyto} treated, mice strongly suggest some degree of mucosal priming. An additional source of variation could be derived from the nature of the vaccines used, and the vaccine-derived antigen expressed in bacteria. Epitopes from the Ova-mRNA vaccine were expressed in EcN, and ELISAs measured immune responses to the full antigen from which the epitope was sourced. However, in BL21 the carrier protein CRM was expressed, and ELISAs measured humoral responses toward the whole PCV13 vaccine, which includes CRM, but also 13 unique polysaccharides. While we still expect the polysaccharide-specific response to be enhanced, through the induction of CRM-specific helper cells, as described earlier, it is possible that only the CRM-specific response was enhanced and that signal is being 'lost' among the polysaccharide-specific response. It would be worthwhile to measure the CRM-specific response alone, to see if this was enhanced in BL21-CRM treated mice. Although the flow cytometry data using CRM-probes suggests that it may not be altered.

Limitations

This study was conducted over a relatively short period, and I believe longer-term studies are needed to assess the efficiency and durability of the bacteria-enhanced vaccine-specific immune responses. Furthermore, the small number of mice per group may have limited the statistical power to detect subtle differences in immune responses, particularly in secondary lymphoid organs (n = 4 or 5 per group) and, at a minimum, an independent repeat should be performed. Additionally, the *E. coli* BL21 strain used in the second *in vivo* experiment is not naturally part of the gut microbiome and may have a shorter persistence time, which could limit the duration of antigen presentation. These bacteria are also not known to be immunomodulatory, which may have led to suboptimal immune responses. Moreover, the analysis of GCB cells and memory B cells in mRNA-Ova vaccinated mice is somewhat limited as it was performed on all host B cells, which would include B cells not specific for the Ova protein. These Ova-specific B cells could have been better captured with the use of fluorescent Ova probes, potentially revealing more subtle differences in secondary lymphoid organs.

Future directions

Although the engineered *Escherichia coli* Nissle strain was successful in enhancing Ova-specific vaccine responses, future work could explore the use of other probiotics strains known for immunomodulatory activity such as *Lactobacillus* or *Bifidobacterium*, which may enhance this effect. Additionally, we could focus on exploring other anchoring or fusion proteins that might improve surface expression of antigens. We could also explore assessing for cell-mediated immunity (T cells) using tetramers or *in vitro* peptide stimulations to assess their formation and activity following administration of engineered bacteria and vaccination. If addressed, these alterations could improve the impact of these engineered microbes and lead to clinical trials in humans to assess their impact when combined with vaccination on the human immune system.

While the administration of genetically modified bacteria to humans may seem unlikely, numerous studies have demonstrated the potential of engineered bacteria for the benefit of human health in a clinical setting. One Phase I study evaluated a genetically engineered strain of *Lactococcus lactis* to deliver trefoil factor 1 (TFF1) to help reduce or prevent oral mucositis caused by chemotherapy (Limaye et al., 2013). In another study *Listeria monocytogenes* was engineered as a cervical cancer vaccine where the human papilloma virus (HPV) E7 protein was fused to Listeria protein listerolysin O (LLO) to stimulate a robust immune response targeting HPV cancer cells and prevent tolerance (Galicia-Carmona et al., 2021). In another Phase 1 study, researchers genetically modified *E. coli* to breakdown phenylalanine (Phe) in humans with a genetic defect in Phe metabolism, reducing Phe levels in blood and alleviating disease symptoms (Puurunen et al., 2021). Together, these examples highlight the growing trend of engineered bacteria used for palliative, prophylactic, or curative purposes in a clinical setting.

Clinical implications

If further developed, these studies have the potential in enhancing not only mucosal immunity, but cell mediated immunity, thereby reducing morbidity and disease transmission particularly in individuals that respond sub optimally to vaccines such as the elderly, infants, or immunocompromised individuals. Using these engineered probiotics has the potential to be safe and cheap way of effectively enhancing vaccine mediate protection against infectious diseases, or even be used to retain vaccine-induced immunity in the months post-vaccination.

References

Agrawal, B. (2019). Heterologous Immunity: Role in Natural and Vaccine-Induced Resistance to Infections. *Front Immunol*, *10*, 2631. https://doi.org/10.3389/fimmu.2019.02631

Al Nabhani, Z., Dulauroy, S., Marques, R., Cousu, C., Al Bounny, S., Dejardin, F., Sparwasser, T., Berard, M., Cerf-Bensussan, N., & Eberl, G. (2019). A Weaning Reaction to Microbiota Is Required for Resistance to Immunopathologies in the Adult. *Immunity*, *50*(5), 1276-1288 e1275. https://doi.org/10.1016/j.immuni.2019.02.014

Atarashi, K., Tanoue, T., Shima, T., Imaoka, A., Kuwahara, T., Momose, Y., Cheng, G., Yamasaki, S., Saito, T., Ohba, Y., Taniguchi, T., Takeda, K., Hori, S., Ivanov, II, Umesaki, Y., Itoh, K., & Honda, K. (2011). Induction of colonic regulatory T cells by indigenous Clostridium species. *Science*, *331*(6015), 337-341. https://doi.org/10.1126/science.1198469

Bacher, P., Rosati, E., Esser, D., Martini, G. R., Saggau, C., Schiminsky, E., Dargvainiene, J., Schroder, I., Wieters, I., Khodamoradi, Y., Eberhardt, F., Vehreschild, M., Neb, H., Sonntagbauer, M., Conrad, C., Tran, F., Rosenstiel, P., Markewitz, R., Wandinger, K. P.,…Scheffold, A. (2020). Low-Avidity CD4(+) T Cell Responses to SARS-CoV-2 in Unexposed Individuals and Humans with Severe COVID-19. *Immunity*, *53*(6), 1258-1271 e1255. https://doi.org/10.1016/j.immuni.2020.11.016

Bartolo, L., Afroz, S., Pan, Y. G., Xu, R., Williams, L., Lin, C. F., Tanes, C., Bittinger, K., Friedman, E. S., Gimotty, P. A., Wu, G. D., & Su, L. F. (2022). SARS-CoV-2-specific T cells in unexposed adults display broad trafficking potential and cross-react with commensal antigens. *Sci Immunol*, *7*(76), eabn3127. https://doi.org/10.1126/sciimmunol.abn3127

Bemark, M., & Angeletti, D. (2021). Know your enemy or find your friend?-Induction of IgA at mucosal surfaces. *Immunol Rev*, *303*(1), 83-102. https://doi.org/10.1111/imr.13014

Bennek, E., Mandic, A. D., Verdier, J., Roubrocks, S., Pabst, O., Van Best, N., Benz, I., Kufer, T., Trautwein, C., & Sellge, G. (2019). Subcellular antigen localization in commensal E. coli is critical for T cell activation and induction of specific tolerance. *Mucosal Immunol*, *12*(1), 97-107. https://doi.org/10.1038/s41385-018-0061-0

Blum, J. E., Kong, R., Schulman, E. A., Chen, F. M., Upadhyay, R., Romero-Meza, G., Littman, D. R., Fischbach, M. A., Nagashima, K., & Sattely, E. S. (2024). Discovery and characterization of dietary antigens in oral tolerance. *bioRxiv*. https://doi.org/10.1101/2024.05.26.593976

Bondareva, M., Budzinski, L., Durek, P., Witkowski, M., Angermair, S., Ninnemann, J., Kreye, J., Letz, P., Ferreira-Gomes, M., Semin, I., Guerra, G. M., Momsen Reincke, S., Sanchez-Sendin, E., Yilmaz, S., Sempert, T., Heinz, G. A., Tizian, C., Raftery, M., Schonrich, G.,…Kruglov, A. A. (2023). Cross-regulation of antibody responses against the SARS-CoV-2 Spike protein and commensal microbiota via molecular mimicry. *Cell Host Microbe*, *31*(11), 1866-1881 e1810. https://doi.org/10.1016/j.chom.2023.10.007

Bousbaine, D., Bauman, K. D., Chen, Y. E., Yu, V. K., Lalgudi, P. V., Naziripour, A., Veinbachs, A., Phung, J. L., Nguyen, T. T. D., Swenson, J. M., Lee, Y. E., Dimas, A., Jain, S., Meng, X., Pham, T. P. T., Zhao, A., Barkal, L., Gribonika, I., Van Rompay, K. K. A.,…Fischbach, M. A. (2024). Discovery and engineering of the antibody response against a prominent skin commensal. *bioRxiv*. https://doi.org/10.1101/2024.01.23.576900

Cerutti, A. (2008). The regulation of IgA class switching. *Nat Rev Immunol*, *8*(6), 421-434. https://doi.org/10.1038/nri2322

Chen, Y. E., Bousbaine, D., Veinbachs, A., Atabakhsh, K., Dimas, A., Yu, V. K., Zhao, A., Enright, N. J., Nagashima, K., Belkaid, Y., & Fischbach, M. A. (2023). Engineered skin bacteria induce antitumor T cell responses against melanoma. *Science*, *380*(6641), 203-210. https://doi.org/10.1126/science.abp9563

Ciabattini, A., Nardini, C., Santoro, F., Garagnani, P., Franceschi, C., & Medaglini, D. (2018). Vaccination in the elderly: The challenge of immune changes with aging. *Semin Immunol*, *40*, 83-94. https://doi.org/10.1016/j.smim.2018.10.010

Cubillos-Ruiz, A., Guo, T., Sokolovska, A., Miller, P. F., Collins, J. J., Lu, T. K., & Lora, J. M. (2021). Engineering living therapeutics with synthetic biology. *Nat Rev Drug Discov*, *20*(12), 941-960. https://doi.org/10.1038/s41573-021-00285-3

De Silva, N. S., & Klein, U. (2015). Dynamics of B cells in germinal centres. *Nat Rev Immunol*, *15*(3), 137-148. https://doi.org/10.1038/nri3804

DiazGranados, C. A., Dunning, A. J., Kimmel, M., Kirby, D., Treanor, J., Collins, A., Pollak, R., Christoff, J., Earl, J., Landolfi, V., Martin, E., Gurunathan, S., Nathan, R., Greenberg, D. P., Tornieporth, N. G., Decker, M. D., & Talbot, H. K. (2014). Efficacy of high-dose versus standard-dose influenza vaccine in older adults. *N Engl J Med*, *371*(7), 635-645. https://doi.org/10.1056/NEJMoa1315727

Du, F., Liu, Y. Q., Xu, Y. S., Li, Z. J., Wang, Y. Z., Zhang, Z. X., & Sun, X. M. (2021). Regulating the T7 RNA polymerase expression in E. coli BL21 (DE3) to provide more host options for recombinant protein production. *Microb Cell Fact*, *20*(1), 189. https://doi.org/10.1186/s12934-021-01680-6

Fluckiger, A., Daillere, R., Sassi, M., Sixt, B. S., Liu, P., Loos, F., Richard, C., Rabu, C., Alou, M. T., Goubet, A. G., Lemaitre, F., Ferrere, G., Derosa, L., Duong, C. P. M., Messaoudene, M., Gagne, A., Joubert, P., De Sordi, L., Debarbieux, L.,…Zitvogel, L. (2020). Cross-reactivity between tumor MHC class I-restricted antigens and an enterococcal bacteriophage. *Science*, *369*(6506), 936-942. https://doi.org/10.1126/science.aax0701

Galicia-Carmona, T., Arango-Bravo, E., Serrano-Olvera, J. A., Flores-de La Torre, C., Cruz-Esquivel, I., Villalobos-Valencia, R., Moran-Mendoza, A., Castro-Eguiluz, D., & Cetina-Perez, L. (2021). ADXS11-001 LM-LLO as specific immunotherapy in cervical cancer. *Hum Vaccin Immunother*, *17*(8), 2617-2625. https://doi.org/10.1080/21645515.2021.1893036

Hagan, T., Cortese, M., Rouphael, N., Boudreau, C., Linde, C., Maddur, M. S., Das, J., Wang, H., Guthmiller, J., Zheng, N. Y., Huang, M., Uphadhyay, A. A., Gardinassi, L., Petitdemange, C., McCullough, M. P., Johnson, S. J., Gill, K., Cervasi, B., Zou, J.,…Pulendran, B. (2019). Antibiotics-Driven Gut Microbiome Perturbation Alters Immunity to Vaccines in Humans. *Cell*, *178*(6), 1313-1328 e1313. https://doi.org/10.1016/j.cell.2019.08.010

Hamel, K. M., Liarski, V. M., & Clark, M. R. (2012). Germinal center B-cells. *Autoimmunity*, *45*(5), 333-347. https://doi.org/10.3109/08916934.2012.665524

Hapfelmeier, S., Lawson, M. A., Slack, E., Kirundi, J. K., Stoel, M., Heikenwalder, M., Cahenzli, J., Velykoredko, Y., Balmer, M. L., Endt, K., Geuking, M. B., Curtiss, R., 3rd, McCoy, K. D., & Macpherson, A. J. (2010). Reversible microbial colonization of

germ-free mice reveals the dynamics of IgA immune responses. *Science*, *328*(5986), 1705-1709. https://doi.org/10.1126/science.1188454

Harris, V., Ali, A., Fuentes, S., Korpela, K., Kazi, M., Tate, J., Parashar, U., Wiersinga, W. J., Giaquinto, C., de Weerth, C., & de Vos, W. M. (2018). Rotavirus vaccine response correlates with the infant gut microbiota composition in Pakistan. *Gut Microbes*, *9*(2), 93-101. https://doi.org/10.1080/19490976.2017.1376162

Harris, V. C., Armah, G., Fuentes, S., Korpela, K. E., Parashar, U., Victor, J. C., Tate, J., de Weerth, C., Giaquinto, C., Wiersinga, W. J., Lewis, K. D., & de Vos, W. M. (2017). Significant Correlation Between the Infant Gut Microbiome and Rotavirus Vaccine Response in Rural Ghana. *J Infect Dis*, *215*(1), 34-41. https://doi.org/10.1093/infdis/jiw518

Hassan, S., Keshavarz-Moore, E., & Ward, J. (2016). A cell engineering strategy to enhance supercoiled plasmid DNA production for gene therapy. *Biotechnol Bioeng*, *113*(9), 2064-2071. https://doi.org/10.1002/bit.25971

Hegazy, A. N., West, N. R., Stubbington, M. J. T., Wendt, E., Suijker, K. I. M., Datsi, A., This, S., Danne, C., Campion, S., Duncan, S. H., Owens, B. M. J., Uhlig, H. H., McMichael, A., Oxford, I. B. D. C. I., Bergthaler, A., Teichmann, S. A., Keshav, S., & Powrie, F. (2017). Circulating and Tissue-Resident CD4(+) T Cells With Reactivity to Intestinal Microbiota Are Abundant in Healthy Individuals and Function Is Altered During Inflammation. *Gastroenterology*, *153*(5), 1320-1337 e1316. https://doi.org/10.1053/j.gastro.2017.07.047

Isabella, V. M., Ha, B. N., Castillo, M. J., Lubkowicz, D. J., Rowe, S. E., Millet, Y. A., Anderson, C. L., Li, N., Fisher, A. B., West, K. A., Reeder, P. J., Momin, M. M., Bergeron, C. G., Guilmain, S. E., Miller, P. F., Kurtz, C. B., & Falb, D. (2018). Development of a synthetic live bacterial therapeutic for the human metabolic disease phenylketonuria. *Nat Biotechnol*, *36*(9), 857-864. https://doi.org/10.1038/nbt.4222

Jandhyala, S. M., Talukdar, R., Subramanyam, C., Vuyyuru, H., Sasikala, M., & Nageshwar Reddy, D. (2015). Role of the normal gut microbiota. *World J Gastroenterol*, *21*(29), 8787-8803. https://doi.org/10.3748/wjg.v21.i29.8787

Jarmander, J., Gustavsson, M., Do, T. H., Samuelson, P., & Larsson, G. (2012). A dual tag system for facilitated detection of surface expressed proteins in Escherichia coli. *Microb Cell Fact*, *11*, 118. https://doi.org/10.1186/1475-2859-11-118

Kostylev, M., Otwell, A. E., Richardson, R. E., & Suzuki, Y. (2015). Cloning Should Be Simple: Escherichia coli DH5alpha-Mediated Assembly of Multiple DNA Fragments with Short End Homologies. *PLoS One*, *10*(9), e0137466. https://doi.org/10.1371/journal.pone.0137466

Lavelle, E. C., & Ward, R. W. (2022). Mucosal vaccines - fortifying the frontiers. *Nat Rev Immunol*, *22*(4), 236-250. https://doi.org/10.1038/s41577-021-00583-2

Laver, J. R., Gbesemete, D., Dale, A. P., Pounce, Z. C., Webb, C. N., Roche, E. F., Guy, J. M., Berreen, G., Belogiannis, K., Hill, A. R., Ibrahim, M. M., Ahmed, M., Cleary, D. W., Pandey, A. K., Humphries, H. E., Allen, L., de Graaf, H., Maiden, M. C., Faust, S. N.,…Read, R. C. (2021). A recombinant commensal bacteria elicits heterologous antigen-specific immune responses during pharyngeal carriage. *Sci Transl Med*, *13*(601). https://doi.org/10.1126/scitranslmed.abe8573

Leventhal, D. S., Sokolovska, A., Li, N., Plescia, C., Kolodziej, S. A., Gallant, C. W., Christmas, R., Gao, J. R., James, M. J., Abin-Fuentes, A., Momin, M., Bergeron, C., Fisher, A., Miller, P. F., West, K. A., & Lora, J. M. (2020). Immunotherapy with engineered bacteria by targeting the STING pathway for anti-tumor immunity. *Nat Commun*, *11*(1), 2739. https://doi.org/10.1038/s41467-020-16602-0

Levin, E. G., Lustig, Y., Cohen, C., Fluss, R., Indenbaum, V., Amit, S., Doolman, R., Asraf, K., Mendelson, E., Ziv, A., Rubin, C., Freedman, L., Kreiss, Y., & Regev-Yochay, G. (2021). Waning Immune Humoral Response to BNT162b2 Covid-19 Vaccine over 6 Months. *N Engl J Med*, *385*(24), e84. https://doi.org/10.1056/NEJMoa2114583

Limaye, S. A., Haddad, R. I., Cilli, F., Sonis, S. T., Colevas, A. D., Brennan, M. T., Hu, K. S., & Murphy, B. A. (2013). Phase 1b, multicenter, single blinded, placebo-controlled, sequential dose escalation study to assess the safety and tolerability of topically applied AG013 in subjects with locally advanced head and neck cancer receiving induction chemotherapy. *Cancer*, *119*(24), 4268-4276. https://doi.org/10.1002/cncr.28365

Lipsitch, M., Krammer, F., Regev-Yochay, G., Lustig, Y., & Balicer, R. D. (2022). SARS-CoV-2 breakthrough infections in vaccinated individuals: measurement, causes and impact. *Nat Rev Immunol*, *22*(1), 57-65. https://doi.org/10.1038/s41577-021-00662-4

Lu, L. L., Suscovich, T. J., Fortune, S. M., & Alter, G. (2018). Beyond binding: antibody effector functions in infectious diseases. *Nat Rev Immunol*, *18*(1), 46-61. https://doi.org/10.1038/nri.2017.106

Lynch, J. P., Gonzalez-Prieto, C., Reeves, A. Z., Bae, S., Powale, U., Godbole, N. P., Tremblay, J. M., Schmidt, F. I., Ploegh, H. L., Kansra, V., Glickman, J. N., Leong, J. M., Shoemaker, C. B., Garrett, W. S., & Lesser, C. F. (2023). Engineered Escherichia coli for the in situ secretion of therapeutic nanobodies in the gut. *Cell Host Microbe*, *31*(4), 634-649 e638. https://doi.org/10.1016/j.chom.2023.03.007

Lynn, D. J., Benson, S. C., Lynn, M. A., & Pulendran, B. (2022). Modulation of immune responses to vaccination by the microbiota: implications and potential mechanisms. *Nat Rev Immunol*, *22*(1), 33-46. https://doi.org/10.1038/s41577-021-00554-7

Lynn, M. A., Eden, G., Ryan, F. J., Bensalem, J., Wang, X., Blake, S. J., Choo, J. M., Chern, Y. T., Sribnaia, A., James, J., Benson, S. C., Sandeman, L., Xie, J., Hassiotis, S., Sun, E. W., Martin, A. M., Keller, M. D., Keating, D. J., Sargeant, T. J.,…Lynn, D. J. (2021). The composition of the gut microbiota following early-life antibiotic exposure affects host health and longevity in later life. *Cell Rep*, *36*(8), 109564. https://doi.org/10.1016/j.celrep.2021.109564

Lynn, M. A., Tumes, D. J., Choo, J. M., Sribnaia, A., Blake, S. J., Leong, L. E. X., Young, G. P., Marshall, H. S., Wesselingh, S. L., Rogers, G. B., & Lynn, D. J. (2018). Early-Life Antibiotic-Driven Dysbiosis Leads to Dysregulated Vaccine Immune Responses in Mice. *Cell Host Microbe*, *23*(5), 653-660 e655. https://doi.org/10.1016/j.chom.2018.04.009

Mao, T., Israelow, B., Pena-Hernandez, M. A., Suberi, A., Zhou, L., Luyten, S., Reschke, M., Dong, H., Homer, R. J., Saltzman, W. M., & Iwasaki, A. (2022). Unadjuvanted intranasal spike vaccine elicits protective mucosal immunity against sarbecoviruses. *Science*, *378*(6622), eabo2523. https://doi.org/10.1126/science.abo2523

Mazmanian, S. K., Round, J. L., & Kasper, D. L. (2008). A microbial symbiosis factor prevents intestinal inflammatory disease. *Nature*, *453*(7195), 620-625. https://doi.org/10.1038/nature07008

McMahan, K., Wegmann, F., Aid, M., Sciacca, M., Liu, J., Hachmann, N. P., Miller, J., Jacob-Dolan, C., Powers, O., Hope, D., Wu, C., Pereira, J., Murdza, T., Mazurek, C. R., Hoyt, A., Boon, A. C. M., Davis-Gardner, M., Suthar, M. S., Martinot, A. J.,…Barouch, D. H. (2024). Mucosal boosting enhances vaccine protection against SARS-CoV-2 in macaques. *Nature*, *626*(7998), 385-391. https://doi.org/10.1038/s41586-023-06951-3

Moginger, U., Resemann, A., Martin, C. E., Parameswarappa, S., Govindan, S., Wamhoff, E. C., Broecker, F., Suckau, D., Pereira, C. L., Anish, C., Seeberger, P. H., & Kolarich, D. (2016). Cross Reactive Material 197 glycoconjugate vaccines contain privileged conjugation sites. *Sci Rep*, *6*, 20488. https://doi.org/10.1038/srep20488

Moradi-Kalbolandi, S., Majidzadeh, A. K., Abdolvahab, M. H., Jalili, N., & Farahmand, L. (2021). The Role of Mucosal Immunity and Recombinant Probiotics in SARS-CoV2 Vaccine Development. *Probiotics Antimicrob Proteins*, *13*(5), 1239-1253. https://doi.org/10.1007/s12602-021-09773-9

Murray, S. M., Ansari, A. M., Frater, J., Klenerman, P., Dunachie, S., Barnes, E., & Ogbe, A. (2023). The impact of pre-existing cross-reactive immunity on SARS-CoV-2 infection and vaccine responses. *Nat Rev Immunol*, *23*(5), 304-316. https://doi.org/10.1038/s41577-022-00809-x

Nagashima, K., Zhao, A., Atabakhsh, K., Bae, M., Blum, J. E., Weakley, A., Jain, S., Meng, X., Cheng, A. G., Wang, M., Higginbottom, S., Dimas, A., Murugkar, P., Sattely, E. S., Moon, J. J., Balskus, E. P., & Fischbach, M. A. (2023). Mapping the T cell repertoire to a complex gut bacterial community. *Nature*, *621*(7977), 162-170. https://doi.org/10.1038/s41586-023-06431-8

Naik, S., Bouladoux, N., Linehan, J. L., Han, S. J., Harrison, O. J., Wilhelm, C., Conlan, S., Himmelfarb, S., Byrd, A. L., Deming, C., Quinones, M., Brenchley, J. M., Kong, H. H., Tussiwand, R., Murphy, K. M., Merad, M., Segre, J. A., & Belkaid, Y. (2015). Commensal-dendritic-cell interaction specifies a unique protective skin immune signature. *Nature*, *520*(7545), 104-108. https://doi.org/10.1038/nature14052

Nutt, S. L., Hodgkin, P. D., Tarlinton, D. M., & Corcoran, L. M. (2015). The generation of antibody-secreting plasma cells. *Nat Rev Immunol*, *15*(3), 160-171. https://doi.org/10.1038/nri3795

Pan, Y. G., Aiamkitsumrit, B., Bartolo, L., Wang, Y., Lavery, C., Marc, A., Holec, P. V., Rappazzo, C. G., Eilola, T., Gimotty, P. A., Hensley, S. E., Antia, R., Zarnitsyna, V. I., Birnbaum, M. E., & Su, L. F. (2021). Vaccination reshapes the virus-specific T cell repertoire in unexposed adults. *Immunity*, *54*(6), 1245-1256 e1245. https://doi.org/10.1016/j.immuni.2021.04.023

Pedersen, T. K., Brown, E. M., Plichta, D. R., Johansen, J., Twardus, S. W., Delorey, T. M., Lau, H., Vlamakis, H., Moon, J. J., Xavier, R. J., & Graham, D. B. (2022). The CD4(+) T cell response to a commensal-derived epitope transitions from a tolerant to

an inflammatory state in Crohn's disease. *Immunity*, *55*(10), 1909-1923 e1906. https://doi.org/10.1016/j.immuni.2022.08.016

Ponziani, F. R., Coppola, G., Rio, P., Caldarelli, M., Borriello, R., Gambassi, G., Gasbarrini, A., & Cianci, R. (2023). Factors Influencing Microbiota in Modulating Vaccine Immune Response: A Long Way to Go. *Vaccines (Basel)*, *11*(10). https://doi.org/10.3390/vaccines11101609

Pulendran, B., & Ahmed, R. (2011). Immunological mechanisms of vaccination. *Nat Immunol*, *12*(6), 509-517. https://doi.org/10.1038/ni.2039

Puurunen, M. K., Vockley, J., Searle, S. L., Sacharow, S. J., Phillips, J. A., 3rd, Denney, W. S., Goodlett, B. D., Wagner, D. A., Blankstein, L., Castillo, M. J., Charbonneau, M. R., Isabella, V. M., Sethuraman, V. V., Riese, R. J., Kurtz, C. B., & Brennan, A. M. (2021). Safety and pharmacodynamics of an engineered E. coli Nissle for the treatment of phenylketonuria: a first-in-human phase 1/2a study. *Nat Metab*, *3*(8), 1125-1132. https://doi.org/10.1038/s42255-021-00430-7

Redenti, A., Im, J., Redenti, B., Li, F., Rouanne, M., Sheng, Z., Sun, W., Gurbatri, C. R., Huang, S., Komaranchath, M., Jang, Y., Hahn, J., Ballister, E. R., Vincent, R. L., Vardoshivilli, A., Danino, T., & Arpaia, N. (2024). Probiotic neoantigen delivery vectors for precision cancer immunotherapy. *Nature*. https://doi.org/10.1038/s41586-024-08033-4

Riglar, D. T., & Silver, P. A. (2018). Engineering bacteria for diagnostic and therapeutic applications. *Nat Rev Microbiol*, *16*(4), 214-225. https://doi.org/10.1038/nrmicro.2017.172

Roco, J. A., Mesin, L., Binder, S. C., Nefzger, C., Gonzalez-Figueroa, P., Canete, P. F., Ellyard, J., Shen, Q., Robert, P. A., Cappello, J., Vohra, H., Zhang, Y., Nowosad, C. R., Schiepers, A., Corcoran, L. M., Toellner, K. M., Polo, J. M., Meyer-Hermann, M., Victora, G. D., & Vinuesa, C. G. (2019). Class-Switch Recombination Occurs Infrequently in Germinal Centers. *Immunity*, *51*(2), 337-350 e337. https://doi.org/10.1016/j.immuni.2019.07.001

Rossouw, C., Ryan, F. J., & Lynn, D. J. (2024). The role of the gut microbiota in regulating responses to vaccination: current knowledge and future directions. *FEBS J*. https://doi.org/10.1111/febs.17241

Saggau, C., Martini, G. R., Rosati, E., Meise, S., Messner, B., Kamps, A. K., Bekel, N., Gigla, J., Rose, R., Voss, M., Geisen, U. M., Reid, H. M., Sumbul, M., Tran, F.,

Berner, D. K., Khodamoradi, Y., Vehreschild, M., Cornely, O., Koehler, P.,…Bacher, P. (2022). The pre-exposure SARS-CoV-2-specific T cell repertoire determines the quality of the immune response to vaccination. *Immunity*, *55*(10), 1924-1939 e1925. https://doi.org/10.1016/j.immuni.2022.08.003

Sano, K., Bhavsar, D., Singh, G., Floda, D., Srivastava, K., Gleason, C., Group, P. S., Carreno, J. M., Simon, V., & Krammer, F. (2022). SARS-CoV-2 vaccination induces mucosal antibody responses in previously infected individuals. *Nat Commun*, *13*(1), 5135. https://doi.org/10.1038/s41467-022-32389-8

Sarnelli, G., Del Re, A., Palenca, I., Franzin, S. B., Lu, J., Seguella, L., Zilli, A., Pesce, M., Rurgo, S., Esposito, G., Sanseverino, W., & Esposito, G. (2024). Intranasal administration of Escherichia coli Nissle expressing the spike protein of SARS-CoV-2 induces long-term immunization and prevents spike protein-mediated lung injury in mice. *Biomed Pharmacother*, *174*, 116441. https://doi.org/10.1016/j.biopha.2024.116441

Sarnelli, G., Del Re, A., Pesce, M., Lu, J., Esposito, G., Sanseverino, W., Corpetti, C., Basili Franzin, S., Seguella, L., Palenca, I., Rurgo, S., De Palma, F. D. E., Zilli, A., & Esposito, G. (2023). Oral Immunization with Escherichia coli Nissle 1917 Expressing SARS-CoV-2 Spike Protein Induces Mucosal and Systemic Antibody Responses in Mice. *Biomolecules*, *13*(3). https://doi.org/10.3390/biom13030569

Shin, H., & Iwasaki, A. (2012). A vaccine strategy that protects against genital herpes by establishing local memory T cells. *Nature*, *491*(7424), 463-467. https://doi.org/10.1038/nature11522

Shishido, S. N., Varahan, S., Yuan, K., Li, X., & Fleming, S. D. (2012). Humoral innate immune response and disease. *Clin Immunol*, *144*(2), 142-158. https://doi.org/10.1016/j.clim.2012.06.002

Su, L. F., Kidd, B. A., Han, A., Kotzin, J. J., & Davis, M. M. (2013). Virus-specific CD4(+) memory-phenotype T cells are abundant in unexposed adults. *Immunity*, *38*(2), 373-383. https://doi.org/10.1016/j.immuni.2012.10.021

Wang, S., Geng, N., Zhou, D., Qu, Y., Shi, M., Xu, Y., Liu, K., Liu, Y., & Liu, J. (2019). Oral Immunization of Chickens With Recombinant Lactobacillus plantarum Vaccine Against Early ALV-J Infection. *Front Immunol*, *10*, 2299. https://doi.org/10.3389/fimmu.2019.02299

Watson, O. J., Barnsley, G., Toor, J., Hogan, A. B., Winskill, P., & Ghani, A. C. (2022). Global impact of the first year of COVID-19 vaccination: a mathematical modelling study. *Lancet Infect Dis*, *22*(9), 1293-1302. https://doi.org/10.1016/S1473-3099(22)00320-6

Welsh, R. M., & Fujinami, R. S. (2007). Pathogenic epitopes, heterologous immunity and vaccine design. *Nat Rev Microbiol*, *5*(7), 555-563. https://doi.org/10.1038/nrmicro1709

Winklmeier, S., Rubsamen, H., Ozdemir, C., Wratil, P. R., Lupoli, G., Stern, M., Schneider, C., Eisenhut, K., Ho, S., Wong, H. K., Taskin, D., Petry, M., Weigand, M., Eichhorn, P., Foesel, B. U., Mader, S., Keppler, O. T., Kumpfel, T., & Meinl, E. (2024). Intramuscular vaccination against SARS-CoV-2 transiently induces neutralizing IgG rather than IgA in the saliva. *Front Immunol*, *15*, 1330864. https://doi.org/10.3389/fimmu.2024.1330864

Woof, J. M., & Russell, M. W. (2011). Structure and function relationships in IgA. *Mucosal Immunol*, *4*(6), 590-597. https://doi.org/10.1038/mi.2011.39

Yagnik, B., Sharma, D., Padh, H., & Desai, P. (2019). Oral immunization with LacVax(R) OmpA induces protective immune response against Shigella flexneri 2a ATCC 12022 in a murine model. *Vaccine*, *37*(23), 3097-3105. https://doi.org/10.1016/j.vaccine.2019.04.053

Zhang, Y., Yang, L., Zhang, J., Huang, K., Sun, X., Yang, Y., Wang, T., Zhang, Q., Zou, Z., & Jin, M. (2022). Oral or intranasal immunization with recombinant Lactobacillus plantarum displaying head domain of Swine Influenza A virus hemagglutinin protects mice from H1N1 virus. *Microb Cell Fact*, *21*(1), 185. https://doi.org/10.1186/s12934-022-01911-4

Appendices

Buffers and reagents

	Composition
rCutSmart buffer 10x	50 mM Potassium Acetate 20 mM Tris-acetate 10 mM Magnesium Acetate 100 µg/ml Recombinant Albumin

	Composition
Tris acetate EDTA (TAE) buffer 1x	40 mM Tris(hydroxymethyl)aminomethane 20 mM Acetic acid 1 mM EDTA (disodium salt)

	Composition
T4 DNA Ligase Buffer	50 mM Tris-HCl 10 mM $MgCl_2$ (magnesium chloride) 10 mM Dithiothreitol 1 mM ATP

	Composition
DreamTaq master PCR mix 2x	0.05 U/µL Taq DNA polymerase and reaction buffer 4 mM $MgCl_2$ (magnesium chloride)

	0.4 mM of each dNTP (dATP, dCTP, dGTP and dTTP)

	Composition
ZymoPURE binding buffer	10 mM Tris-Cl 0.1 mM EDTA (Ethylenediaminetetraacetic acid) 0.04% NaN_3 (Sodium-azide)
ZymoPURE elution buffer	10 mM Tris-Cl 0.1 mM EDTA (Ethylenediaminetetraacetic acid) 0.04% NaN_3 (Sodium-azide)

	Composition
Dulbecco's phosphate-buffered saline (DPBS)	8.0 gm NaCl (Sodium Chloride) 200 mg KCl (potassium chloride) 1.15 gm Na_2HPO_4 (Disodium Phosphate) 200 mg KH_2PO_4 (Monopotassium Phosphate)

	Composition
Luria-Bertani broth (LB)	10 gm Tryptone 10 gm NaCl (Sodium Chloride) 5 gm Yeast extract

	Composition
ELISA coating buffer	1.5 gm mM Na_2CO_3 (Sodium carbonate) 3 gm $NaHCO_3$ (Sodium bicarbonate) 500 ml distilled water
ELISA buffer	1 x concentrated phosphate buffered saline solution

	Composition
Red Blood Cell lysis buffer	8.02 gm NH4Cl (ammonium chloride) 0.84 gm NaHCO3 (sodium bicarbonate) 0.37 gm EDTA (disodium)